

USAGE OF HYALURONIC ACID - CHITOSAN COACERVATES FOR CARTILAGE
TISSUE ENGINEERING



by
Özge Acar

Submitted to Graduate School of Natural and Applied Sciences
in Partial Fulfillment of the Requirements
for the Degree of Doctor of Philosophy in
Biotechnology

Yeditepe University
2017

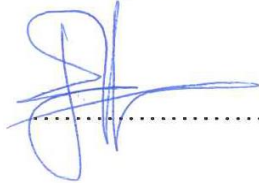
USAGE OF HYALURONIC ACID - CHITOSAN COACERVATES FOR CARTILAGE
TISSUE ENGINEERING

APPROVED BY:

Prof. Dr. Gamze Köse
(Thesis Supervisor)



Prof. Dr. Ebru Toksoy Öner



Assoc. Prof. Dr. Başak Kayıtmazer



Assoc. Prof. Dr. Fatma Neşe Kök



Assist. Prof. Dr. Hüseyin Çimen



DATE OF APPROVAL:/...../2017

ACKNOWLEDGEMENTS

I am deeply grateful to my advisor Prof. Dr. Gamze Köse for her leading, support and guidance to pursue my academic study in Yeditepe University Tissue Engineering group (YUTEG). I absolutely appreciate her efforts and mentorship that have helped me to improve my carrier. Her critical and professional comments guided me through my Ph.D. study.

In advance, I would like to thank Assoc. Prof. Başak Kayitmazer for her time and brilliant ideas that helped me to see different aspects of my thesis project with her expertise. I would also like to acknowledge my thesis committee members, Prof. Ebru Toksoy Öner, Assoc. Prof. Fatma Nese Kok and Assist. Prof. Hüseyin Çimen.

I wish to thank YUTEG members, my undergrad students and university staffs that were very kind and collaborator to me during my thesis. I would like to thank to my friends, life is beautiful and easy with them.

Overall, I would gratefully thank to my family for their worthless support and love. Finally, I thank to my beloved husband, Erşan Acar that he is always there for me and doing everything with patience to help my dreams come true.

ABSTRACT

USAGE OF HYALURONIC ACID - CHITOSAN COACERVATES FOR CARTILAGE TISSUE ENGINEERING

Cartilage injuries can lead to severe pain and tissue degeneration. Articular cartilage has low natural repair capacity that have turned into a leading objective for tissue engineers. Complex coacervation technique is a promising way of generating 3D scaffolds using oppositely charged polyelectrolytes that have cell entrapment capacity. Those scaffolds have potential for usage in cartilage tissue engineering studies to regenerate the damaged tissues.

In this study biodegradable, viscous scaffolds were generated by complex coacervation method using hyaluronic acid (HA) and chitosan chloride (CHI-Cl) or chitosan glutamate salt (CHI-G) prepared in NaCl or CaCl₂ solutions. Optimal conditions for coacervation was detected by turbidity, optical microscopy, dynamic light scattering (DLS) and zeta potential techniques and found as the charge ratio of [-]/[+] = 0.31 and 0.48 for HA/CHI-Cl and HA/CHI-G, respectively. Coacervate droplets (~700 nm diameter) were centrifuged and coalesced to form scaffolding material. However, complexes formed above the identified optimal charge ratios ([-]/[+]) observed to transform into precipitates instead of coacervates.

Biocompatibility of the scaffolds were observed by MSC seeding and complexation process was further evaluated by MSC encapsulation studies. All coacervates supported cell cultivation and proliferation (viability $\geq 84\%$) by providing highly porous microstructure with consistent degradation profile.

MSC encapsulation studies were very encouraging that those cells were induced to differentiate into chondrocytes. After chondrogenic induction, cartilage-specific genes were up-regulated in both HA/CHI-Cl and HA/CHI-G coacervates in addition to remarkable cartilaginous matrix synthesis. Therefore, coacervates can be used as a promising scaffolds for cartilage tissue engineering studies.

ÖZET

HİYALÜRONİK ASİT – KİTOSAN KOASERVATLARININ KIKIRDAK DOKU MÜHENDİSLİĞİ İÇİN KULLANIMI

Kıkırdak yaralanmaları doku dejenerasyonuna ve ciddi ağrıya neden olabilir. Doğal tamir kapasitesi düşük olan artiküler kıkırdak, bu sebeple doku mühendisleri için öncü bir hedef haline gelmiştir. Kompleks koaservasyon tekniği, karşıt yüklü polielektrolitleri kullanarak hücre enkapsüle etme kapasitesine sahip, üç boyutlu doku iskeleleri üretilmesi için umut vaad etmektedir. Bu iskelelerinin kullanımı, kıkırdak doku mühendisliği çalışmalarında hasar gören dokuların yenilenmesi için önemli bir potansiyele sahiptir.

Bu çalışmada, biyobozunur, viskoz doku iskeleleri, kompleks koaservasyon yöntemi ile NaCl veya CaCl₂ çözeltileri içerisinde hazırlanan hiyalüronik asit (HA) ve kitosan klorür (KT-K) veya kitosan glutamat tuzu (KT-G) kullanılarak üretilmiştir.

Koaservasyon için optimal koşullar, optik mikroskopi, bulanıklık, dinamik ışık saçılması ve zeta potansiyel teknikleri ile tespit edilmiş ve sırasıyla HA/KT-K ve HA/KT-G için 0.31 ve 0.48'lik yük oranı ([-]/[+]) olarak bulunmuştur. Koaservat damlacıkları (~ 700 nm çap) santrifüj edilerek doku iskelesi malzemesi oluşturmak üzere toplanmıştır. Fakat, belirlenen optimal yük oranlarının üzerinde oluşturulan komplekslerin, koaservatlar yerine çökeltilere dönüştüğü gözlemlenmiştir.

İskelelerinin biyoyoumluluğu mezenkimal kök hücre (MKH) ekilmesiyle gözlemlenirken, kompleksleşme süreci ise MKH enkapsülasyonu ile ayrıca değerlendirilmiştir. Bütün koaservatlar, istikrarlı bozunma profili ile yüksek gözenekli mikro-yapı sağlayarak hücre büyümesi ve çoğalmasını (canlılık \geq % 84) desteklemiştir.

Cesaret verici enkapsülasyon sonuçları sayesinde, bu hücreler kondrositlere farklılaşmaları için uyarılmıştır. Kondrojenik uyarılma sonrasında, hem HA/KT-K hem de HA/KT-G koaservatlarında belirgin kartilaginöz matriks sentezine ek olarak kıkırdağa özelleşmiş genlerin ekspresyonu da artmıştır. Bu nedenle, koaservatların kıkırdak doku mühendisliği çalışmalarında gelecek vaad eden doku iskeleleri olarak kullanılabilirlikleri öngörülmüştür.

TABLE OF CONTENTS

ACKNOWLEDGEMENTS.....	iii
ABSTRACT.....	iv
ÖZET	v
LIST OF FIGURES	ix
LIST OF TABLES.....	xiii
LIST OF SYMBOLS/ABBREVIATIONS.....	xiv
1. INTRODUCTION.....	1
1.1 CARTILAGE	1
1.1.1 Cartilage Extracellular Matrix	2
1.2 ZONAL ARRANGEMENT OF ARTICULAR CARTILAGE.....	4
1.2.1 Chondrocytes	5
1.3 ARTICULAR CARTILAGE DEFECTS.....	6
1.4 TREATMENTS OF ARTICULAR CARTILAGE DEFECTS	7
1.5 CARTILAGE TISSUE ENGINEERING	9
1.5.1 Cell Sources	10
1.5.2 Stimulating Factors	12
1.5.3 Scaffolds	15
1.5.4 Scaffold Fabrication Techniques	19
1.6 COMPLEX COACERVATION (PHASE SEPARATION).....	22
1.6.1 Precipitate	24
1.6.2 Flocculate.....	24
1.6.3 Hydrogel	24
1.6.4 Layer by Layer Assembly.....	25
1.7 AIM OF THE STUDY	26
2. MATERIALS	27
2.1 CHEMICALS AND REAGENTS	27
2.2 ANTIBODIES.....	28
2.3 INSTRUMENTS.....	29
3. METHODS.....	30

3.1	PREPARATION OF POLYMER SOLUTIONS AND COACERVATES	30
3.1.1	Polymer Concentration	30
3.1.2	pH of Solution.....	30
3.1.3	Ionic Strength of Solution.....	31
3.1.4	Coacervate Preparation	32
3.2	CHARACTERIZATION OF THE COACERVATE SUSPENSIONS	33
3.2.1	Optical Microscopy.....	33
3.2.2	Turbidity	33
3.2.3	Dynamic Light Scattering	34
3.2.4	Zeta Potential	34
3.2.5	Visual Inspection	34
3.3	CHARACTERIZATION OF THE COACERVATE SCAFFOLDS	35
3.3.1	Environmental Scanning Electron Microscopy (ESEM).....	35
3.3.2	Dry Weight Analysis of Coacervates.....	35
3.3.3	Degradation Behavior of the Coacervates	35
3.3.4	Antimicrobial Activity of the Coacervates	36
3.4	ISOLATION AND CULTURE OF MESENCHYMAL STEM CELLS	37
3.4.1	Characterization of MSCs.....	38
3.4.2	CM-Dil Staining of MSCs	38
3.5	COACERVATE SCAFFOLDS WITH CELLS.....	38
3.5.1	Cell Seeding.....	38
3.5.2	Cell Encapsulation	39
3.5.3	Scanning Electron Microscopy (SEM).....	39
3.5.4	LIVE/DEAD [®] Cell Viability Assay.....	39
3.5.5	Fluorescent Staining	40
3.5.6	<i>In Vitro</i> Chondrogenic Differentiation	40
3.5.7	Statistical Analysis.....	44
4.	RESULTS AND DISCUSSION.....	45
4.1	CHARACTERIZATION OF COACERVATE SUSPENSIONS	45
4.1.1	Optical Microscopy.....	45
4.1.2	Turbidity	51
4.1.3	Dynamic Light Scattering (DLS).....	53

4.1.4	Zeta Potential	56
4.1.5	Visual Inspection	58
4.1.6	Environmental Scanning Electron Microscopy (ESEM).....	60
4.1.7	Dry Weight Analysis of Coacervates.....	61
4.1.8	Degradation Behavior of the Coacervate Scaffolds.....	62
4.1.9	Antimicrobial Activity	64
4.2	CHARACTERIZATION OF BONE MARROW STEM CELLS	67
4.3	CELL CONTAINING COACERVATES.....	68
4.3.1	Bright Field and Fluorescent Microscopy	69
4.3.2	Scanning Electron Microscopy (SEM)	72
4.3.3	LIVE/DEAD Cell Viability Assay	74
4.3.4	Immunofluorescence Staining to Analyze Cell Morphology	79
4.3.5	<i>In Vitro</i> Chondrogenic Differentiation	84
5.	CONCLUSION	91
6.	FUTURE PROSPECTS.....	92
	REFERENCES	93

LIST OF FIGURES

Figure 1.1. Schematic illustration of cartilage types	2
Figure 1.2. Molecular organization of hyaline cartilage ECM	4
Figure 1.3. The zonal arrangement of articular cartilage.....	5
Figure 1.4. Schematic illustration of the development of a mesenchymal cell into a chondrocyte.....	6
Figure 1.5. The Outerbridge system for grading damage degree of articular cartilage	7
Figure 1.6. Schematic illustration of the therapeutic techniques used in cartilage repair	9
Figure 1.7. Schematic illustration of tissue engineering concept that involves seeding <i>in vitro</i> expanded cells within 3D scaffolds using suitable bioactive factors.	10
Figure 1.8. Schematic illustration of the origins and types of stem cells	12
Figure 1.9. Schematic representation of the bioreactors mostly used in cartilage tissue engineering.....	14
Figure 1.10. Frequently used synthetic biodegradable polymers in cartilage tissue engineering and their structures	16
Figure 1.11. Structure of hyaluronic acid polymer	18
Figure 1.12. Structures of chitin, chitosan and protonated chitosan polymers.....	19

Figure 1.13. Schematic representation of cell encapsulation by complex coacervation between a polyanion and a polycation	25
Figure 4.1. Optical microscopy images of HA:CHI-Cl coacervate suspensions in the charge ratio of $[-]/[+] = 0.07$, at ionic strength of 50 mM and 150 mM.....	46
Figure 4.2. Optical microscopy images of HA:CHI-Cl coacervate suspensions at ionic strength of 300 mM NaCl solution	48
Figure 4.3. Optical microscopy images of HA:CHI-Cl coacervate suspensions at ionic strength of 300 mM CaCl_2 solution	49
Figure 4.4. Optical microscopy images of HA:CHI-G coacervate suspensions at ionic strength of 300 mM NaCl solution	50
Figure 4.5. Visual turbidity of mixtures at ionic strength of 300 mM HA/CHI-Cl in NaCl, HA/CHI-Cl in CaCl_2 and HA/CHI-G in NaCl salt solution	52
Figure 4.6. Turbidity as a function of HA to CHI charge ratio $[-]/[+]$, at 300 mM ionic strength.....	53
Figure 4.7. Scattering intensity as a function of HA to CHI charge ratio $[-]/[+]$, at 300 mM ionic strength.....	54
Figure 4.8. Z-average (hydrodynamic) diameter as a function of HA to CHI charge ratio $[-]/[+]$, at 300 mM ionic strength.....	56
Figure 4.9. Zeta potential as a function of HA to CHI charge ratio $[-]/[+]$, at 300 mM ionic strength.....	58

Figure 4.10. Visual appearance of coacervates after centrifugation at a charge ratio of [-]/[+] = 0.31 HA/CHI-Cl and [-]/[+] = 0.48 HA/CHI-G suspensions.	59
Figure 4.11. Environmental Scanning Electron microscopy images of HA/CHI-Cl coacervates at 3 rd day of incubation prepared with 300 mM CaCl ₂	61
Figure 4.12. Environmental Scanning Electron microscopy images of HA/CHI-Cl coacervates at 3 rd day of incubation prepared with 300 mM NaCl	61
Figure 4.13. <i>In situ</i> degradation behavior of coacervates at different incubation time intervals (up to 120 days).....	64
Figure 4.14. Bacterial growth inhibition of disc diffusion method. Coacervates were incubated with <i>Esheria coli</i> and <i>Staphylococcus aureus</i>	66
Figure 4.15. Flow cytometry histogram of rBMSC labeled with CD11a, CD 31, CD45, CD29 and CD90.....	68
Figure 4.16. Brighth field microscopy images of MSCs encapsulated in coacervates.....	69
Figure 4.17. Fluorescent microscopy of CM-Dil-labeled MSCs at first day of incubation for coacervates cell seeded and cell encapsulated	71
Figure 4.18. Scanning Electron microscopy images of HA/CHI-Cl coacervates.....	73
Figure 4.19. Scanning Electron microscopy images of cell encapsulated coacervates after 3 days of incubation	74
Figure 4.20. Images of rBMSCs seeded coacervates after LIVE/DEAD assay analysis.....	76

Figure 4.21. Images of rBMSCs encapsulated coacervates after LIVE/DEAD assay analysis.....	78
Figure 4.22. The graphs show the mean values \pm standard deviations for live cells from 3 different zones for each experimental group	79
Figure 4.23. Phalloidin/DAPI stainings of rBMSCs seeded on coacervates after 3 days of incubation.....	80
Figure 4.24. Images of encapsulated rBMSCs stained with phalloidin/DAPI representing the cell morphology inside coacervates after 3 and 21 days of incubation	82
Figure 4.25. Images of encapsulated rBMSCs stained with phalloidin/DAPI representing the cell morphology inside coacervates (40X magnification)	83
Figure 4.26. Collagen type II, aggrecan and cell nuclei immunostaining images of rBMSCs encapsulated in coacervates after chondrogenic induction of 7 and 14 days	86
Figure 4.27. Collagen type II, aggrecan and cell nuclei immunostaining images of rBMSCs encapsulated in coacervates after chondrogenic induction of 21 and 30 days	87
Figure 4.28. Analysis of gene expression levels for the coacervates after cultured in differentiation media (14 and 21 days) and growth media (21 days)	90

LIST OF TABLES

Table 1.1 Typical polymers employed in complex coacervation	22
Table 3.1 Critical overlap concentrations of chitosan and hyaluronic acid polymers	30
Table 3.2 Preparation of salt solutions.....	31
Table 3.3 Polymer information for the calculation of charge ratio	32
Table 3.4 Volume to charge ratio conversion.....	33
Table 3.5 Samples placed on the inoculated agar surfaces.....	36
Table 3.6 cDNA reaction mix.....	43
Table 3.7 Real-time PCR reaction mix	43
Table 3.8 Primer pairs used for real-time PCR.....	44
Table 4.1 Positivity (%) of the CD markers	68

LIST OF SYMBOLS/ABBREVIATIONS

c^*	Critical overlap concentration
β	Beta
ζ	Zeta
3D	Three dimension
a.u.	Absorption units
ACAN	Aggrecan
ACI	Autologous chondrocyte implantation
ANOVA	Analysis of variance
BMP	Bone morphogenetic protein
BSA	Bovine serum albumin
CAD	Computer assisted design
CD	Cluster of differentiation
CDM	Chondrogenic differentiation medium
cDNA	Complementary DNA
CHI	Chitosan
CHI-Cl	Chitosan chloride salt
CHI-G	Chitosan glutamate salt
Cl	Chloride
CO ₂	Carbon dioxide
COL2A1	Collagen type II
CT	Computed tomography
DAPI	4',6-diamidino-2-phenylindole
DD	Deacetylation degree
d_H	Hydrodynamic diameter
DLS	Dynamic light scattering
DMEM	Dulbecco's modified Eagle's medium
DMSO	Dimethyl sulfoxide
DNA	Deoxyribonucleic acid

dNTP	Deoxynucleotide
DPBS	Dulbecco's phosphate buffer saline
<i>E. coli</i>	<i>Esheria coli</i>
ECM	Extracellular matrix
ESC	Embryonic stem cell
ESEM	Environmental scanning electron microscopy
EthD-1	Ethidium homodimer-1
FBS	Fetal bovine serum
FGF-2	Fibroblast growth factor-2
G	Glutamate
GAG	Glycosaminoglycan
GAPDH	Glyceraldehyde-3-phosphate dehydrogenase
GF	Growth factor
H ₂ O	Water
HA	Sodium hyaluronate / Hyaluronic acid
HCl	Hydrochloric acid
HSC	Hematopoietic stem cells
<i>I</i>	Ionic strength
ICRS	International cartilage repair society
IGF-1	Insulin-like growth factor-1
iPSC	Induced pluripotent stem cell
ISCT	International society for cellular therapy
LbL	Layer by layer assembly
MACI	Matrix-induced autologous chondrocyte implantation
MEM	Minimum essential medium
MRI	Magnetic resonance imaging
MSC	Mesenchymal stem cell
M _w	Molecular weight
NaOH	Sodium hydroxide
O ₂	Oxygen
OFX	Ofloxacin
PAA	Poly (acrylic acid)
PCL	Poly (ε-caprolactone)

PCR	Polymerase chain reaction
PDADMAC	Poly (diallyldimethylammonium chloride)
PdI	Polydispersity index
PDMAEMA	Poly (N,N-dimethylaminoethyl methacrylate)
PE	Polyelectrolytes
PEG	Poly (ethylene glycols)
PG	Proteoglycan
PGA	Poly (glycolic acid)
PLA	Poly (lactic acid)
PLGA	Poly (lactic-co-glycolic acid)
PLL	Poly-L-lysine
q-PCR	Quantitative polymerase chain reaction
rBMSC	Rat bone marrow stromal (stem) cell
RGD	Arginine-glycine-aspartic acid
RHAMM	Hyaluronan-mediated motility receptor
rhTGF β	Recombinant human transforming growth factor beta
RP	Rapid prototyping
RT	Reverse transcriptase
<i>S. aureus</i>	<i>Staphylococcus aureus</i>
SDF	Stromal cell-derived factor
SEM	Scanning electron microscopy
sGAG	Sulfated glycosaminoglycan
SGM	Standard growth medium
SOX9	SRY (sex determining region Y)-box 9
STD	Standard deviation
TGF	Transforming growth factor
WC	Water content
W _d	Dry weight
W _f	Final weight
W _i	Initial weight
WL	Weight loss
W _w	Wet weight

1. INTRODUCTION

The human body has an amazing regeneration capacity to maintain the tissues viable and functional throughout life. Vascularization is the important feature for full regeneration using delivery of the cells and nutrients. Articular cartilage has very low intrinsic regenerative capacity because of being avascular and aneural [1].

Chondral and osteochondral injuries of the knee are potentially serious and very common in our country. The damage can result in severe pain, knee swelling and some restrictions in mobility. There are several medical and clinical approaches to repair joint function. Current surgical treatments; arthroscopic debridement, stem cell based repair, tissue transplantation and prosthesis implantation are not satisfactory especially for the young patients.

Tissue engineering is a promising approach to overcome the problems and limitations of the current treatments. It is defined as the application of scientific principles to the synthesis of living tissues using appropriate cells combined with biodegradable scaffolds including the stimulation of additional biological factors [2].

In this study, the aim was to determine the effects of novel coacervate encapsulation system for cartilage regeneration. MSC-encapsulated coacervates were induced to undergo chondrogenic differentiation to mimic hyaline cartilage. To achieve this goal, complex coacervation method was used to have a gel-like fluid using chitosan (CHI) and hyaluronic acid (HA) due to their biocompatibility and structural similarity to glycosaminoglycan (GAG) found in cartilage. These constructs were examined in *in vitro* conditions in terms of tissue regeneration.

1.1 CARTILAGE

Cartilage is a highly-specialized connective tissue. It has a valuable biomechanical capacity to bear different kinds of loads in many areas of the body, including; joints between bones, ends of the ribs, in the spine (between the vertebrae), ears, nose and bronchial tubes.

There are three types of cartilage; hyaline cartilage, elastic cartilage and fibrocartilage (Figure 1.1). The most abundant type is hyaline cartilage which is present within joints and designed to withstand and distribute weight with less friction. It is strong as a protector for bones but softer and flexible as a cushion, especially, at the joints. Articular cartilage is the mostly injured tissue because of functioning under the loads transmitted across joints.

Elastic cartilage is more flexible than hyaline cartilage due to elastin fiber content. It is present at the places where the maintenance of a specific shape is important to continue its function, like outer ear and the larynx [3].

Fibrocartilage is the toughest type of cartilage having type I collagen. It is found in areas requiring great support or tensile strength, like intervertebral discs and sites where ligaments and tendons are connected to bones [4].

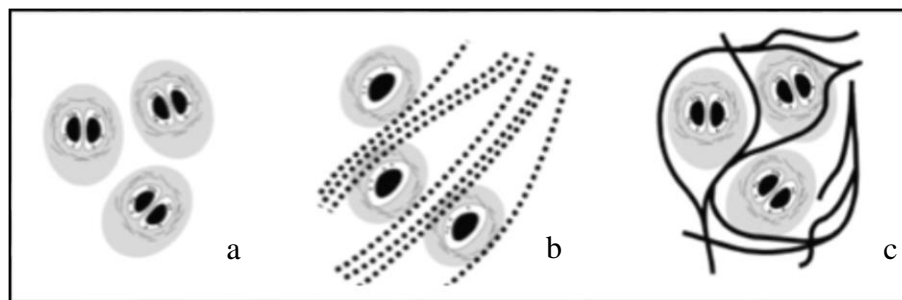


Figure 1.1. Schematic illustration of cartilage types; (a) Hyaline cartilage, (b) Fibrocartilage, (c) Elastic cartilage [5]

1.1.1 Cartilage Extracellular Matrix

Cartilage consists of chondrocytes in an extracellular matrix (ECM) containing collagen, proteoglycans, and water. In articular cartilage, clear majority of the tissue (65-80%) weight is composed of water. Chondrocytes are the only cell type found in the cartilage tissue and have low density (<10%) over the total volume [6, 7]. During maturation, chondrocytes usually have roundish shape which differs with age and the cartilage zone it stands [8]. They have a well-developed synthesis mechanism and ensure the production of collagen type II, proteoglycans and hyaluronic acid. Ultimately, chondrocytes maintain the regulation of synthesis and breakdown of the ECM. This regulation is still unclear but it is

thought that cytokines and growth factors have important catabolic and anabolic effects [9, 10].

1.1.1.1 Collagens

Collagen is the most abundant protein found in the ECM of all mammalian connective tissues. In humans, there are more than 28 different types of collagen and collagen-like proteins, but type II collagen is the predominant collagen type found in articular cartilage [11]. There are also type IV, V, VI, IX, X and XI collagens in limited amounts [12]. Type VI collagen is mostly found in pericellular matrix (the narrow layer encapsulating the chondrocytes) and thought to be regulating the chondrocyte-ECM interaction [13]. Type X collagen is found in the calcified zone and present around the hypertrophic chondrocytes [14].

1.1.1.2 Proteoglycans

Proteoglycans are large macromolecules comprised of a protein core with attached polysaccharide chains (glycosaminoglycans). Mature articular cartilage contains five types of glycosaminoglycans; hyaluronan, chondroitin sulfate, dermatan sulfate, heparan sulfate, and keratan sulfate [15]. Aggrecan is the primary proteoglycan in articular cartilage, which binds to a hyaluronan core with numerous sulfated glycosaminoglycan side chains (Figure 1.2). Multiple aggrecan molecules bind to hyaluronic acid and are stabilized by a link protein to form large aggregated proteoglycans. Other small proteoglycans found in articular cartilage include decorin, biglycan, and fibromodulin that all interact with collagen in different capacities to stabilize the ECM [16]. Proteoglycans have a negative charge due to the presence of carboxyl and sulfate groups. Negative charge absorbs water molecules and promotes resistance to compression due to the increased swelling capacity [17]. Also, presence of water helps the exchange of nutrients and oxygen (O₂).

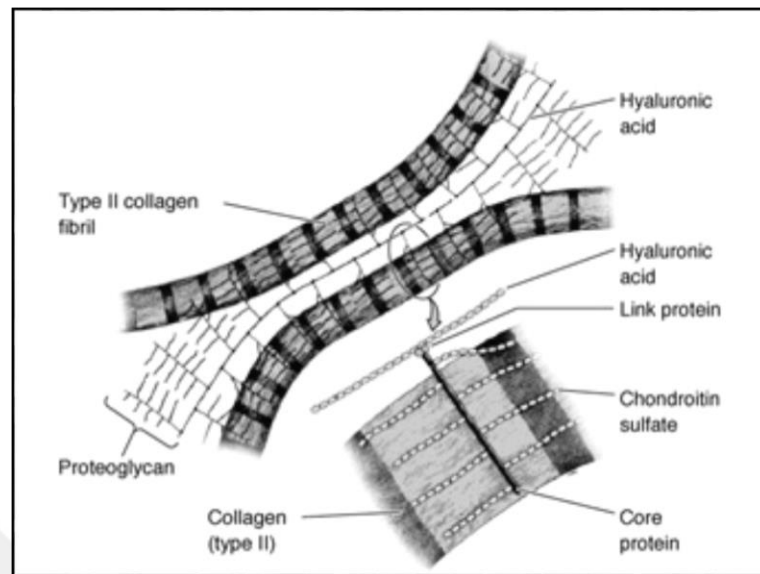


Figure 1.2. Molecular organization of hyaline cartilage ECM [18]

1.2 ZONAL ARRANGEMENT OF ARTICULAR CARTILAGE

Articular cartilage can be divided into 4 zones; tangential, transitional, radial and calcified zones based on the differences in matrix morphology, biochemistry and function [19]. The structure and composition of each cartilage zone is shown in Figure 1.3 [20].

The tangential zone is around 10% of the cartilage thickness. The collagen in this zone is oriented parallel to the articular surface. The proteoglycan content is lower and chondrocytes are flattened and denser than in other zones. In the transitional zone which has 40% to 60% of the thickness, the collagen is more randomly oriented and chondrocytes are more spherical. Proteoglycan content reaches its maximum in this zone. The collagen in the radial zone is perpendicular to the calcified zone and the chondrocytes are lined up between the collagen bundles. There is a boundary between radial and calcified zone named tide mark. Below this area proteoglycan content is reduced and chondrocytes become hypertrophic.

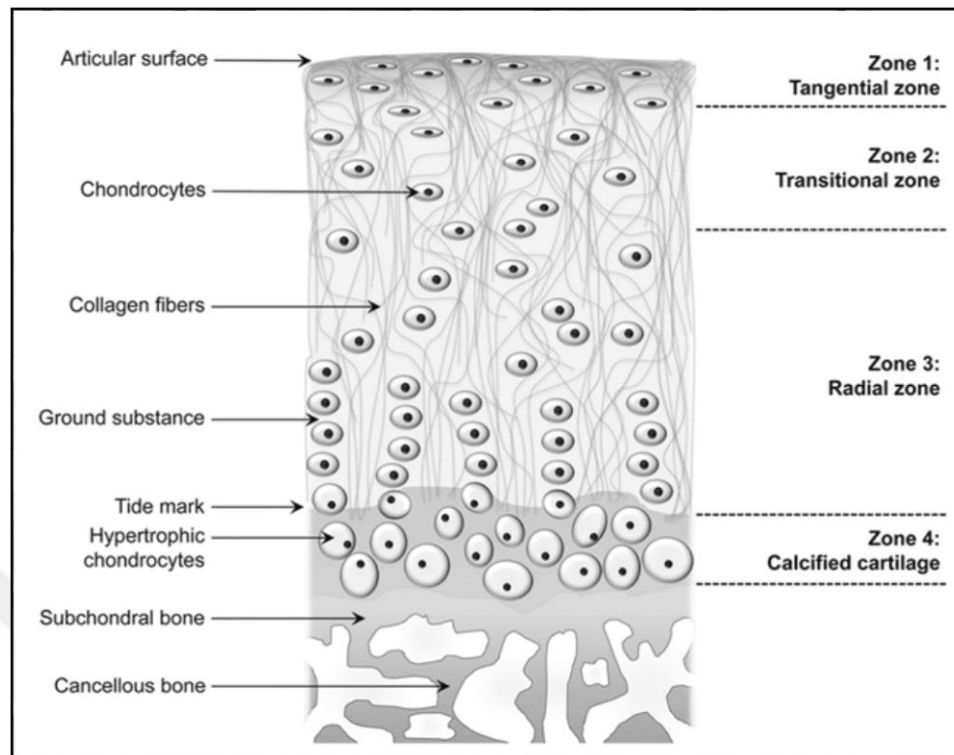


Figure 1.3. The zonal arrangement of articular cartilage. The image includes the arrangements of collagen fibers and the morphologies of chondrocytes in each zone [20]

1.2.1 Chondrocytes

Chondrocyte is the unique cell type in articular cartilage tissue and essential for cartilage formation and functionality. The progenitors of these cells arise in the bone marrow, in a form of mesenchymal stem cell. They can differentiate into several different types of cell. When they differentiate into cartilage cells, they first become chondroblasts. They are flattened cells capable of division. When they embed themselves in the cartilage matrix, they are called chondrocytes and lie in the matrix lacunae (Figure 1.4). Once they are in cartilage matrix, they stop proliferation and continue growth by starting to secrete more cartilage extracellular matrix [21].

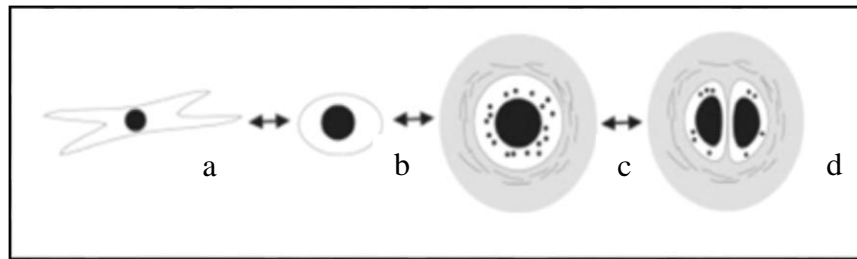


Figure 1.4. Schematic illustration of the development of a mesenchymal cell into a chondrocyte; (a) Mesenchymal cell, (b) Chondroblast, (c) Lacuna embedded immature chondrocyte, (d) Lacuna embedded mature chondrocyte [22]

Unlike the other connective tissue types, cartilage is avascular; all nutrients including oxygen, diffuse through the cartilage matrix to reach the cells. This lack of blood flow creates a hypoxic environment, with accessible oxygen levels that range from 2% to 6%, depending on the location and depth [23].

1.3 ARTICULAR CARTILAGE DEFECTS

Articular cartilage damage is one of the most widespread and potentially serious type of cartilage damage. It has a low natural repair capacity because there is no blood supply and the limited cellularity of the tissue. As a result, usually knee joint is affected. The damage can result in severe pain, knee swelling and some restrictions in mobility [24].

There are two main ways that articular cartilage injuries can occur;

- i) Traumatic mechanical destruction that occurs with a direct hit, for instance traffic accident, a fall or a sports injury.
- ii) Progressive mechanical degeneration (wear and tear) that occurs with the progressive loss of the normal cartilage structure and continues as an increased friction on the underlying bone and developing osteoarthritis.

There are several parameters that may influence the injured surface such as intensity and direction of loading, repetitive injuries, inflammatory conditions of the joint, age and genetic factors [25].

There is a grading system found by the International Cartilage Repair Society (ICRS) for determination the damage degree of cartilage. This grade is based on the appearance of the articular cartilage identified at arthroscopy (Figure 1.5) [26].

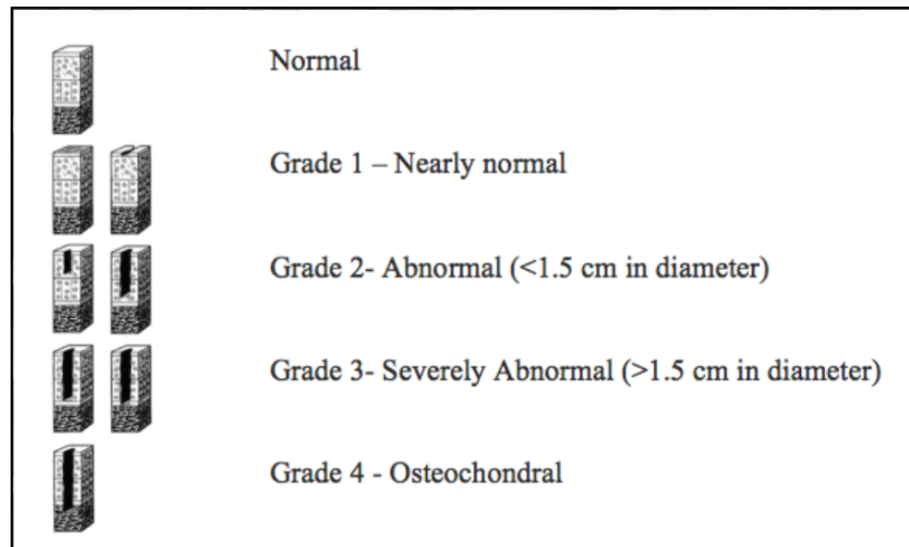


Figure 1.5. The Outerbridge system for grading damage degree of articular cartilage [26]

1.4 TREATMENTS OF ARTICULAR CARTILAGE DEFECTS

To renovate joint function, multiple treatment options exist. Conservative treatments including medications, physiotherapy, supportive devices and lifestyle changes, take first place [27]. In more severe cases surgical treatments, including arthroscopic debridement, stem cell based repair, tissue transplantation, chondrocyte implantation and joint replacement are required.

Arthroscopic debridement (lavage) is performed to remove unstable cartilage (Figure 1.6 a). It is a palliative approach that limits the rate of degeneration. After that operation, resurfacing can be performed (Figure 1.6 b) [28].

Abrasion arthroplasty [29], drilling [30] and microfracturing [31] are similar methods after cleaning the defect, they are simple and fast. Those methods can be used for the treatment of small defects. In all methods, the underlying bone is stimulated by holes and injured bone induce the release of multipotent stem cells from the marrow (Figure 1.6 c). Those bone marrow stem cells then begin to stimulate production of a cartilage-like tissue. These

lesions heal with the formation of fibrocartilage rather than the normal characteristics of hyaline cartilage [32]. Fibrocartilage is not a good replacer since it is not biochemically and biomechanically like hyaline cartilage [33].

Mosaicplasty is a relatively invasive technique for replacing the degenerated cartilage with healthy cartilage from the non-weight bearing areas of a joint. This approach generally used for larger defects and uses autogenous tissue to create a hyaline cartilage surface. However, removal of too much healthy cartilage could damage the matrix integrity of the body [34]. As an alternative procedure, allogeneous tissues can be taken from a cadaver in which tissue should be fresh, sterile and disease free. This procedure is called as allograft osteochondral transplantation and mostly suitable for the larger defects [35].

Autologous chondrocyte implantation (ACI) was first introduced by Brittberg *et al.* in 1994 [36]. There are some disadvantages, such as this method forms more like fibrocartilage than the normal characteristics of hyaline cartilage and it consists of two operations. First, small piece of articular cartilage is harvested arthroscopically from a non-weight bearing area of the joint. This biopsy is sent to a laboratory to isolate chondrocytes. When the cells are expanded in number, they are used in the second operation which is an open surgery. A piece of periosteal patch is cut from a healthy part and sewn over the defect, then amplified chondrocytes are injected underneath this patch [37] (Figure 1.6 d).

Matrix-induced autologous chondrocyte implantation (MACI) is a fundamental example of tissue engineering and short-term results are encouraging for further investigations [38]. For MACI, apart of ACI, amplified chondrocytes are seeded onto a matrix such as type I/III porcine collagen membrane and implanted into the defect lesion [39] (Figure 1.6 e).

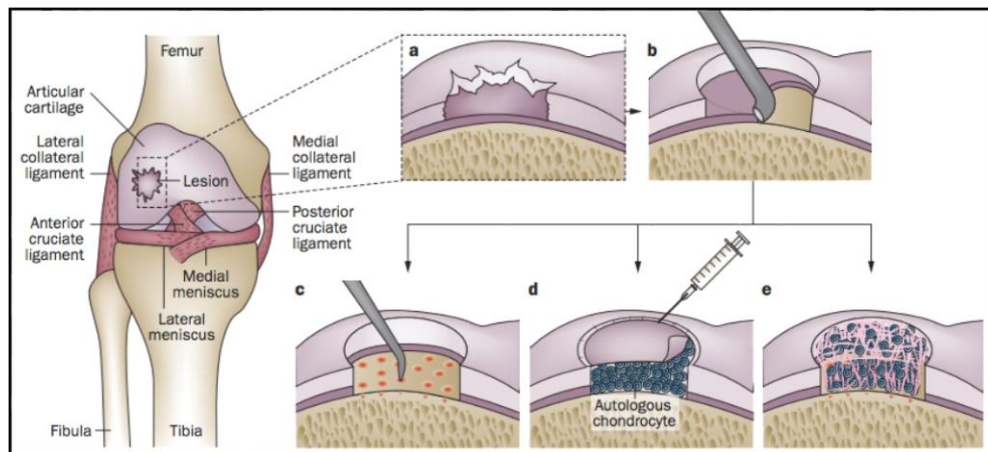


Figure 1.6. Schematic illustration of the therapeutic techniques used in cartilage repair; (a) Chondral lesion, (b) Arthroscopic debridement application for cleaning the lesion, (c) Microfracture application to stimulate subchondral bone, (d) ACI application; lesion filled with chondrocytes, (e) MACI application; chondrocytes seeded on a 3D matrix and then secured inside lesion [40]

For severely damaged joint or advanced osteoarthritis, articular cartilage can not be recovered by any of the treatments above discussed. In these cases, total or partial joint replacements are performed to decrease pain and restore joint's normal function [41]. In joint replacement surgeries, the damaged osteochondral tissue is totally or partially removed and an artificial implant (prosthetic) is replaced in the damaged joint. However, there are some problems due to the complications including infection, implant loosening or wear and tear [42]. Beside that implants are not recommended for young and active patients [43].

1.5 CARTILAGE TISSUE ENGINEERING

Tissue engineering is a promising approach for regeneration of the damaged or no longer functional tissues by improving the function in the maximum efficiency [44].

Engineering cartilage tissue is a complex procedure that involves the use of biodegradable scaffolds that are seeded with appropriate cells and grown in an environment including stimulating factors (Figure 1.7) [2].

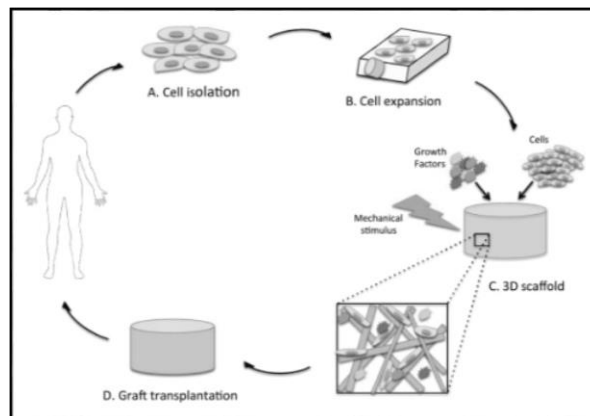


Figure 1.7. Schematic illustration of tissue engineering concept that involves seeding *in vitro* expanded cells within 3D scaffolds using suitable bioactive factors

1.5.1 Cell Sources

For selecting the optimal source of cells, two important points should be considered: performance of the cells and accessibility. Autogenic, allogeneic and xenogeneic (from an animal) chondrocytes are mostly used in articular cartilage repair and regeneration because they are the native cells, responsible for the production and maintenance of the cartilage tissue. However, there are some limitations [45]. Both allogeneic and xenogeneic chondrocytes have the risk of disease transmission and immune rejection [46]. For large-scale defects, the autologous chondrocyte number is insufficient. Cell expansion is required but those cells tend to lose their phenotype (dedifferentiate towards fibroblastic cells) with a decreased capacity to secrete extracellular matrix [47]. Autologous chondrocyte harvesting and injection progress in two invasive surgeries which means pain and risk. Because of these limitations, alternative cell sources are necessary.

Stem cells are important alternative cell sources for cartilage tissue engineering because they can be isolated from the patient's own body. Stem cells can be classified into four types: totipotent, pluripotent, multipotent and unipotent stem cells (Figure 1.8). Morula cells are totipotent stem cells. They are derived from the first two divisions of the fertilized egg, and have the ability to differentiate into any tissue in human body. Embryonic stem cells (ESCs) are pluripotent stem cells and have the ability to differentiate into any cell type. However, they can not differentiate into placental cells. There are restrictive ethical

concerns regarding to their use, since they are harvested from the inner cell mass in a 5–6 day old blastocyst from pre-implantation embryo [48]. Besides that, directing and sorting the ESCs differentiation to a specific lineage is difficult. It is possible that multiple tissues can be formed from ESC-differentiation resulting in an undesirable teratoma and teratocarcinoma formation as shown in knee joints of mice after transplantation of ESCs [49].

Hematopoietic stem cells (HSCs) and mesenchymal stem cells (MSCs) are both multipotent (lineage-restricted) stem cells and called as adult stem cells. They have high proliferation rate and capacity to differentiate into closely related family of cells. For example, MSCs are able to differentiate into musculoskeletal system such as cartilage, bone, muscle cells; while hematopoietic stem cells differentiate into only blood cell types, such as red and white blood cells. Adult mesenchymal stem cells can easily be harvested from bone marrow, adipose tissue, periosteum, synovial membrane, umbilical cord and dental sources [50-52]. Adult stem cells are approved as a promising alternative cell source for use in articular cartilage repair and regeneration strategies because of their ease of isolation and retaining their multi-lineage potential during expansion [53]. However, the number and differentiation capacity of the MSCs are restricted with age, when isolated from elderly patients, almost 200-fold decrease was observed [54]. MSCs are characterized by their capacity to adhere to tissue culture plastics, their phenotypical characterization including positive and negative surface antigen markers and their *in vitro* differentiation potential into adipocytes, chondrocytes and osteoblasts [55].

Although bone marrow aspiration is painful, within MSCs, bone marrow stromal cells (BMSCs) are shown to be the most promising cell source for cartilage tissue regeneration [56]. Different studies have shown the potential of BMSC after seeding on a compatible scaffold with chondrogenic inducers, these cells undergo chondrogenesis and produce ECMs mainly composed of aggrecan, collagen type II and VI [57-59].

Unipotent stem cells have the ability to differentiate along only one lineage but have self-renewal capabilities. Among the entire stem cells, unipotent stem cells have the lowest differentiation potential [60].

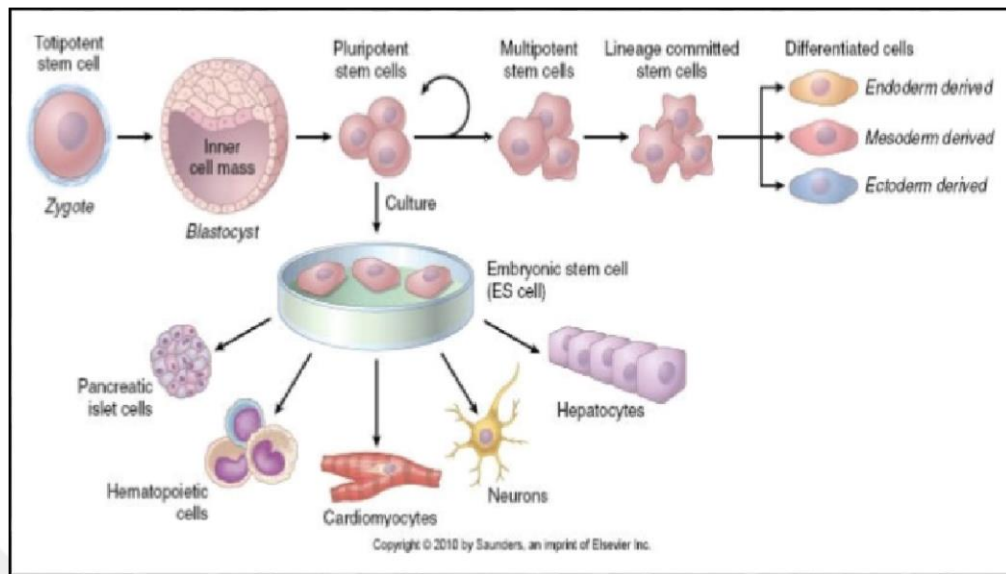


Figure 1.8. Schematic illustration of the origins and types of stem cells [61]

Induced pluripotent stem cells (iPSC) have great potential as a cell source for cartilage tissue engineering. They are somatic cells reprogrammed by the transfer of transcription factors such as OCT4, SOX2, KLF4, and c-MYC involved in pluripotency [62]. These cells exhibit the same morphology, high proliferative and differentiation capabilities as ESCs. iPSCs have the ability to differentiate into a desired cell type under specific culture conditions, but it is hard to achieve uniformly differentiated cell population. This increases the risk of tumorigenicity [63].

1.5.2 Stimulating Factors

1.5.2.1 Growth Factors

The role of bioactive factors is essential in articular cartilage development and maintenance of the cells in differentiated state. Growth factors induce specific differentiation pathways (by membrane receptors and signalling pathways or directly transcription control) to maintain chondrocyte proliferation and achieve native hyaline cartilage ECM synthesis.

Transforming growth factor beta (TGF- β), bone morphogenetic protein (BMP), insulin-like growth factor (IGF) and fibroblast growth factor (FGF) are demonstrated soluble growth factors that can be used individually or in combination to enhance chondrogenesis [64].

Members of TGF- β family are mostly investigated growth factors for the cartilage tissue engineering. They have essential roles in cellular processes including proliferation, differentiation and cell death [65]. TGF- β s (especially TGF- β 1 and β 3) were proven by Grimaud *et al.* to have capability to induce chondrogenesis of MSCs and also increase the expression of collagen type II and aggrecan [66].

BMPs are important in both chondrogenesis [67] and osteogenesis [68]. BMPs (especially BMP-4, -6, and -7) increase production of collagen type II and proteoglycan. MSCs after especially transduced by BMP-4 have acquired a chondrocyte phenotype *in vitro* [69].

IGFs are important proteins that regulate growth and differentiation. The expression of IGF-1 is positive in both developing cartilage and mature cartilage. Either with mesenchymal or chondrocyte cells, IGF-1 promotes proliferation and stimulates the expression of cartilage specific markers such as proteoglycan and collagen type II synthesis in *in vitro* and *in vivo* [70].

Fibroblast growth factors (FGFs) are involved in various cellular events, such as proliferation, differentiation, survival and motility. FGF-2 is the most widely investigated member of this family in terms of chondrogenesis. Solchaga *et al.*, (2010) demonstrated that addition of FGF-2 enhanced proliferation of MSCs and differentiated cells preserved chondrogenic potential longer [71].

It has been already demonstrated that GFs promote chondrogenic differentiation in *in vitro* studies [72, 73] while in some animal studies, detrimental effects were also observed [71] so for further clinical applications especially in human medication, biosafety should be priority.

1.5.2.2 Mechanical Stimuli

In cartilage tissue engineering, the challenge is to mimic the tissue's original structure and function. During daily activities, articular cartilage is usually exposed mechanical forces,

including direct compression, hydrostatic pressure, tensile or shear forces. Recently, importance of the mechanical stimuli application is realised in cartilage tissue engineering and shown to regulate the expression of extracellular matrix *in vivo* [74, 75]. For this reason, bioreactors have been designed both for the adjustment of environmental factors such as pH, temperature, oxygen supply and application of mechanical loading to cell-seeded 3D constructs. There are many different types of bioreactors available for cartilage tissue engineering. Most of them are custom made modified but popular ones are spinner flask bioreactors, rotating-wall vessel bioreactors and wavy-walled bioreactors.

Spinner flask bioreactor is designed to overcome diffusion limitations and enhances mass transfer into the cell seeded 3D constructs. System generates a complex flow environment by mixing the growth medium (Figure 1.9 a) [76].

In the wavy-walled bioreactor, smooth waves are applied to the vessel as shown in the Figure 1.9 b to enhance mixing at controlled shear stress levels. This system promotes chondrocyte aggregation and ECM formation [77]. Improved cartilage formation of porcine cartilage constructs was demonstrated when compared to static culture [78].

Rotating-wall vessel bioreactor is a microgravity environment simulator to stimulate the growth of tissue-engineered cartilage. There are 2 cylinders with inner and outer rotation at the same rate independently and cell seeded constructs inside the media are kept stationary between them (Figure 1.9 c) [79].

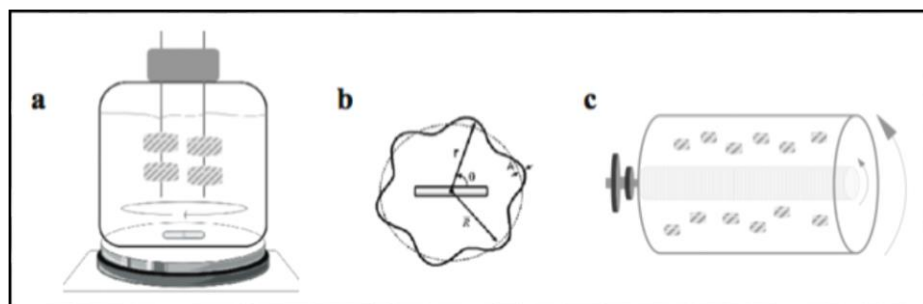


Figure 1.9. Schematic representation of the bioreactors mostly used in cartilage tissue engineering (a) Spinner flask bioreactor, (b) Wavy-walled bioreactor, (c) Rotating-wall vessel bioreactor [80]

There are some issues making the effect of mechanical stimuli on cartilage constructs complicated. For instance, multiple mechanical loading, custom designed bioreactors and

limited knowledge about *in vivo* cell behaviour in response to mechanical stimuli are the first comings. Ultimately, further research is needed for optimizing the parameters to control differentiation.

1.5.2.3 Oxygen Level

Due to the absence of vascularization in articular cartilage, chondrocytes receive required nutrient and oxygen from synovial fluid by diffusion. Nevertheless, in most studies, prepared cell seeded constructs are cultivated under atmospheric oxygen tensions (21%) that is much higher than the oxygen tension in native joints. Consequently, there are some studies tried to mimic the native joint environment. When hypoxia conditions (5%) were used, results generally showed enhancement of chondrogenesis [81, 82], but not all hypoxic effects were beneficial. Undistinguished or even suppressed cartilaginous ECM production was also shown under hypoxic oxygen levels [83].

1.5.3 Scaffolds

For tissue engineering applications, scaffolds play a critical role to mimic 3D environment of the extracellular matrix. There are important characteristics of ideal tissue engineering scaffolds: (i) be biocompatible to minimize local tissue response but maximize cell growth and integration into surrounding tissue; (ii) be biodegradable with non-toxic by-products and exhibit favourable resorption rate, which can provide structural support for the initial cell growth and then gradually degrade after new tissue formation; (iii) have suitable porosity and interconnectivity to allow cell migration and allow exchange of nutrients and wastes; (iv) guide and frame tissue formation by its architecture and possess appropriate mechanical properties to support tissue growth under native mechanical loads [84-86]. There is no ideal combination or methodology to achieve the required scaffold. Yet, there are several biomaterial options exist, the most extensively used natural and synthetic scaffolds for articular cartilage tissue engineering will be summarized below.

1.5.3.1 Synthetic Scaffolds

Synthetic polymers are popular due to easy fabrication, controllable biodegradability and useful range of mechanical properties [87, 88]. Members of poly (α -hydroxy esters) are the most widely used synthetic biodegradable polymers for cartilage tissue engineering (Figure 1.10). They are poly (glycolic acid) (PGA), poly (lactic acid) (PLA), their copolymer poly (lactic-co-glycolic acid) (PLGA), poly (ethylene glycols) (PEG) and poly (ϵ -caprolactone) (PCL). They have been extensively investigated since they were approved by the United States Food and Drug Administration (FDA) for clinical use. Hsu *et al.*, (2006) demonstrated that PLA and PGA polymers increased chondrocyte proliferation and glycosaminoglycan synthesis [89]. Chondrocytes cultured in nanofibrous PCL scaffolds maintained their chondrocyte phenotype [90] and MSCs at the same conditions were successfully differentiated into chondrocytes [91].

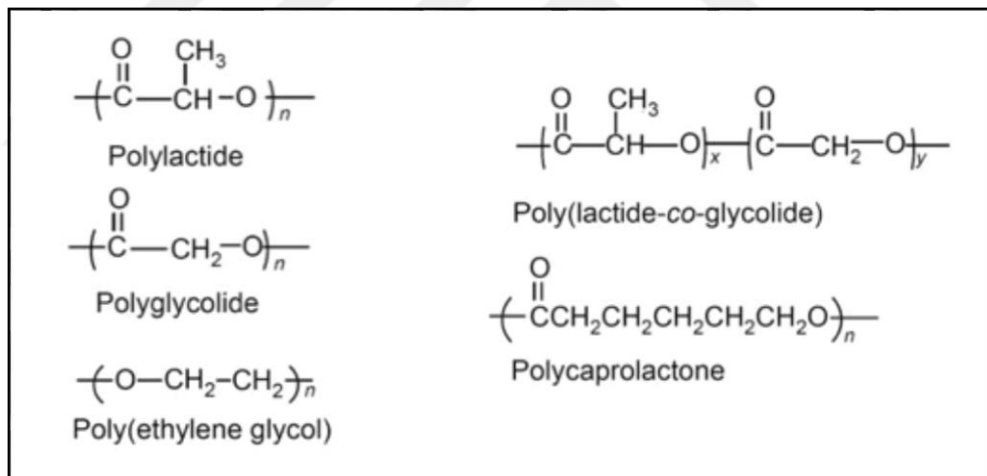


Figure 1.10. Frequently used synthetic biodegradable polymers in cartilage tissue engineering and their structures [88]

Conversely, some of the synthetic polymers have some disadvantages. They are degraded by hydrolytic reactions that result in release of high concentrations of acidic by-products. Release of small particles during degradation can cause inflammation and chondrocyte death due to the reduction in pH [92].

1.5.3.2 Natural Scaffolds

Natural polymers are popular scaffolds for cartilage repair and regeneration due to their biofunctional molecular domains that are specifically recognized by cells and tissues in the body. They are as well biodegradable and easily available. They enhance cell attachment and differentiation also they are featured as the first biomaterials used in clinical applications [93].

Although they are biocompatible, they may exhibit some problems such as variability differences from batch-to-batch and limited mechanical properties. Considerably, natural scaffolds mostly used in articular cartilage tissue engineering include carbohydrate-based materials such as hyaluronic acid, agarose, alginate, chitosan and protein-based materials such as collagen and fibrin glue.

Collagen is the major protein type in natural ECM of various tissues, including cartilage and other connective tissues and most common natural polymer type used in cartilage tissue engineering. Collagen offers low immunogenicity, good biocompatibility with tuneable mechanical properties [94]. Many studies have shown a combination of collagens (such as type I and type II collagens) with chondrocytes or stem cells facilitated cartilage tissue growth both *in vitro* and *in vivo* [95, 96].

Fibrin is a protein, involved in the clotting of blood. It is produced from the fibrinogen protein by polymerization in the presence of thrombin. Fibrin offers some advantages such as adhesive properties and producibility from patient's own blood [97]. Injectable fibrin-based gels or glues are widely used as a clinical fixative to secure other scaffolds at the repair site to culture chondrocytes [98].

Hyaluronan (Hyaluronic acid) is a natural polysaccharide and found in the ECM of soft connective tissues as non-sulphated GAG backbone. This makes HA, an ideal scaffolding material for cartilage tissue engineering. It is composed of β -1,3-N-acetyl-D-glucosamine and β -1,4-D-glucuronic acid repeating disaccharide units (Figure 1.11) [99]. Hyaluronan is the form of hyaluronic acid. The carboxyl groups on the glucuronic acid residues are become negatively charged under physiological conditions (pH and ionic strength) [100]. HA can be obtained by two main methods, by extraction from animal tissues such as umbilical cord, eyeball and rooster comb or bacterial fermentation using the strains of

Streptococci [101]. It is biocompatible and biodegradable. Grigolo *et al.* (2001) demonstrated that chondrocytes cultured on a modified hyaluronan scaffold (HYAFF 11-commercially available 3D construct) expressed both collagen type II and aggrecan, while collagen type I production was downregulated [102].

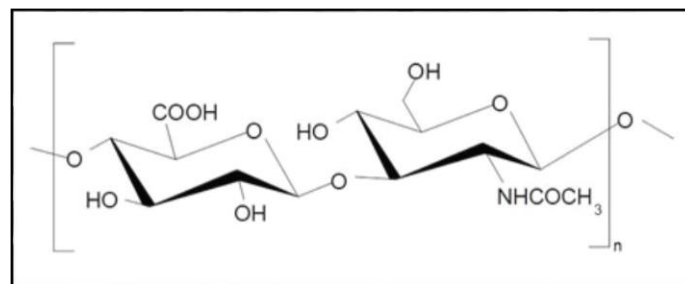


Figure 1.11. Structure of hyaluronic acid polymer [99]

Agarose and alginate are polysaccharides derived from seaweed. They have the ability to form inert hydrogel, which allows encapsulation when mixed with chondrocytes. For cartilage tissue engineering, agarose gels are used as a 3D scaffold to differentiate MSCs into chondrocytes for long term *ex vivo* culture [103]. Due to poor biodegradability (there is no enzyme degradation system for agarose in mammalian tissues), its use for *in vivo* applications is limited [104].

Alginate gels are formed in the presence of cations such as Na^+ and Ca^{2+} through ionic bonding. Due to cell encapsulation ability, chondrocytes maintain their spherical shape in the 3D alginate beads. Besides dedifferentiation of chondrocytes is prevented [105] or with MSCs, chondrogenic differentiation is promoted [106]. However, the limitation is the slow degradation rate in *in vivo* studies of alginate beads.

Chitin, the most abundant second natural biopolymer is extracted from the exoskeleton of crustaceans (crabs, lobster, shrimps etc.). Chitosan is derived from linear strand of chitin by deacetylation, removal of acetyl groups ($\text{CH}_3\text{-CO}$). This reaction forms randomly distributed β -(1-4)-linked D-glucosamine groups added to N-acetyl-D-glucosamine groups. Deacetylation makes chitosan soluble in acidic environments ($\text{pH} < 6.0$) and rendering the polymer positively charged ($-\text{NH}_3^+$) by protonation of amino groups (Figure 1.12) [107]. In order to be used in biomedical or tissue engineering applications, many derivatives of chitosan are synthesized, for example chitosan salts are the most widely used

polymers because they are water soluble at neutral pH [108]. Those chitosan salts also have the similar favourable characteristics as biocompatibility, biodegradability, low immunogenicity and anti-microbial property. It is popular in cartilage tissue engineering because of the structural similarity to GAG found in native articular cartilage ECM [109]. Lahiji *et al.*, (2000) showed that chondrocytes cultured in a chitosan hydrogel maintained their chondrocyte morphology and produced collagen type II [110].

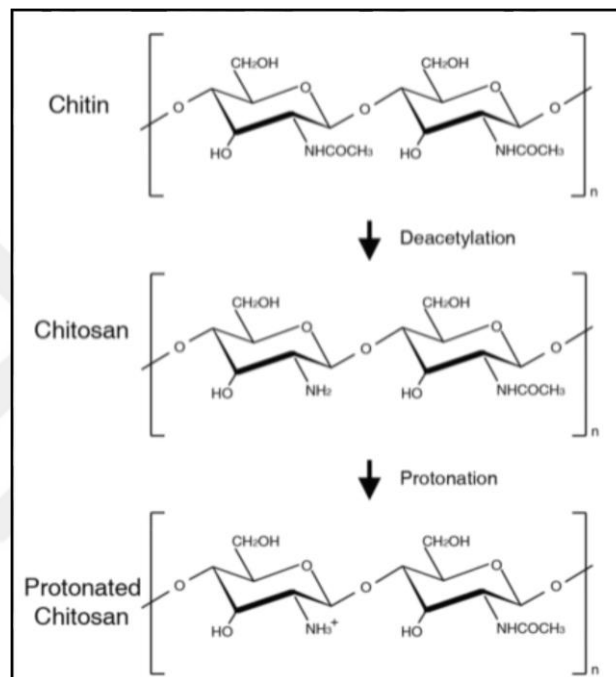


Figure 1.12. Structures of chitin, chitosan and protonated chitosan polymers [107]

Frequent challenge seen in natural polymers is having poor mechanical strength and flexibility. Crosslinking or making blend with natural or synthetic polymers can overcome this problem [111].

1.5.4 Scaffold Fabrication Techniques

Scaffold fabrication is an important challenge in tissue engineering for guiding cell growth. The current popular techniques are solvent casting/particulate leaching, freeze-drying, electrospinning, 3D printing and phase separation.

1.5.4.1 Solvent casting/particulate leaching

Solvent casting/particulate leaching is a widely-used technique which is a simple way to prepare porous scaffolds. It utilizes a solution with polymer that is dissolved in an organic solvent and particles of a known size. This solution is shaped to produce a scaffold and after evaporation, polymer with particles stay. This construct is immersed in particle solving bath to leach away the particles and forming a highly porous foam [112, 113].

Shi *et al.* produced porous scaffold using salt leaching of PLGA polymer and showed that this technique has the potential for cartilage regeneration when combined with chondrocytes [114].

1.5.4.2 Freeze drying

Freeze drying is a well-established method and can be used for preparation of a porous polymer. This method is utilized by applying two phases for sublimation. In the first phase, the prepared polymer solution is completely frozen and in the second phase solvent is removed by application of high vacuum. After sublimation of all ice crystals, highly porous dry polymer remains [115].

Xia *et al.* prepared a natural polymer mixture of chitosan-gelatin scaffolds using freeze-drying method and histology analysis showed collagen type II and sGAG production after seeding with pig-derived chondrocytes [116].

1.5.4.3 Electrospinning

Electrospinning technique uses the electric field to produce nanofibers that are similarly found in ECM [117]. Polymer solutions (natural or synthetic polymers) are placed into the syringe filter and collected from the target point. By the application of high voltage, the solvent evaporates and the fibre deposition is accelerated. Those fibres can be laid randomly or aligned in terms of the purpose [118]. There are crucial parameters that effect the morphology of the collected fibres which are applied voltage, flow rate of the polymer,

distance of the syringe to collector, humidity and temperature of the district area [119, 120].

Li *et al.* used electrospun meshes of PCL scaffolds for the cultivation of human MSCs and after 21 day of chondrogenic differentiation, results showed *in vitro* chondrogenesis was achieved by high PG matrix deposition [91].

1.5.4.4 3D Printing

For producing a better designed 3D constructs, rapid prototyping (RP) and bioprinting are new and relatively successive techniques in tissue engineering field [121]. There are 3 important steps: imaging, computer assisted design (CAD) and material or cell choice. For imaging, inoffensive clinical imaging techniques are mostly used, computed tomography (CT) or magnetic resonance imaging (MRI) is integrated to provide structural and functional information about the tissue. After this data is computerized, CAD software takes cross sectional layers and constructs a solid design. After an appropriate cell and material detection, the information is used for fabrication of desired tissue. Uptill now, fully functional organ or tissue has not been printed, but some small portions in limited applications were implemented [122].

Human chondrocyte used PEG hydrogels were bioprinted by Cui *et al.*, those scaffolds were investigated in terms of viability and neocartilage formation [123].

1.5.4.5 Phase Separation

Polyelectrolytes (PEs) are polymers that contain charged functional groups that make them named as anions or cations. Due to the ionic interaction capacity, PEs can form polyelectrolyte complexes [124]. One of the most important complexation named as coacervation.

Coacervation has been entitled into simple and complex coacervation considering the polymer number contributing to the system. In simple coacervation only one macromolecule, whereas in complex coacervation more than one macromolecule is involved [125, 126].

1.6 COMPLEX COACERVATION (PHASE SEPARATION)

Coacervation method is based on the phase separation between positively and negatively charged macromolecules (such as polymers, nucleic acids, proteins) in aqueous solutions. This separation occurs spontaneously due to electrostatic interactions and gained entropy by the release of salt ions in solution and results in the formation of a dense macro ion-rich liquid phase named as coacervate [127]. This process was first observed by Bungenberg de Jong *et al.*, [126] with natural polymers, gelatin and gum arabic. In coacervation method either a gel like fluid or a precipitate occurs depending on the parameters such as pH, ionic strength, temperature, molecular weight and concentrations of the polymers [128]. Priftis *et al.* [129] used a model system to provide useful insights and showed that complex formation was strongly affected by those parameters.

Table 1.1 lists the positively and negatively charged polymers that are mostly used in the formation of complex coacervates.

Table 1.1 Typical polymers employed in complex coacervation [129]

Polyanions	Polycations
Alginate	Chitosan
Carrageenan	Poly (diallyldimethylammonium chloride)
Carboxymethylcellulose	Poly (L-lysine)
Chondroitin sulfate	Poly (vinylamine)
Gellan	
Hyaluronic acid	
Poly (acrylic acid)	
Xanthan	

Complex coacervation method has gained much interest in the microencapsulation field as drugs in pharmaceutical industry [130], as flavours in food industry [131], as growth factors [132] and viable cells [133] in biotechnology. Coacervates are concurrently used for industrial applications such as encapsulation of paints and liquid inks [134].

Several groups showed that microencapsulation by coacervation of alginate with poly-L-lysine (PLL) system was useful for the entrapment of Langerhans islets [135, 136] but PLL had low mechanical stability so cell encapsulated multilayered alginate/silicate system was

used as an alternative and successfully transplanted into mice. It was found more stable than alginate/poly-L-lysine system [133]. Further attractive feature was shown with the coacervation of chitosan and alginate polymers. In this study cells were micro-encapsulated and system maintained cell viability and phenotype [137].

In another promising coacervation system, encapsulation found to enhance the effectiveness of growth factors by enabling a sustained release profile and on-site delivery. Epidermal growth factor (EGF), fibroblast growth factor-2 (FGF-2) and stromal cell-derived factor (SDF-1 α) were all encapsulated in coacervates for several purposes such as wound healing [138, 139], vascular graft remodeling [140] and angiogenesis [132].

More recently, promising tissue engineering applications of the coacervates were reported. For tissue engineering purposes, coacervates could be used as a complete scaffold or coating material on the grafted scaffolds. Presented coacervates enhanced viability [141], *in vitro* proliferation [142] and differentiation potential [143] of the included cell types. Furthermore, high viscosity of the coacervates made them desirable tissue adhesives to be used in bone fractures [144-147].

A proper understanding and control of the environmental factors (ionic strength, pH or temperature) in complex coacervation had enabled tissue engineers to design stimuli-responsive biomaterials in order to be used at desired places. For instance, changing the pH and ionic strength modulated the attachment capacity of the coacervates prepared using poly (allylamine hydrochloride) with pyrophosphate or tripolyphosphate [148]. In another system, temperature changes manipulated the coacervation of 5-amino-1-pentanol and trimethylolpropane ethoxylate triacrylate [149], similarly phase separation of poly (allylamine-co-allylurea) was also altered by temperature increase [150].

There are some other electrostatically driven phase separations such as flocculation, precipitation, ionic hydrogel and layer by layer assembly which are different than coacervation. Important aspects of those processes were clarified by Kayitmazer *et al.* [151].

1.6.1 Precipitate

Precipitation corresponds to solid–liquid phase separation instead of liquid-liquid phase separation as observed in coacervation and the dense phase has crystalline features. It is comparatively easy to differentiate coacervates from precipitates. Precipitates can be identified as pieces of white, deformable (miscible) material. Instead of liquid droplets, solid particles can be observed by optical microscopy. For more obvious distinguishing between precipitation and coacervation, centrifugation can be applied for visual observation. Using high charge density polymers, high molecular weight polymers and low salt concentrations; phase separation becomes liquid-solid (precipitate) because of having higher complementarity and stronger interactions between polymers [152].

1.6.2 Flocculate

Flocculates are also formed through solid–liquid phase separation when the solid phase formed is less dense than that of precipitation and first suspended coagulants are formed and those small complexes become flocs or flakes staying in the solution before sedimentation. It is not so easy to differentiate coacervates from flocculates, but flocs seem as densified coacervates, more like solidified gels [153].

1.6.3 Hydrogel

Hydrogels are 3D polymeric structures that can absorb large amounts of water and still exhibit solid-like mechanical properties due to the presence of a crosslinked network structure [154]. In coacervate formation, phase separation exists from physical interactions, not due to the presence of crosslinkers [155]. Ionic hydrogels made from polyelectrolyte networks, require more than 5% weight polymers. Coacervation is suppressed in concentrated solutions, in these concentrated mixtures, the oppositely charged macromolecules are in close proximity with each other and the molecular chains may overlap to become a gel. Coacervation effects occur in low concentrations as low as 0.1% weight polymers.

1.6.4 Layer by Layer Assembly

Layer by Layer assembly (LbL) uses self-assembling properties of charged molecules like polyelectrolytes (PE). This technique is based on the electrostatic attraction between oppositely charged molecules, which results in stable multilayer structures [156]. For this purpose, an anionic (or cationic) polyelectrolyte is adsorbed onto a colloidal particle for a period of time and then rinsed to remove excess amount of the polymer. When a cationic (or anionic) charged polyelectrolyte is introduced, they adhere to negatively (or positively) charge the surface of previous PE and this procedure can be cycled for hundred times until wanted multilayer thickness is achieved. In LbL assembly, only one ionic charge is free and its opposite charge is fixed on a system but in coacervate both of the ionic charges are free and tend to become closer to each other (no adherence as in LbL).

The main challenge for engineering articular cartilage tissue is the massive transition of chondrocytes into fibroblastic cells which form fibrocartilage instead of hyaline cartilage during *in vitro* culture process [157]. Eventually, it is possible to encapsulate MSCs or chondrocytes without dedifferentiation.

For cartilage tissue engineering, polysaccharides as chitosan (CHI) and hyaluronic acid (HA) are the most sophisticated natural polymers due to their biocompatibility, biodegradability and structural similarity to glycosaminoglycan (GAG) found in cartilage. Synthesis of complex coacervate is a novel approach in cartilage tissue engineering by using electrostatic interaction between the cationic chitosan and anionic hyaluronic acid with the capability of entrapping cells (Figure 1.13).

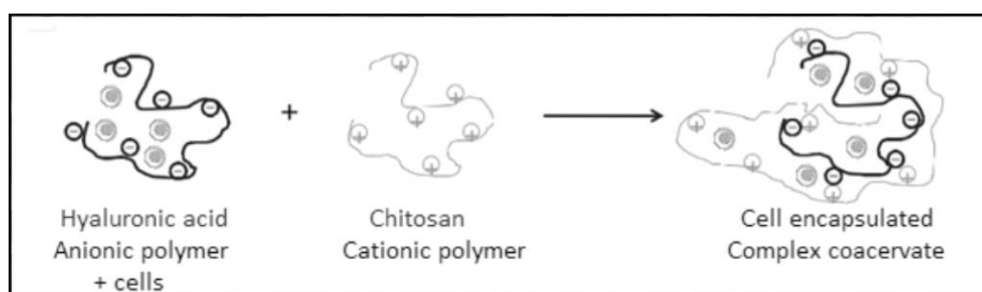


Figure 1.13. Schematic representation of cell encapsulation by complex coacervation between a polyanion and a polycation [158]

1.7 AIM OF THE STUDY

Aim of this study was to develop porous, biodegradable scaffolds using complex coacervation technique, investigate the stability and characterize the prepared coacervates. The 3D coacervates were prepared using weak polyelectrolytes chitosan glutamate salt (CHI-G), chitosan chloride salt (CHI-Cl) and sodium hyaluronate (HA) dissolved in NaCl as monovalent and CaCl_2 as divalent salts. MSC encapsulation was applied after characterization for evaluating the potentials of the coacervates for cartilage tissue engineering purposes.



2. MATERIALS

2.1 CHEMICALS AND REAGENTS

- Dulbecco's Phosphate Buffer Saline (DPBS) (Gibco, Germany)
- Minimum Essential Medium (MEM) Alpha (Gibco, Germany)
- High Glucose Dulbecco's Modified Eagle Medium (Gibco, Germany)
- Penicillin-Streptomycin (Gibco, Germany)
- Fetal Bovine Serum (FBS) (Gibco, Germany)
- Trypsin-EDTA (Sigma-Aldrich Corporation, Germany)
- Recombinant Human Transforming Growth Factor (rhTGF β 1) (R&D Systems, USA)
- PROTASAN Ultrapure Chitosan CL 213, 83% deacetylation degree (DD) (FMC Biopolymer, Norway)
- PROTASAN Ultrapure Chitosan G 213, 83% deacetylation degree (DD) (FMC Biopolymer, Norway)
- Sodium Hyaluronate Pharma Grade 150 (FMC Biopolymer, Norway)
- Calcium Chloride (Merck, USA)
- Sodium Chloride (Sigma-Aldrich Corporation, Germany)
- CellTracker CM-DiI (Invitrogen, Thermo Scientific, USA)
- Hydrochloric acid (HCl) (Sigma-Aldrich Corporation, Germany)
- Sodium hydroxide (NaOH) (Sigma-Aldrich Corporation, Germany)
- Formaldehyde solution 37% by weight (Riedel-de Haën, Germany)
- Alexa Fluor[®] 546 Phalloidin (Invitrogen, Thermo Scientific, USA)
- 4',6-Diamino-2-phenylindole (DAPI) (Sigma-Aldrich Corporation, Germany)
- ProLong[®] Gold Antifade Mountant (Invitrogen, Thermo Scientific, USA)
- Sodium azide (Sigma-Aldrich Corporation, Germany)
- ITS Pre-mix tissue culture supplement (Corning, USA)
- TritonX-100 (Invitrogen, Thermo Scientific, USA)
- Cacodylic acid sodium salt trihydrate (AppliChem, USA)

- Double Distilled Water (Milli-Q) (SARTORIUS AG, Germany)
- Live/Dead[®] Viability/Cytotoxicity Kit *for mammalian cells* (Invitrogen, Thermo Scientific, USA)
 - Ethidium homodimer1
 - Calcein-AM
- L-Ascorbic acid 2-phosphate (Santa Cruz Biotechnology, Inc., USA)
- L-Proline (Sigma-Aldrich Corporation, Germany)
- Sodium Pyruvate (Sigma-Aldrich Corporation, Germany)
- Gluteraldehyde 25% Aqueous Solution (Sigma-Aldrich Corporation, Germany)
- Fresh *E.coli* (ATCC 10536) and *S.aureus* (ATCC 6538) cultures
- Oxoid[™], Ofloxacin (OFX) antimicrobial susceptibility disks (Invitrogen, Thermo Scientific, USA)
- Nucleospin RNA mini kit (Macherey-Nagel, Germany)
- β -mercaptoethanol (Sigma-Aldrich Corporation, Germany)
- Sensiscript Reverse Transcription Kit (Qiagen, Germany)
- RNase inhibitor (Thermo Scientific, USA)
- Oligo dT primer (Thermo Scientific, USA)
- Maxima SYBR Green/ROX qPCR master mix (2X) (Thermo Scientific, USA)

2.2 ANTIBODIES

- FITC anti-rat CD 90 (BD Pharmingen, USA)
- FITC anti-rat CD 11a (BD Pharmingen, USA)
- PE anti-rat CD 31 (BD Pharmingen, USA)
- PE-Cy anti-rat CD 45 (BD Pharmingen, USA)
- FITC anti-rat CD 29 (BD Pharmingen, USA)
- COL2A1 Antibody (M2139) mouse monoclonal IgG2b (Santa Cruz Biotechnology, Inc., USA)
- Aggrecan Antibody (H-300) rabbit polyclonal IgG (Santa Cruz Biotechnology, Inc., USA)

- Goat anti-Mouse IgG (H+L) Secondary Antibody, Alexa Fluor® 488 conjugate (Invitrogen, Thermo Scientific, USA)
- Goat anti-Rabbit IgG (H+L) Secondary Antibody, Alexa Fluor® 647 conjugate (Invitrogen, Thermo Scientific, USA)

2.3 INSTRUMENTS

- Inverted microscopy (Nikon Eclipse TC 100, USA)
- Laminar flow cabinet (ESCO Labculture Class II Biohazard Safety Cabinet 2A, Singapore)
- CO₂ incubator (Thermo Scientific, USA)
- Centrifuge (Hettich micro 22R and Sigma 2-5 centrifuge, Germany)
- Vortex (Stuart, UK)
- pH meter (Hanna, Germany)
- ELISA plate reader (Bio-Tek EL x 800, USA)
- Lyophilizator (Thermo Savant)
- EVO Scanning electron microscope device (Carl Zeiss)
- Fluorescent microscope (Vert.A1 ZEISS)
- Confocal microscope (ZEISS)
- FACSCalibur flow cytometer (BD Biosciences, USA)
- Nanodrop spectrophotometer (Thermo Scientific, USA)
- CFX96 Touch™ sequence detection system (Bio-Rad, USA)

3. METHODS

3.1 PREPARATION OF POLYMER SOLUTIONS AND COACERVATES

3.1.1 Polymer Concentration

The critical overlap concentrations (c^*) for chitosan and hyaluronic acid polymers were adopted from the literature as given in Table 3.1. Towards those informations, for chitosan polymers (having 83% DD) with 260 kDa and 345.5 kDa molecular weight (CHI-CI and CHI-G, respectively), 0.9 mg/mL or 0.09 % (w/v) and for hyaluronic acid with 1,700 kDa molecular weight (Mw), 0.7 mg/mL or 0.07 % (w/v) concentrations were used.

Table 3.1 Critical overlap concentrations of CHI and HA polymers [3, 159, 160]

Polymer Name	Molecular weight (kDa)	c^* values (mg/mL)
Chitosan	4-5	179.86-271.00
	22-30	38.40-55.77
	61-79	14.72-20.55
	280-300	4.27-6.11
	850	1
Hyaluronic Acid	660	1.4
	2,200	0.7

3.1.2 pH of Solution

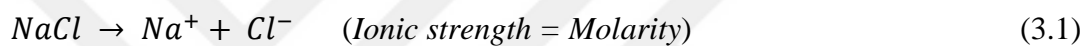
Maximum growth of mammalian cells occurs at pH 7.4 which is the standard cell culturing pH. Coacervation is favored at pH values lying between the pKa values of the used polymers (HA and CHI) due to the increasing numbers of charged species (COO^- and NH_3^+). HA and CHI are both fully soluble between pH = 2.0 and 6.7. Therefore, the pH of the polymer solutions was decided as 6.25 and adjusted before introducing complexation using 1 M HCl or NaOH.

3.1.3 Ionic Strength of Solution

Yan *et al.*, (2009) showed the ionic strength of growth medium (Dulbecco's Modified Eagles Medium (DMEM) containing 10% fetal bovine serum (FBS) and 1% penicillin/streptomycin) as 189 mM [161]. Therefore, complex formation was observed by coacervation with NaCl or CaCl₂ salt solutions with an ionic strength of 50 mM, 150 mM and 300 mM.

Ionic strength (*I*) calculation formula [162]:

$$I = \frac{1}{2} \sum_{i=1}^n c_i z_i^2$$



3.1.3.1 Preparation of NaCl and CaCl₂ Salt Solutions

The amount of salt required for a given ionic strength (Table 3.2) was measured into ultrapure water (Milli-Q water) from NaCl or CaCl₂ stock. Prepared salt solutions were mixed on a magnetic stirrer at RT until completely dissolved.

Table 3.2 Preparation of salt solutions

Molarity (mM)	Ionic Strength (mM)	Mass (gram)	Salt
50	50	0.292	NaCl
150	150	0.876	NaCl
300	300	1.752	NaCl
16.67	50	0.184	CaCl ₂
50	150	0.554	CaCl ₂
100	300	1.109	CaCl ₂

3.1.4 Coacervate Preparation

CHI (0.09% w/v) and HA (0.07% w/v) were dissolved separately in NaCl or CaCl₂ solutions to have the required ionic strength (*I*). The complete dissolution of both polymers was achieved by constant stirring overnight via magnetic stirrer. The pH of each polymer solution was adjusted to c.a 6.25 and each solution was sterilized by filtering through a 0.45 µm pore size filter in a laminar flow hood. HA solution was added drop by drop into CHI solution at different mixing ratios (charge ratios [-]/[+]) while keeping the mixture stirred. Those coacervate suspensions were used for the examination of droplet formation, turbidity, dynamic light scattering (DLS) and zeta potential.

For further *in vitro* experiments, charge ratio of [-]/[+] = 0.31 and 0.48 for HA/CHI-Cl and HA/CHI-G, respectively (0.4:1 v/v HA:CHI mixing ratio (see results part for the selection of this ratio) was applied. The prepared coacervate suspension was centrifuged at 4,000 rpm for 23 minutes to facilitate phase separation into the coacervate and dilute (supernatant) phases. After centrifugation, the supernatant was carefully decanted without disturbing the coacervate layer.

3.1.4.1 Charge Calculation and Volume to Charge Conversion

Charge ratio was calculated using the HA and CHI polymer characteristics denoted at pH 6.25. It is essential to analyze the phases of the HA/CHI mixtures in terms of charge ratio of negative to positive groups ([-]/[+]) so that comparable results could be achieved with the literature. Moreover, charge ratio differs through chitosan chloride and glutamate salt.

Charge ratio calculated from the Tables 3.3 and 3.4:

Table 3.3 Polymer information for the calculation of charge ratio

	Polymer Conc. (mg/ml)	Volume (ml)	Degree of ionization	Polymer repeat unit Mw (g/mol)	Charge group (%)
HA	0.7	(variable)	0.99	401.3	1
CHI-Cl	0.9	(constant)	0.52	198.566	0.83
CHI-G	0.9	(constant)	0.52	308.30	0.83

Table 3.4 Volume to charge ratio conversion

		For CHI-Cl	For CHI-G
CHI Volume	HA Volume	Charge Ratio [-]/[+]	Charge Ratio [-]/[+]
1	0.1	0.077	0.119
1	0.2	0.153	0.238
1	0.3	0.230	0.356
1	0.4	0.306	0.475
1	0.5	0.383	0.594
1	0.6	0.459	0.713
1	0.7	0.536	0.832
1	0.8	0.612	0.950
1	0.9	0.689	1.069
1	1	0.765	1.188

3.2 CHARACTERIZATION OF THE COACERVATE SUSPENSIONS

3.2.1 Optical Microscopy

Optical microscopy was used to confirm the presence of liquid coacervate droplets. The coacervate suspensions were placed on glass slides to observe the droplets. Optical micrographs of each type of polyelectrolyte complexes such as precipitates or coacervates formed were represented with a final ionic strength of 50 mM, 150 mM and 300 mM NaCl or CaCl₂ salt solutions. Moreover, different mixing ratios (charge ratio of [-]/[+]) of HA solution into CHI solutions (v/v) were examined in detail for ionic strength of 300 mM NaCl or CaCl₂ salt solutions.

3.2.2 Turbidity

Effect of mixing ratio (charge ratio of [-]/[+]) on the extent of HA/CHI coacervation was investigated by turbidity measurement. Different mixing ratios of HA solution into CHI solution (v/v) was measured for $I = 300$ mM and pH = 6.25. Turbidity was measured using a plate reader equipped with a UV spectrophotometer (BioTek Instruments, USA) at a

wavelength of 630 nm at room temperature. None of the polymers absorb light at this wavelength. Turbidity was measured in absorption units (a.u.) and applied into a 96-well plate. All samples were referenced against the respective salt solution. All the experiments were run in triplicate.

3.2.3 Dynamic Light Scattering

Dynamic light scattering (DLS) experiments were performed on a Zetasizer Nano ZS (Malvern Instruments, UK), which records data at a scattering angle of 173° with a 633 nm He/Ne laser. All experiments were carried out at 25°C . Size for the coacervate suspension was reported as a Z-average hydrodynamic diameter; i.e. intensity weighted mean hydrodynamic radius (using Stokes-Einstein equation). Size values were reported as average and standard deviation of three repeated measurements. Cumulants analysis (“general purposes mode”) was employed for fitting of the correlation curve. Intensity was recorded as derived count rate, which was the 0.3 % of the measured mean count rate.

3.2.4 Zeta Potential

The zeta potential (ζ) measurements were performed on a Zetasizer Nano ZS (Malvern Instruments, UK). Coacervate suspensions were loaded into folded capillary cells (Malvern Instruments, UK). Charge values were converted to zeta potential (using Smoluchowski equation) and reported as average and standard deviation of three repeated measurements.

3.2.5 Visual Inspection

For visual inspection, coacervate suspensions were centrifuged to accelerate the phase separation for 23 minutes at 4,000 rpm to coalesce the dispersed complexes to a single phase at the bottom of the falcon tubes.

3.3 CHARACTERIZATION OF THE COACERVATE SCAFFOLDS

3.3.1 Environmental Scanning Electron Microscopy (ESEM)

After centrifugation of the HA/CHI-Cl and HA/CHI-G, charge ratio of [-]/[+] = 0.31 and 0.48, respectively, the phase formation was observed at the bottom of the falcon tubes. HA/CHI coacervates were collected from the bottom and used as scaffolds. These coacervates were washed with sodium cacodylate buffer (pH 7.4), incubated with 2.5 % glutaraldehyde solution at room temperature (RT) for 1.5 hours and then kept at 4 °C until observation with environmental scanning electron microscopy (ZEISS EVO LS 15, Germany). ESEM was applied at a voltage of 5 kV and different magnifications. The mean pore size was estimated using ImageJ software.

3.3.2 Dry Weight Analysis of Coacervates

After centrifugation of the coacervate suspensions, the collected HA/CHI coacervates were weighed to determine the wet weight. Then the samples were completely dried at 60 °C (overnight) in the oven and dry weight was recorded to determine the water content of the coacervates. All experiments were conducted in triplicate.

The degree of water content (% WC) of coacervates was calculated according to the following equation:

$$\% WC = \left[\frac{(W_w - W_d)}{W_w} \right] \times 100 \quad (3.2)$$

where W_w is the wet weight of coacervate and W_d is the weight of the coacervate after dried in the oven.

3.3.3 Degradation Behavior of the Coacervates

Coacervate degradation rates were evaluated by measuring the mass loss for up to 16 weeks. Triplicate samples of HA/CHI-Cl and HA/CHI-G coacervates were weighed and then immersed individually in sealed falcon tubes that were containing PBS solution with

0.09 % (w/v) of sodium azide that was added to prevent bacterial growth. The coacervates were incubated at 37 °C, 60 rpm shaking water bath for 1, 7, 14, 30, 60 and 120 days without refreshing media. At the end of predetermined incubation intervals, scaffolds were removed from the buffer, rinsed in deionized water to remove salts and weighed. The buffer left inside the falcon tube was collected for the pH measurements.

The percentage weight loss (% WL) of coacervates was calculated according to the following equation:

$$\% WL = 100 - \left[\frac{(W_i - W_f)}{W_i} \right] \times 100 \quad (3.3)$$

where W_i is the initial weight of scaffold and W_f is the weight of the scaffold after incubation in the PBS-sodium azide solution.

3.3.4 Antimicrobial Activity of the Coacervates

The antibacterial activity of prepared HA/CHI coacervates were examined by agar disk diffusion assay [163]. A sterile cotton swab was used for spreading the *Staphylococcus aureus* (ATCC 6538) and *Esheria coli* (ATCC 10536) cultures by surface method. After 5 minutes, prepared coacervates (~1 cm in diameter) were placed triplicate on the inoculated agar surface. The plates were incubated at 37 °C overnight and examined for the zone of inhibition. Positive (Ofloxacin - OFX) and negative (disk - only wetted by distilled water) controls were used. G indicates the coacervates prepared by chitosan glutamate (HA/CHI-G) in NaCl, Cl indicates the coacervates prepared by chitosan chloride (HA/CHI-Cl) in NaCl, and Cl (CaCl₂) indicates the coacervates prepared by chitosan chloride (HA/CHI-Cl) in CaCl₂ salt solutions. All experiments were performed aseptically (Table 3.5).

Table 3.5 Samples placed on the inoculated agar surfaces

<i>E. coli</i>	Plate 1	(+) control	Cl	Cl	G
	Plate 2	(-) control	Cl	G	G
	Plate 3	(+) control	Cl (CaCl ₂)	Cl (CaCl ₂)	Cl (CaCl ₂)
<i>S. aureus</i>	Plate 4	(+) control	G	G	Cl
	Plate 5	(-) control	Cl	G	Cl
	Plate 6	(-) control	Cl (CaCl ₂)	Cl (CaCl ₂)	Cl (CaCl ₂)

3.4 ISOLATION AND CULTURE OF MESENCHYMAL STEM CELLS

Rat bone-marrow derived mesenchymal stem cells (rBMSCs) were isolated from six-week-old male Sprague-Dawley rats. They were sacrificed, femurs and tibias were carefully cleaned from skin and cut at the ankle bone. The muscle and connective tissue were removed by scraping and clean bones were put in harvest medium (Dulbecco's Modified Eagle Medium (DMEM) high glucose, (4.5 g/L) including 1,000 unit/mL penicillin/streptomycin). Ends of the tibia and femur were cut. Sterile needle was inserted and bone marrow was flushed with standard growth medium (SGM) (α -MEM – Glutamax supplemented with 10 % (v/v) Fetal Bovine Serum (FBS) and 100 unit/mL of penicillin/streptomycin) and collected in a 50-mL falcon tube. The cell suspension was centrifuged at 1,800 rpm for 5 min. The pellet was dissolved in SGM and incubated in an incubator at 37 °C, in a humid atmosphere containing 5 % CO₂. Non-adherent cells were removed by washing with PBS (pH = 7.4) and adherent cells were further cultured in SGM. The media were changed three times a week. The cells were transferred to a new culture flask when they reached confluency.

Previously isolated and characterized rBMSCs had been cryopreserved for later use. For that purpose, rBMSCs were washed with PBS twice and detached from the culture flasks by a 0.25 % trypsin-EDTA solution. Cell suspension was centrifuged at 1,800 rpm for 5 min. Cells were resuspended at 1.0×10^6 cells/mL in freezing medium (FBS:DMSO 20:1 v/v) and they were aliquoted into cryogenic vials. Vials were placed in an isopropanol freezing container and transferred to -80 °C.

For thawing the cells, cryogenic vials were removed from -80 °C and thawed rapidly. Cell suspension was transferred to 15 ml falcon tube and 10 ml of medium was added drop by drop. Diluted cell suspension was centrifuged at 1,800 rpm for 5 min. Supernatant was discarded and cells were resuspended in prewarmed, fresh standard growth medium (α -MEM – Glutamax supplemented with 10 % (v/v) FBS and 100 unit/mL of penicillin/streptomycin). Cells were incubated in an incubator at 37 °C, in a humid atmosphere containing 5 % CO₂. The media were changed three times a week.

3.4.1 Characterization of MSCs

MSCs were characterized according to the advice of the International Society for Cellular Therapy (ISCT). Characterization was applied using cell surface markers by flow cytometry analysis. The cells were stained with different fluorescently labeled monoclonal antibodies (BD bioscience). In brief, the cells were detached from the culture flasks by a 0.25 % trypsin-EDTA solution and then washed with PBS. For each tube, 3×10^5 cells (in 100 μ L PBS) were mixed with the fluorescently labeled antibody (FITC anti-rat CD 90, PE anti-rat CD 31, PE-Cy anti-rat CD 45, FITC anti-rat CD 29, FITC anti-rat CD11a) and incubated in dark, at room temperature (RT) for 45 minutes. After washing to remove the excess antibodies, the cells were analyzed by a FACSCalibur flow cytometer.

3.4.2 CM-Dil Staining of MSCs

Stock solution of the CM-Dil dye was prepared in dimethyl sulfoxide (DMSO) at a concentration of 1 mg/ml. Cells were detached from the culture flasks by a 0.25 % trypsin-EDTA solution and then labelled with the working solution of CM-Dil fluorescent dye (1 μ M concentration for 10^6 cells).

3.5 COACERVATE SCAFFOLDS WITH CELLS

3.5.1 Cell Seeding

Coacervates were prepared exactly as previously described in part 3.1.4 (referred as blank). Obtained coacervates (as pellets) were kept inside the falcon tubes for direct cell seeding on the surface of the coacervates.

After the optimal cell density was reached (100,000 cells/coacervate), cells were resuspended in fresh standart growth medium by pipeting well to become ready for seeding. Cell suspensions were added onto the surface of prepared scaffolds and falcon tubes were incubated at 37 °C, 5 % CO₂ for overnight. Coacervates were transferred to 24 well plate and incubated at incubator throughout the experiment.

For controlling the successful seeding of the cells on semi-opaque coacervates, CM-DiI labeled cells were seeded and imaged using fluorescent microscopy at the third day of incubation.

3.5.2 Cell Encapsulation

Polymer solutions were prepared as previously described in part 3.1.4. After the optimal cell density was reached (500,000 cells/coacervate), cells were resuspended in HA solutions by pipeting well to become ready for encapsulation. HA+cell suspension was added drop by drop on chitosan solutions individually. Mixing ratio of HA:CHI (0.4:1 v/v) was applied according to previously chosen ratio from characterization data (see result part). Coacervate suspensions were centrifugated at 4,000 rpm for 23 minutes. Obtained coacervates (as pellets) were carefully transferred to 24-well plate containing 500 μ L standard growth medium and incubated at 37 °C, 5% CO₂ throughout the experiment.

For controlling the successful encapsulation of the cells inside semi-opaque coacervates, CM-DiI labeled cells were encapsulated and imaged using fluorescent microscopy at the third day of incubation.

3.5.3 Scanning Electron Microscopy (SEM)

The morphology of freeze-dried coacervates and interactions between cells and coacervate scaffolds were observed by SEM analysis. Empty and cell encapsulated coacervates were washed with sodium cacodylate buffer (pH 7.4). Fixation was achieved by adding 2.5 % glutaraldehyde solution, then samples were incubated at room temperature for 1.5 hours. Then, samples were washed with sodium cacodylate buffer and frozen at -80 °C. After freezing, samples were left for lyophilization overnight and kept at RT until observation. All samples were coated with 10 nm gold and SEM was applied at 10 kV.

3.5.4 LIVE/DEAD[®] Cell Viability Assay

Live dead assay reagent was prepared by addition of 4 μ M ethidium homodimer-1 (EthD-1) and 2 μ M Calcein-AM in PBS solution. The coacervate samples were washed with PBS

before incubation with live dead assay reagent. After incubation at room temperature for 30-45 minutes at dark, reagents were removed and washed with PBS. Images were taken by fluorescent microscope after 1, 7, 14 and 21 days of incubation. To assess cell viability, 3 different zones were processed for calculating the number of green and red spots using the ImageJ software. The ratio (cell viability percentage) of the number of live cells to the number of total cells was calculated.

3.5.5 Fluorescent Staining

For analyzing the morphology of the encapsulated or seeded cells, actin filament and nucleus staining was applied. For actin filaments, Alexa Fluor® 546 Phalloidin which is a F-actin probe conjugated to red-fluorescent dye (ex/em: 556/573 nm), for nucleus, DAPI (4',6-diamidino-2-phenylindole) which is a blue fluorescent dye (ex/em: 358/461 nm) that binds to A-T rich regions in DNA were used.

Coacervate samples were washed with PBS and fixed in 3.7 % formaldehyde solution for 30 minutes at room temperature. Samples were washed and permeabilized in 0.1 % Triton X-100 for 5 minutes at RT. Samples were washed and incubated in 3 % FBS. After washing the samples, they were incubated in phalloidin solution (1:100 dilution) at RT for 1 hour at dark. Samples were washed to remove unbound phalloidin. Nucleus staining solution DAPI (1:1000 dilution) was added on the samples and incubated at RT for 15 minutes at dark. Samples were washed, then transferred to prepared slides. ProLong® Gold Antifade mountant was added on the samples and stored at 4 °C until examination. Images were taken by confocal microscope after 3 and 21 days of incubation.

3.5.6 *In Vitro* Chondrogenic Differentiation

Encapsulated bone marrow stem cells inside coacervates were induced to differentiate into chondrocytes by providing the proper soluble and environmental conditions.

For differentiation purposes, cell encapsulated coacervates were placed in chondrogenic differentiation medium (CDM) at the 3rd day of incubation. CDM was constituted from DMEM high glucose, (4.5 g/L) supplemented with 100 unit/mL of penicillin/streptomycin,

1 % ITS + Premix Tissue Culture Supplement (6.25 µg/mL insulin, 6.25 µg/mL transferrin, 6.25 ng/mL selenous acid, 1.25 mg/mL bovine serum albumin, 5.35 mg/mL linoleic acid), 10^{-7} M dexamethasone, 50 µg/mL ascorbate-2-phosphate, 40 µg/mL L-ascorbic acid, 1 % FBS, 2 mM sodium pyruvate and 10 ng/ml transforming growth factor-beta 1 (TGF-β1). The media were changed three times a week.

3.5.6.1 Immunostaining

For analyzing chondrogenic differentiation of the encapsulated cells inside coacervates, collagen type II (COL2A1) and aggrecan (ACAN) with nucleus stainings were applied. For COL2A1, Alexa Fluor® 488 conjugated goat anti-mouse IgG (H+L) which is a secondary antibody conjugated to green-fluorescent dye (ex/em: 490/525 nm); for ACAN, Alexa Fluor® 647 conjugated goat anti-rabbit IgG (H+L) which is a secondary antibody conjugated to red-fluorescent dye (ex/em: 650/665 nm); for nucleus, DAPI (4',6-diamidino-2-phenylindole) which is a blue fluorescent dye (ex/em: 358/461 nm) that binds to A-T rich regions in DNA were used.

Coacervate samples were washed with PBS and fixed in 3.7 % formaldehyde solution for 30 minutes at RT. Samples were washed and permeabilized in 0.1 % Triton X-100 for 5 minutes at RT. Samples were washed and incubated in 3 % FBS. After washing the samples, they were incubated in primary antibody solutions (1:500 dilution) at RT for 1 hour. Samples were washed to remove unbound antibodies. Secondary antibody solutions (5µg/ml) were added on the samples at RT for 1 hour at dark. Samples were washed extensively with PBS to remove unbound conjugate. Nucleus staining solution DAPI (1:1000 dilution) was added on the samples and incubated at RT for 15 minutes at dark. Samples were washed and then transferred to prepared slides. ProLong® Gold Antifade mountant was added on the samples and stored at 4 °C until examination. Images were taken by confocal microscope after 7, 14, 21 and 30 days of incubation.

3.5.6.2 RNA isolation

RNA was isolated from the cells encapsulated inside coacervate samples using RNA isolation kit (Nucleospin RNA mini kit, Macherey-Nagel, Germany) after 7, 14 and 21 days of incubation.

Cell encapsulated coacervate samples were washed twice with PBS and finely minced inside the distinctive eppendorf tubes. Lysis buffer containing β -mercaptoethanol (100:1 v/v) was added onto the minced samples and tubes were vortexed. Absolute ethanol was added and mixed by pipetting. All cell lysates were transferred to new tubes that contain NucleoSpin® RNA column (~700 μ L) and centrifuged at 11,000 g for 30 seconds. Supernatant was discarded. Membrane Desalting Buffer was added and centrifuged at 11,000 g for 1 minute. DNase reaction mixture was directly applied onto the center of the silica membrane of the column and incubated at room temperature for 15 min. Wash buffer RAW2 was added and centrifuged at 11,000 g for 30 sec. Supernatant was discarded. Wash buffer RA3 was added and centrifuged at 11,000 g for 30 sec. Supernatant was discarded. Again wash buffer RA3 was added and centrifuged at 11,000 g for 2 min. Purification columns were separately transferred to sterile 1.5 mL RNase-free microcentrifuge tubes. Nuclease free water was added and centrifuged at 11,000 g for 1 min. to elute RNA. Purification columns were discarded. RNA concentration and purity was detected with NanoDrop spectrophotometer (Thermo Scientific, USA) by using nuclease free water as blank.

3.5.6.3 Reverse Transcriptase (RT) Polymerase Chain Reaction

Reverse transcription was carried out to synthesize cDNA from purified RNAs using Sensiscript Reverse Transcription Kit (Qiagen, Germany). First, RNA samples (~5 μ L) were incubated for 5 min at 65 °C. cDNA was synthesized from ~50 ng of total RNA in a 20 μ L reaction volume with 1X RT buffer, 10 u/rxn RNase inhibitor, 1 μ M oligo dT primer, 0.5 mM of each dNTP, and Sensiscript RT. All mixture was prepared on ice and components were added to tube according to the order in Table 3.6. Reaction was performed at 37 °C for 1 hour.

Table 3.6 cDNA reaction mix

Components	Volume	Final Conc.
RNase free water	variable	
10X RT Buffer	2 μ L	1X
dNTPs (5 mM)	2 μ L	0.5 mM
Oligo dT Primer (10 μ M)	2 μ L	1 μ M
RNase Inhibitor (10u/ μ L)	1 μ L	10 u/rxn
RT enzyme	1 μ L	
RNA Template	variable	< 50 ng

3.5.6.4 Real Time Polymerase Chain Reaction

Real-time PCR analysis was performed by using Maxima SYBR Green/ROX qPCR master mix (2X) (Thermo Scientific, USA). Reaction mixture was prepared using the components listed in Table 3.7. The reaction was performed as follows: For initial denaturation (120 sec 94 °C), 40 cycles of denaturation, annealing and extension (30 sec 94 °C, 30 sec 59-61 °C, 30 sec 72 °C) and final extension (10 min 72 °C). GAPDH gene was used as a housekeeping gene for normalization and iCycler, CFX96 Touch Real Time PCR Detection System (BIO-RAD, USA) was used as the detection system. Data were expressed as fold change and analysed via comparative Ct method ($\Delta\Delta$ Ct). The used primer sequences for the q-PCR are indicated in Table 3.8. Chondrogenic genes were collagen type II (COL2A1), aggrecan (ACAN), SRY-related high-mobility-group box 9 (SOX9) and housekeeping gene was glyceraldehyde-3-phosphate dehydrogenase (GAPDH). Each sample was studied in duplicate.

Table 3.7 Real-time PCR reaction mix

Components	Volume	Final Conc.
Nuclease free water	variable	
Maxima SYBR Green/ROX qPCR Master Mix (2X)	12.5 μ L	1X
Primers F+R (10 μ M)	1.5 μ L	0.3 μ M each
Template DNA	variable	< 500 ng

Table 3.8 Primer pairs used for real-time PCR

Primers		Sequence (5'→3')	Annealing Temp (°C)	Product Length
GAPDH	F	ACCACAGTCCATGCCATCAC	59	452
	R	TCCACCACCCTGTTGCTGTA		
COL2A1	F	CACCGCTAACGTCCAGATGAC	59	276
	R	GGAAGGCGTGAGGTCTTCTGT		
ACAN	F	CATTCGCACGGGAGCAGCCA	61	133
	R	TGGGGTCCGTGGGCTCACAA		
SOX9	F	TGGCAGACCAGTACCCGCATCT	60	139
	R	TCTTTCTT GTGCTGCACGCGC		

3.5.7 Statistical Analysis

Analysis of variance (ANOVA) was performed using GraphPad prism software. One-way ANOVA followed by Tukey post multi-comparison tests for samples with a single variant and two-way ANOVA followed by Bonferroni post tests for samples with more than one variable sets were utilized. Statistical significance was noted when p-value was less than 5% confident (0.05) using three biological replicates unless otherwise stated. Mean values for replicate experiments and standard deviations (STD) were calculated.

4. RESULTS AND DISCUSSION

4.1 CHARACTERIZATION OF COACERVATE SUSPENSIONS

4.1.1 Optical Microscopy

Light microscopy was performed for the detection of phase separation and morphology of the complex coacervates between HA and CHI biopolymers. Spherical droplets are distinctive features of coacervate suspension [164-166] and can be visualized by this technique.

Droplet formation was observed with a final ionic strength (I) of 50 mM, 150 mM and 300 mM NaCl or CaCl₂ salt solutions at pH 6.25. Three different ionic strengths were selected to explore the coacervate droplets within the physiological range.

Salt concentration (ionic strength) had a direct influence on phase separation of the coacervate systems [167, 168]. In Figure 4.1 a,b, the optical microscopy images clearly showed that coacervate complexes directly clustered into precipitates at ionic strength of 50 mM. However, in Figure 4.1 c,d, coacervate droplets could also be recognized together with the precipitates (clustered flocs) at ionic strength of 150 mM. A similar transition phase in which coacervate droplets coexist with precipitates was reported in the literature for a synthetic polycation/anionic mixed micelle system [169]. From the Figure 4.1, we can conclude that even in the charge ratio of HA/CHI ([-]/[+]) 0.07, using small quantities of salt in our system generated irregular shaped or clumped droplets/flocs instead of coacervate droplets and suppressed the phase separation. Our result is consistent with the literature stating that in the absence or presence of low salt concentration conditions, immediate precipitates might be observed even in low mixing ratios [128].

To solve this suppression of phase separation, addition of small amount of salt have shown to enhance coacervation by changing the energy of the system [170, 171], though a lot more addition of salt also suppresses the phase separation and named as salt screening effect [172, 173].

Kayitmazer *et al.* showed the critical salt concentration for phase separation in the HA/CHI system as a function of polymer concentration and pH [174]. Considering those findings, we increased the ionic strength to 300 mM where phase separation still occurred and a more detailed observation was done by modulating the charge ratio of HA/CHI ($[-]/[+]$).

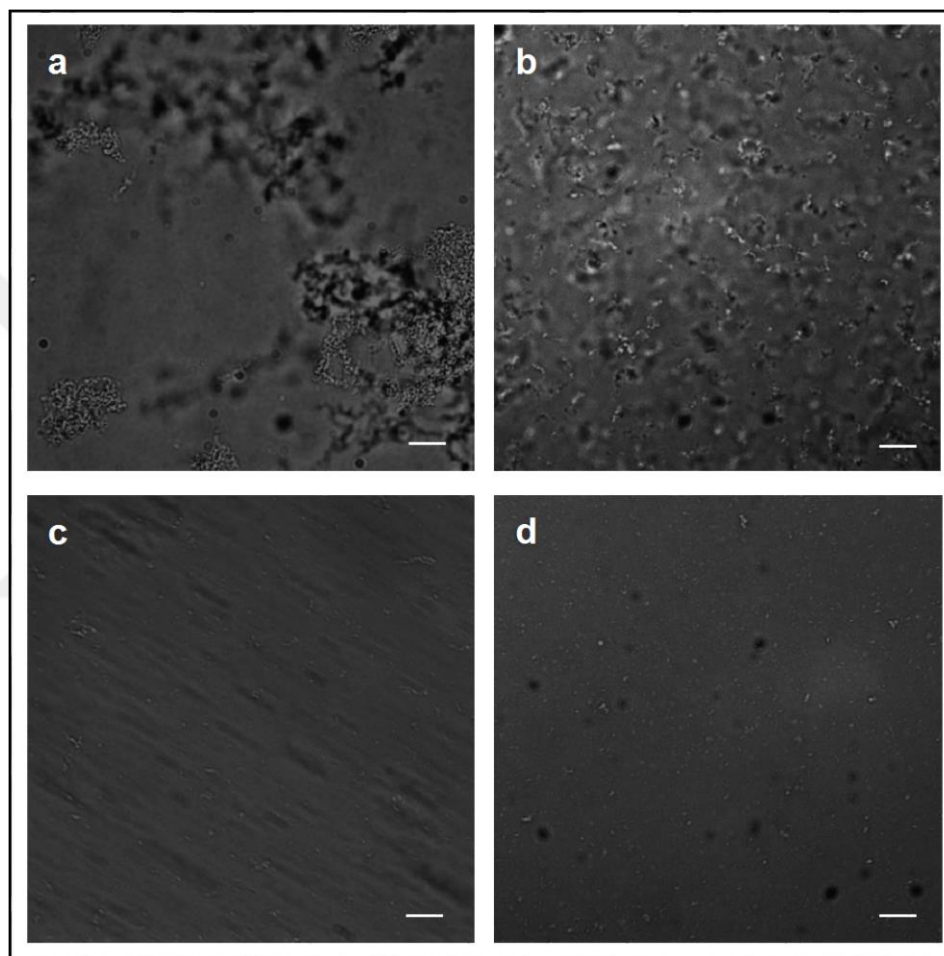


Figure 4.1. Optical microscopy images of HA:CHI-Cl coacervate suspensions at charge ratio of $[-]/[+] = 0.07$, at ionic strength of 50 mM in (a) NaCl, (b) CaCl_2 solution; at ionic strength of 150 mM in (c) NaCl, (d) CaCl_2 solution. The scale bars represent 10 μm

For the HA/CHI-Cl system, micron sized droplets (diameter) were observed up to $[-]/[+] = 0.31$ as seen in Figure 4.2 a-c, prepared in NaCl solution and Figure 4.3 a-c, prepared in CaCl_2 solution. At charge ratio of $[-]/[+] 0.46$ and 0.61 in both solutions (Figure 4.2 d,e and Figure 4.3 d,e), coacervate droplets coexisted with precipitate particles whereas precipitates were the dominant structures at charge ratio of 0.77 (Figure 4.2 f and Figure

4.3 f).

For the HA/CHI-G system, coacervation was only analyzed for the samples prepared in NaCl salt solution, the data observed for HA/CHI-Cl system showed that the results were very similar for the coacervates prepared in NaCl or CaCl₂ solutions. The preliminary examination also showed similar results for HA/CHI-G prepared in CaCl₂ solution (data not shown). So it was decided to continue for HA/CHI-G system only with preparations in NaCl solution.

In HA/CHI-G system, coacervation region was extended to charge ratio of $[-]/[+] = 0.48$ and spherical droplets were observed up to this ratio as seen in Figure 4.4 a-c. At the charge ratio of $[-]/[+] = 0.71$, some of coacervate droplets started to accumulate in clusters (Figure 4.4 d), whereas precipitates appeared as solid flocs with irregular shapes above $[-]/[+] = 0.95$ (Figure 4.4 e,f).

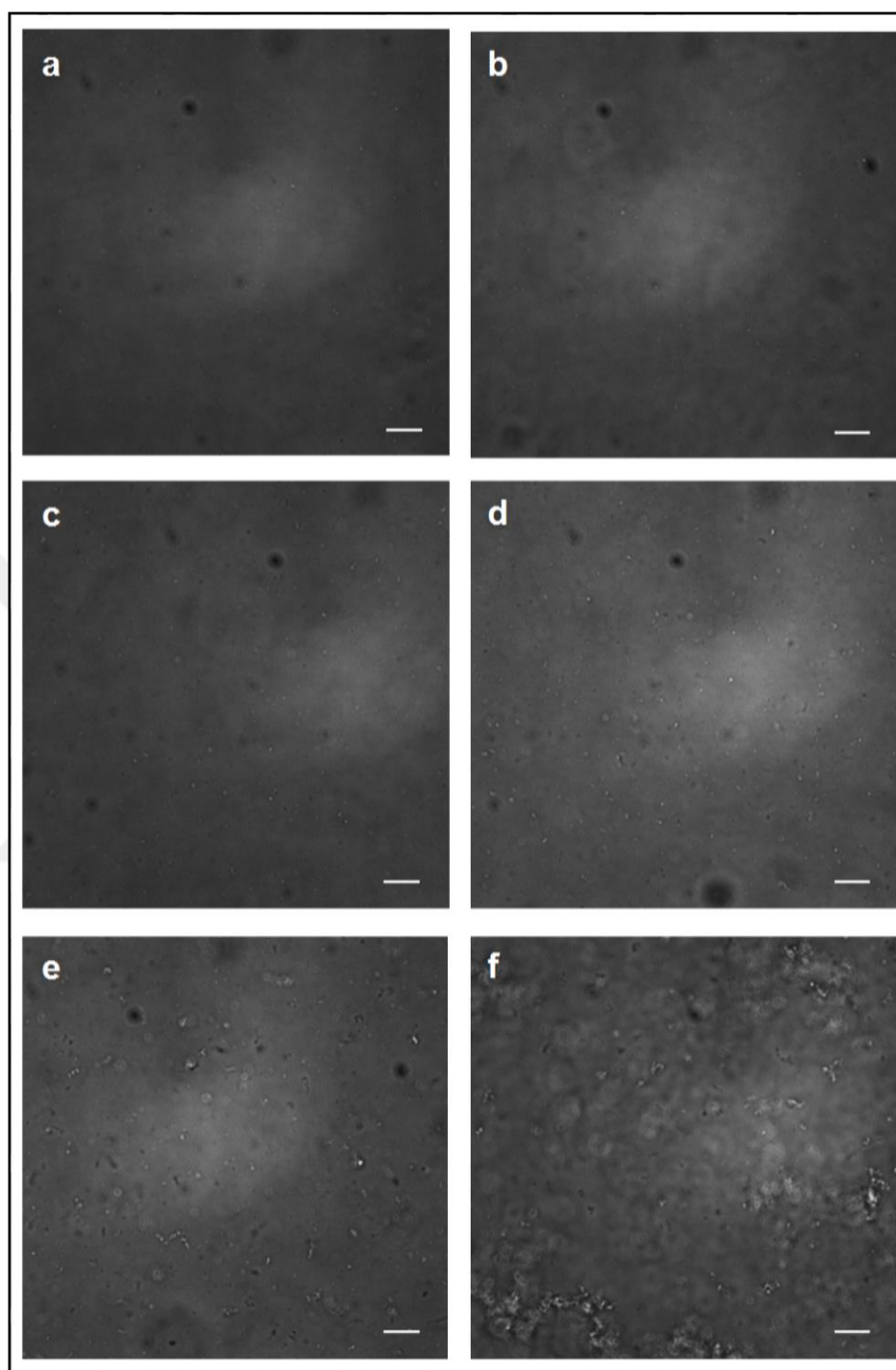


Figure 4.2. Optical microscopy images of HA:CHI-Cl coacervate suspensions at ionic strength of 300 mM NaCl solution at a charge ratio of $[-]/[+]$ (a) 0.08, (b) 0.19, (c) 0.31, (d) 0.46, (e) 0.61, (f) 0.77. The scale bars represent 10 μm

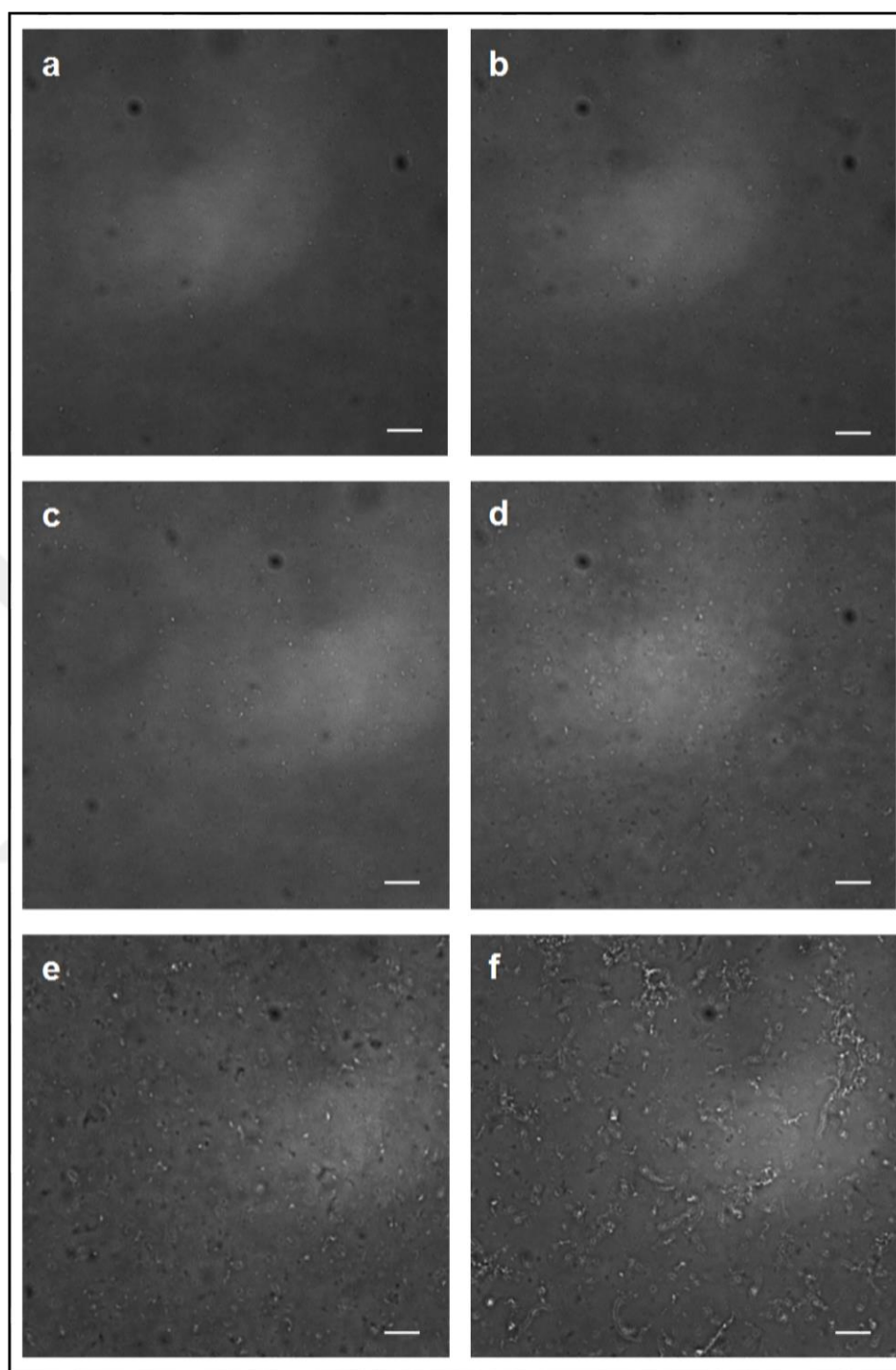


Figure 4.3. Optical microscopy images of HA:CHI-Cl coacervate suspensions at ionic strength of 300 mM CaCl_2 solution at a charge ratio of $[-]/[+]$ (a) 0.08, (b) 0.19, (c) 0.31, (d) 0.46, (e) 0.61, (f) 0.77. The scale bars represent 10 μm

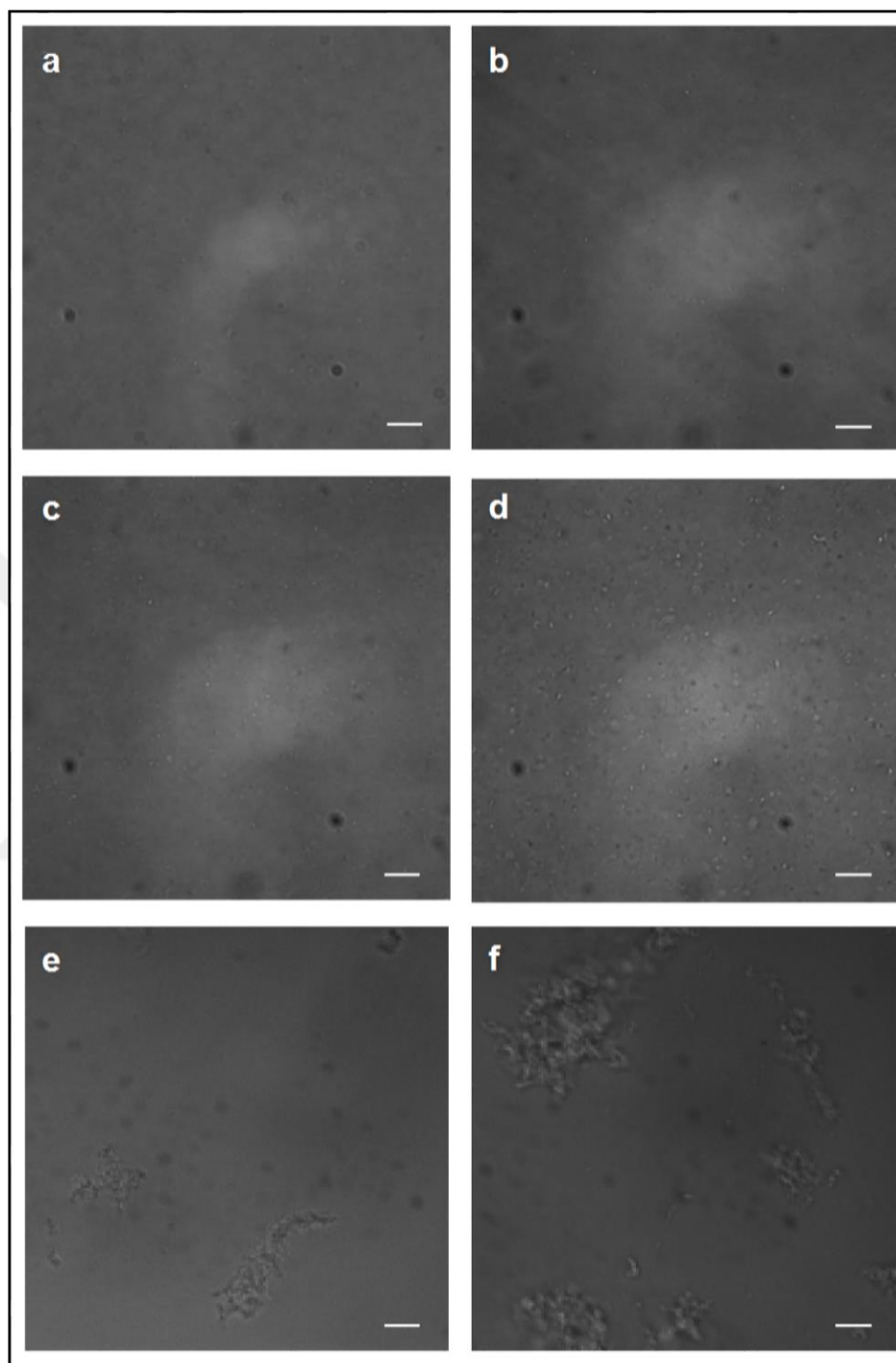


Figure 4.4. Optical microscopy images of HA:CHI-G coacervate suspensions at ionic strength of 300 mM NaCl solution at a charge ratio of $[-]/[+]$ (a) 0.12, (b) 0.30, (c) 0.48, (d) 0.71, (e) 0.95, (f) 1.19. The scale bars represent 10 μm

4.1.2 Turbidity

The nature of the charged complexes formed when HA interacted with the CHI was confirmed by measuring the changes in solution turbidity. This technique is very simple and used extensively [165, 175]. Different mixing ratios of HA/CHI complex solutions were prepared in separate cuvettes (Figure 4.5) and the turbidity at 630 nm of those coacervate solutions were determined after mixing for 10 minutes.

By visual inspection, one-phase turbid solutions were observed up to the charge ratio of $([-]/[+])$ 0.61 for HA/CHI-Cl system using NaCl and CaCl₂ (Figure 4.5 a,b) and 0.71 for HA/CHI-G system using NaCl solutions (Figure 4.5 c). Whereas precipitates could be macroscopically observed beyond charge ratio of 0.69 and 0.83, respectively.

The solutions at low mixing ratios had low turbidity with transparent appearance. Whenever addition of HA was increased, solutions became turbid with whitened appearance (Figure 4.5 a-c). This increase in measured absorbance could be the result of increased complexation since the complexes were large enough to scatter light and it was also shown by Perry *et. al.* [167].

All samples resembled the same behaviour as showing a peak in turbidity and dropped by the excess addition amounts of HA solution. Maximum turbidity for coacervate complexes in the system of HA/CHI-Cl was observed at the charge ratio of $([-]/[+]) = 0.61$ for both NaCl and CaCl₂ salts (Figure 4.6 a,b); however, the turbidity maxima at charge ratio of $([-]/[+]) = 0.71$ was detected for HA/CHI-G system (Figure 4.6 c) which agrees with the visual photographs.

In the literature, same behaviour was also observed for the turbidity measurements of lactoferrin/casein [176] and lactoferrin/ β -lactoglobulin [177, 178] system. In those studies, starting with low mixing ratios, low turbidity was measured and this low turbidity was increased by the addition of lactoferrin to the system. Finally, excess addition resulted in very low turbidity again.

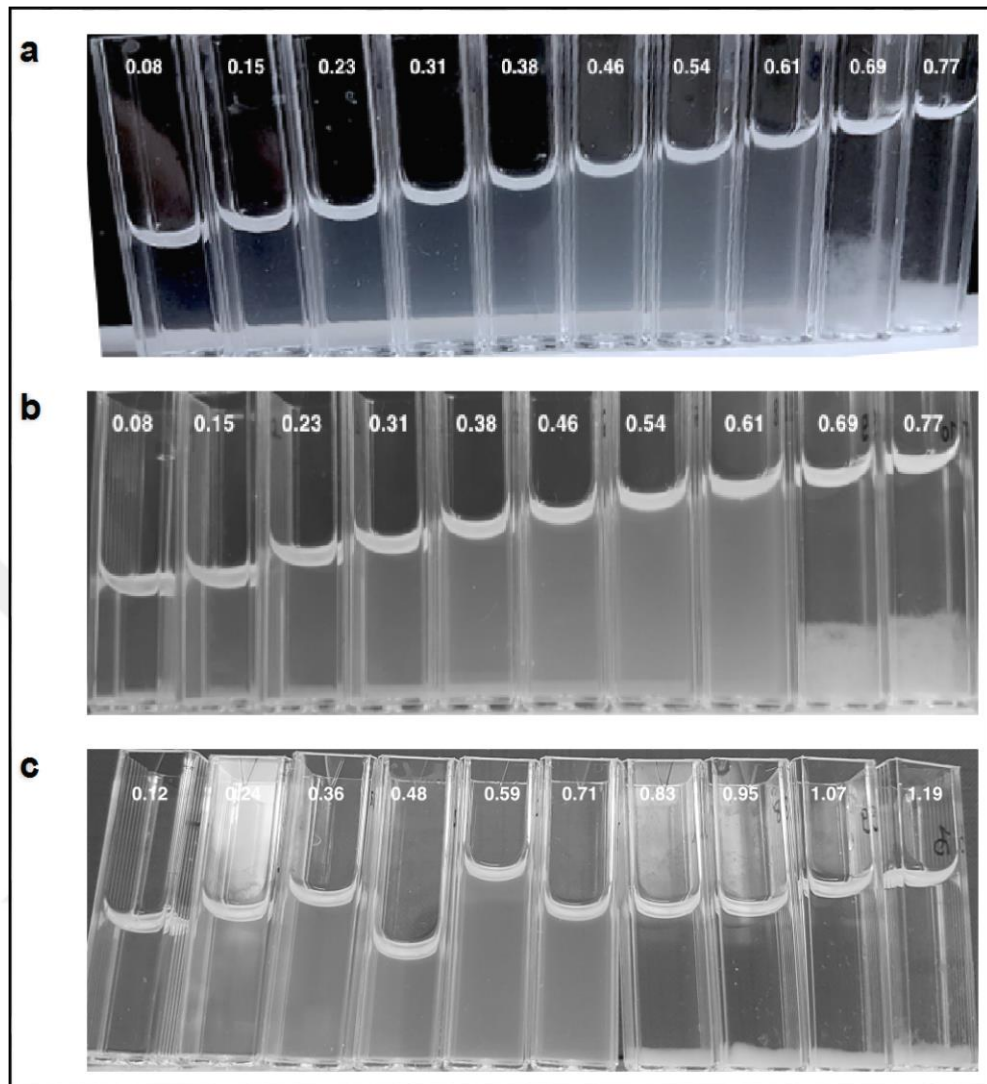


Figure 4.5. Visual turbidity of mixtures at I of 300 mM (a) HA/CHI-Cl in NaCl, (b) HA/CHI-Cl in CaCl_2 , (c) HA/CHI-G in NaCl salt solution. The charge ratios $[-]/[+]$ are given above each cuvette

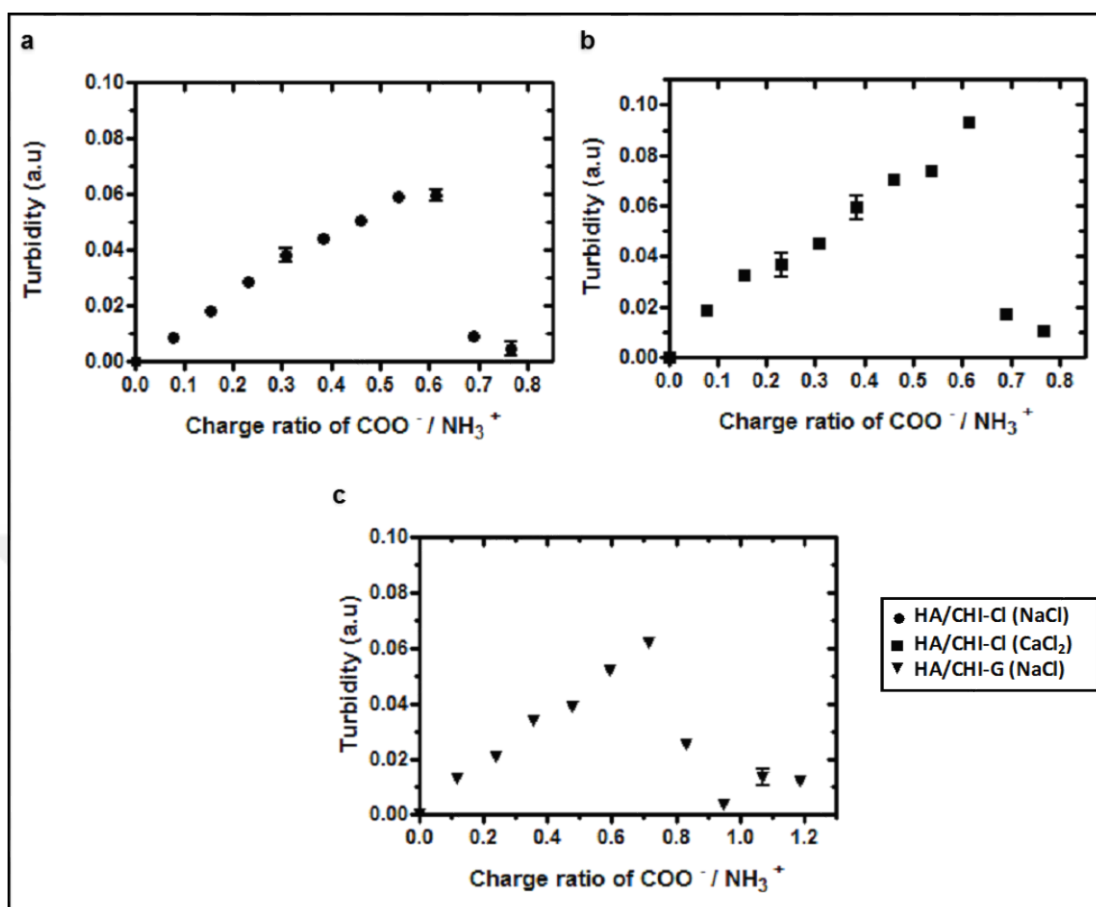


Figure 4.6. Turbidity as a function of HA to CHI charge ratio $[-]/[+]$, at 300 mM ionic strength. (a) Filled circle: HA/CHI-Cl in NaCl salt, (b) Filled square: HA/CHI-Cl in CaCl_2 salt, (c) Filled triangle: HA/CHI-G in NaCl salt

4.1.3 Dynamic Light Scattering (DLS)

For DLS measurements, HA/CHI coacervate complexes were measured as a function of HA/CHI charge ratio. Scattering intensity at 173° and the Z-average hydrodynamic diameter (d_H - nm) graphics were depicted in Figure 4.7 and Figure 4.8, respectively.

In addition to turbidity which is also a scattering measurement, DLS at 173° angle scattering intensity graphic was explored. Scattering intensity technique uses backscattering detection [179] and more sensitive than turbidity about distinguishing coacervate droplets and precipitate particles. Turbidity does not respond to the conditions

where coacervate droplets coexist with the precipitate particles in solution [169]; it only drops where visible separation is observed (Figure 4.5).

In our study, maximum intensity (measured at 173° through DLS) for coacervate complexes in the system of HA/CHI-Cl was observed at the charge ratio of $[-]/[+] = 0.31$ for both NaCl and CaCl_2 salts (Figure 4.7 a,b); however, the maxima reached at charge ratio of $[-]/[+] = 0.48$ for HA/CHI-G system (Figure 4.7 c) which is also consistent with the results of light microscopy.

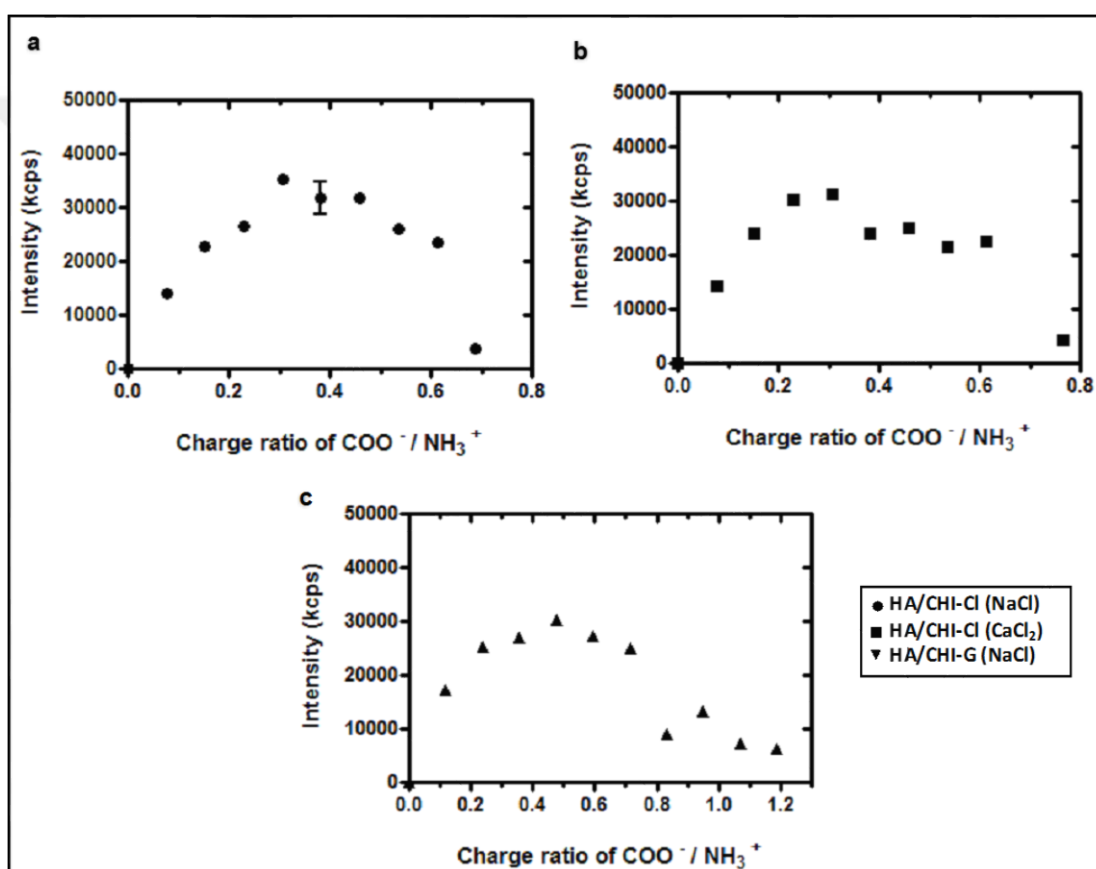


Figure 4.7. Scattering intensity as a function of HA to CHI charge ratio $[-]/[+]$, at 300 mM ionic strength. (a) Filled circle: HA/CHI-Cl in NaCl salt, (b) Filled square: HA/CHI-Cl in CaCl_2 salt, (c) Filled triangle: HA/CHI-G in NaCl salt

The Z-average hydrodynamic diameter (d_H) is constant at 609 ± 19 nm and 668 ± 63 nm between $[-]/[+]$ of 0.08 and 0.31 for the HA/CHI-Cl coacervates prepared in NaCl and CaCl_2 (Figure 4.8 a,b), respectively. For the HA/CHI-G system, d_H was detected constant and measured as 708 ± 18 nm between $[-]/[+]$ of 0.12 and 0.48 (Figure 4.8 c). As

mentioned before, while size stayed constant up to $[-]/[+] = 0.31$ and 0.48 , turbidity and intensity increased. It could be because of the increased number of scattering objects found in coacervate suspensions. Furthermore, in the literature, the light scattering intensity of the coacervation of alginate and silk fibroin was found proportional to the size and the number of the complexes formed [180].

The particles measured with a d_H of 609, 668 and 708 nm (calculated amounts given above) was attributed to coacervate droplets which would coalesce to form the coacervate phase upon centrifugation. Moreover, in the excess addition of HA (charge ratios of $[-]/[+] > 0.54$ for HA/CHI-Cl and $[-]/[+] > 0.83$ HA/CHI-G system), a sharp increase was measured in d_H values (up to $8,891 \pm 1,650$ nm for HA/CHI-Cl in NaCl, $7,470 \pm 1,712$ nm for HA/CHI-Cl in CaCl_2 and $10,834 \pm 2,867$ nm for HA/CHI-G in NaCl solutions) of the HA/CHI complexes suggested formation of precipitate particles ($\text{PdI} > 0.5$). Furthermore, those increased d_H values that were mostly demonstrating huge error bars also well agrees with the study about coacervation of gelatin–dextran conjugate and tea polyphenol [181] by showing heterogeneous population of particles such as droplets, flocculates and aggregates. In brief, measured particles grew in size due to the aggregation of the flocculates.

We can also conclude that the size of coacervate droplets was not established by only one biopolymer since d_H of each biopolymer solution as 130 ± 24 nm for CHI-Cl, 70 ± 3 for CHI-G and 73 ± 13 nm for HA.

The measured d_H value of the coacervation of HA and CHI in our study was also supported by the literature. Kayitmazer *et al.* reported a d_H value of ~ 650 nm at ionic strength of 300 mM NaCl at pH 3.0 using HA/CHI system [174].

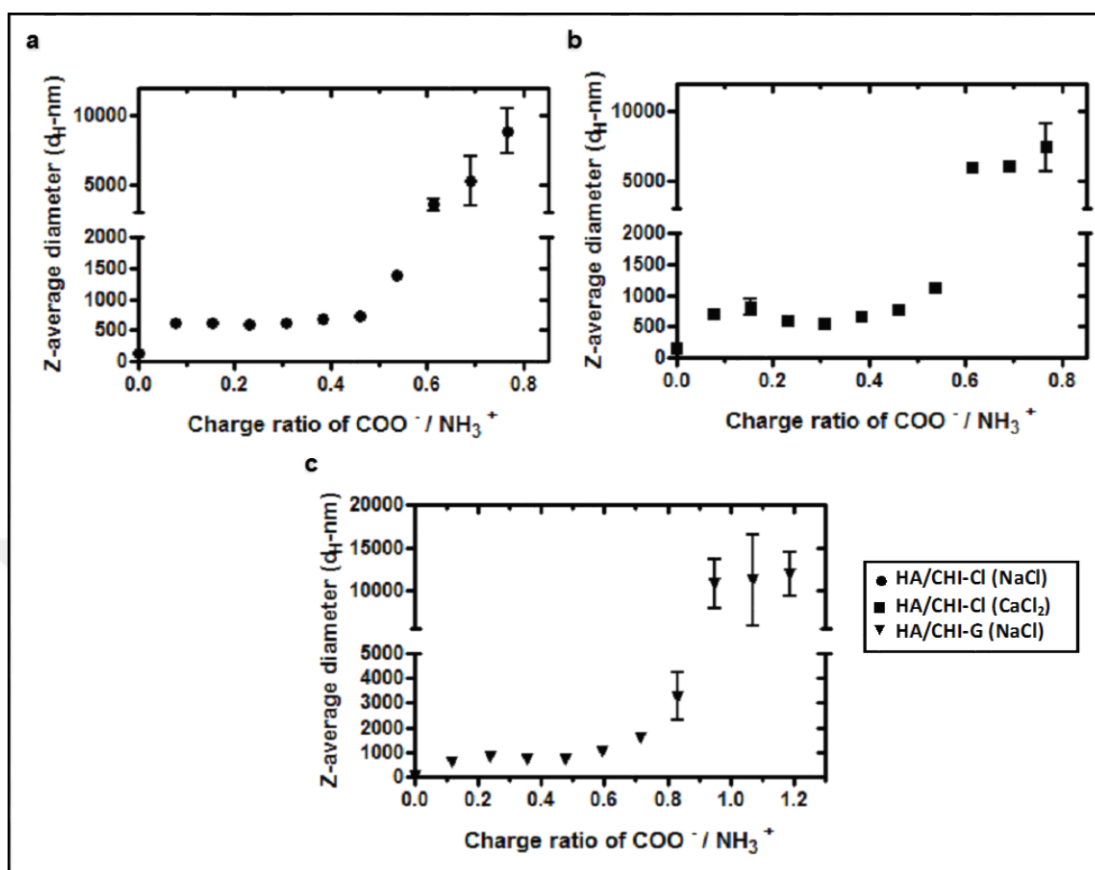


Figure 4.8. Z-average (hydrodynamic) diameter as a function of HA to CHI charge ratio $[-]/[+]$, at 300 mM ionic strength. (a) Filled circle: HA/CHI-Cl in NaCl salt, (b) Filled square: HA/CHI-Cl in CaCl₂ salt, (c) Filled triangle: HA/CHI-G in NaCl salt

4.1.4 Zeta Potential

For zeta potential (ζ -potential), HA/CHI coacervate complexes were measured as a function of charge ratio ($[-]/[+]$) and results are depicted in Figure 4.9.

HA and CHI polymers have either negatively or positively charged surfaces due to the charged COO⁻ and NH₃⁺ groups. In the HA/CHI coacervation system, excess amine or carboxylic acid groups make the charge positive or negative, respectively. The amino groups of chitosan are protonated below the pK_a around pH 6.7 [174], which confers a cationic character to the chitosan. In our study, after the zeta potential measurements of the aqueous chitosan solutions, positive charged values were observed, 11.5 ± 0.9 mV for CHI-Cl in NaCl, 14.6 ± 1 mV for CHI-Cl in CaCl₂ and 15.8 ± 0.29 mV for CHI-G in NaCl

solutions due to the presence of multiple amine groups that were ionized at this pH (6.25).

Coacervation requires charge neutral complexes whose net charge must be almost zero. Nevertheless, in our system, the zeta potential exhibited a slow downward trend as HA solution was added, but at the points in which coacervates were formed, the values were still much higher than zero, 7.23 ± 1.39 mV for HA/CHI-Cl in NaCl, 6.32 ± 0.08 for HA/CHI-Cl in CaCl₂, 6.19 ± 0.67 mV for HA/CHI-G in NaCl solutions (Figure 4.9 a-c). Moreover, as expected, the zeta potential turned into negative values (-11.6 ± 0.3 mV for HA/CHI-Cl in NaCl, -10.36 ± 0.3 mV for HA/CHI-Cl in CaCl₂, -8.50 ± 0.36 mV for HA/CHI-G in NaCl solutions), due to the incorporation of an increasing number of HA chains having excessive amount of carboxyl groups in the coacervation system. Charge reversal only occurred at [-]/[+] bigger than 0.69 and 1.07 for HA/CHI-Cl (both in NaCl and CaCl₂) and HA/CHI-G, respectively, where precipitate particles dominated the mixture.

Although the charge stoichiometry is accepted as a critical parameter that characterises coacervation [165, 182] in our HA/CHI system, instead of coacervation droplets, precipitate formation was observed around stoichiometric (1:1) charge ratios. Zhang and Shklovskii had introduced non-stoichiometric coacervation [183] which also matches well with our system (Figure 4.9) and literature [174, 184]. Kayitmazer *et al.* already reported detailed explanations to non-stoichiometric coacervation of HA/CHI system [174] and we also attributed the non-stoichiometric coacervation to the intracomplex disproportionation (segregation of charges). According to these studies, the coacervate droplets detected in DLS may have a charge-neutral core with a tail where excess cationic charges are located as a tadpole phase, resulting in coacervation.

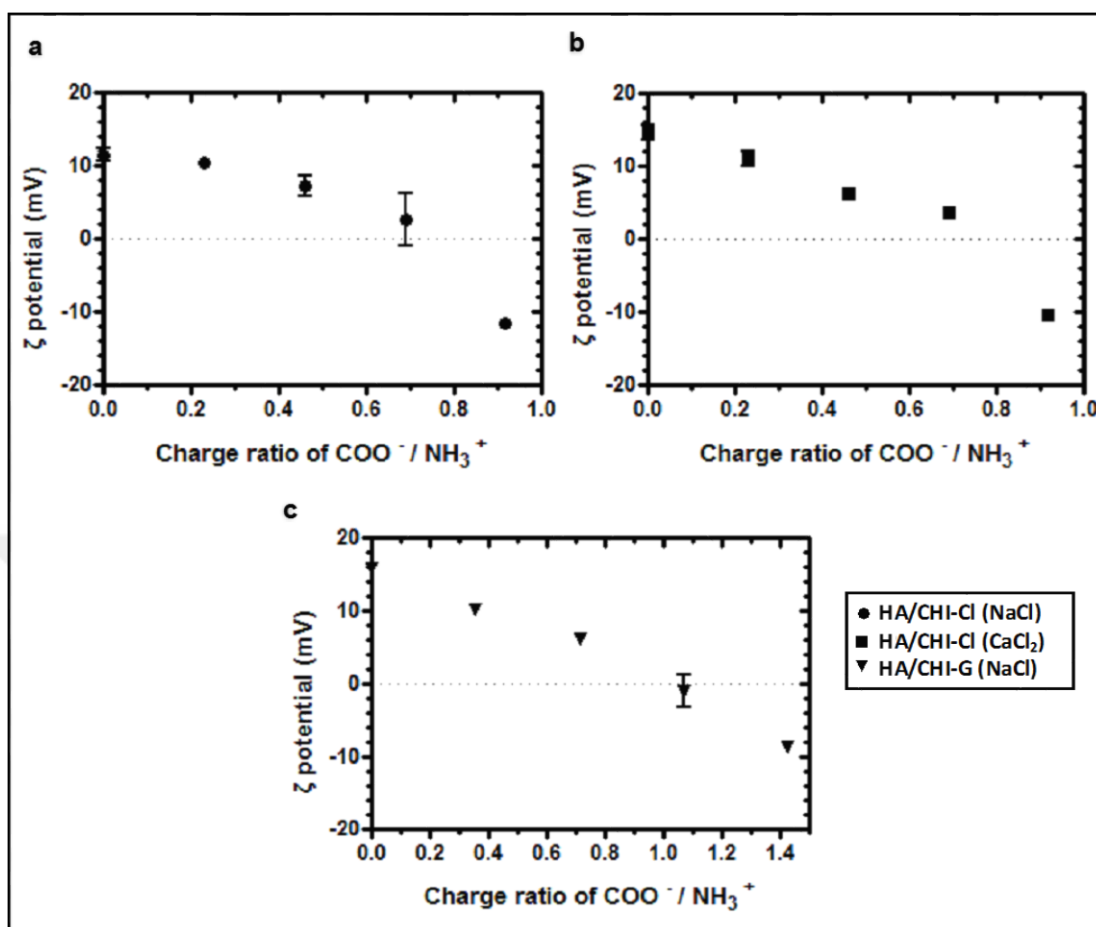


Figure 4.9. Zeta potential as a function of HA to CHI charge ratio $[-]/[+]$, at 300 mM ionic strength. (a) Filled circle: HA/CHI-Cl in NaCl salt, (b) Filled square: HA/CHI-Cl in CaCl_2 salt, (c) Filled triangle: HA/CHI-G in NaCl salt

4.1.5 Visual Inspection

Those natural polymers, CHI and HA have an advantageous properties for tissue engineering applications [185-188], due to their biodegradability and excellent biocompatibility.

Optimum coacervation was detected at charge ratios of $[-]/[+] = 0.31$ (HA/CHI-Cl system) and $[-]/[+] = 0.48$ (HA/CHI-G system). At that ratios, coacervate suspensions displayed the highest yield with better droplet morphology and good size distribution at ionic strength of 300 mM and pH 6.25.

Those liquid coacervate droplets coalesce very slowly under the influence of gravity. Therefore, centrifugation is required for speeding up the coacervate formation rate. Centrifugation is an easy technique that is often used for collecting coacervate layers [168, 189, 190]. A polymer rich phase which is semi-opaque in appearance and a dilute solution phase can be distinctly visualized after centrifugation (Figure 4.10). The reason why the coacervate phase did not appear totally transparent might be due to the level of protein content inside the biopolymers.

Moreover, the centrifuged suspensions confirmed the formation of immisible coacervate layer which was qualified as scaffolding material and all coacervates presented liquid-like and highly viscous (viscoelastic) behaviour (Figure 4.10 b) as identified in the literature [172, 174, 175, 191]

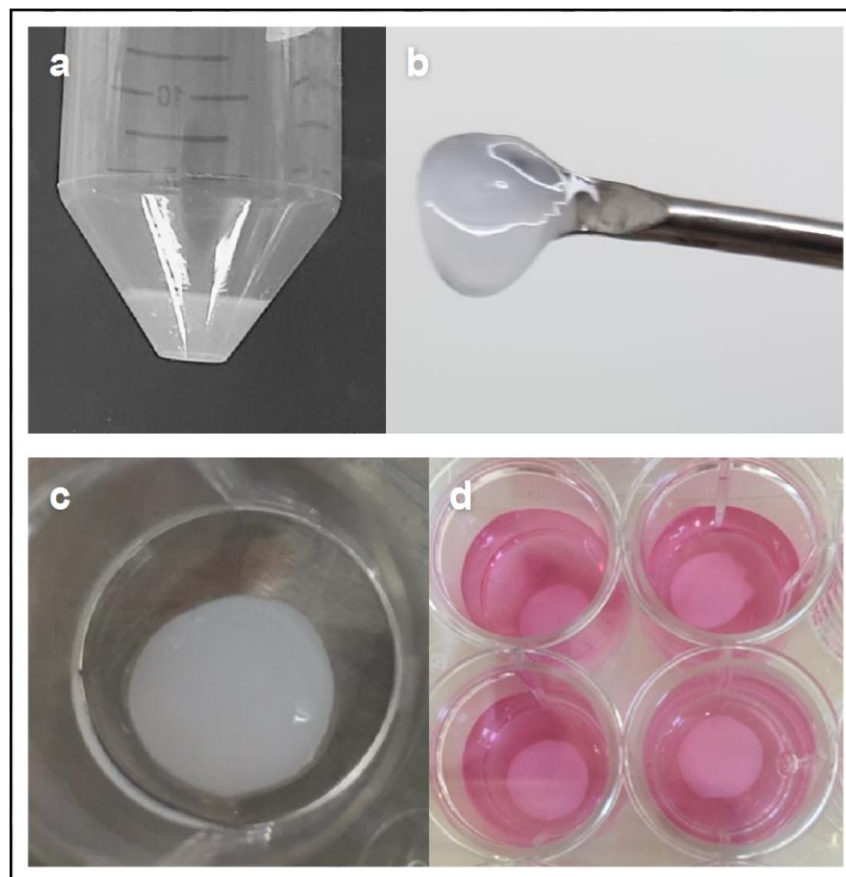


Figure 4.10. Visual appearance of coacervates after centrifugation at a charge ratio of (a,b) $[-]/[+] = 0.31$ HA/CHI-Cl and (c,d) $[-]/[+] = 0.48$ HA/CHI-G suspensions

4.1.6 Environmental Scanning Electron Microscopy (ESEM)

Microstructure of HA/CHI coacervates were examined by environmental scanning electron microscopy. This technique allows to examine the pore structure of the coacervates in a saturated water vapor environment which enables imaging with minimal drying.

Pore size detection and the network morphology are very important measurements for understanding the behaviour/attitude of biomaterials such as cell growth support and host tissue correlation [192].

In this study, ESEM imaging was applied 72 hours later from HA/CHI coacervate preparation. Presence of porous structure was observed for all HA/CHI coacervates. They had randomly oriented pores ranging in size from 5-500 μm and mean pore sizes of 26 μm and 19 μm for coacervates prepared in CaCl_2 (Figure 4.11) and NaCl solutions (Figure 4.12), respectively, as calculated from ImageJ analysis.

Coacervates prepared in CaCl_2 exhibited slightly larger pores when compared to the ones prepared in NaCl salt solution. We can conclude that this difference could be due to the presence of calcium ions (Ca^{+2}) that has larger hydration number (number of water molecules per ion) than that of sodium ions (Na^+) [193]. As a result water content was relatively high in coacervates prepared in CaCl_2 solution (see part 4.1.7) and pores might have swelled in the more hydrated network.

High porosity and interconnected network are required for adequate gas exchange, transport of nutrients and removal of cellular wastes during incubation period [194]. Our HA/CHI coacervates exhibited porous characteristics and provided suitable environment with desirable properties for both cell encapsulation and cultivation.

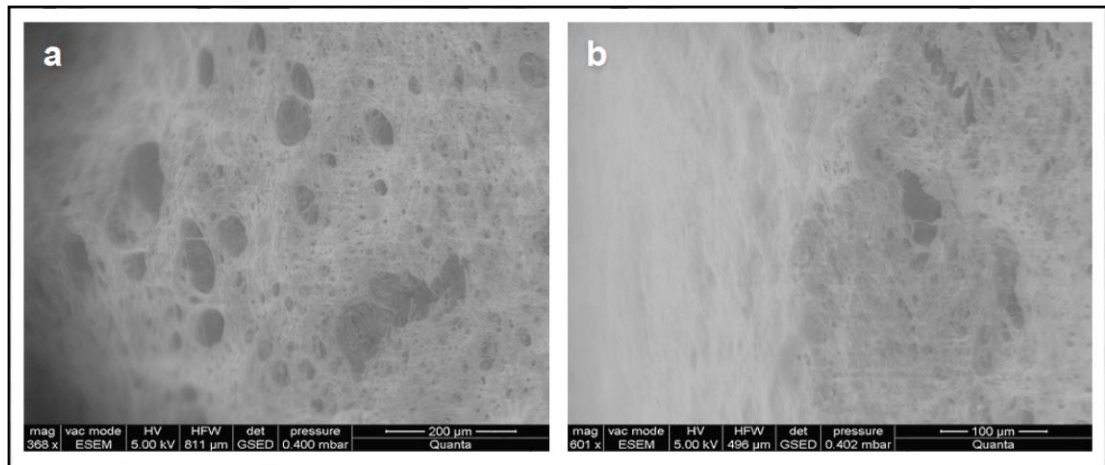


Figure 4.11. Environmental scanning electron microscopy images of (a,b) HA/CHI-Cl coacervates at 3rd day of incubation prepared with 300 mM CaCl₂

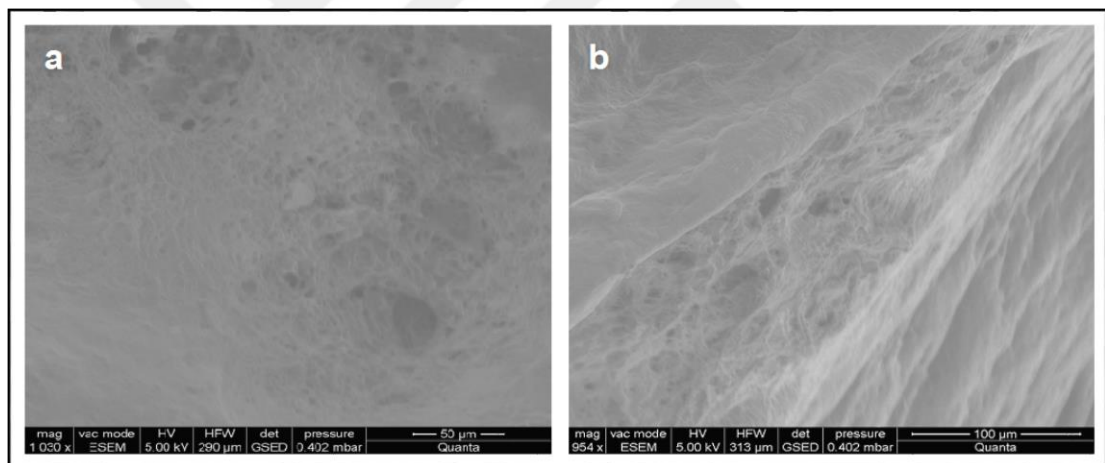


Figure 4.12. Environmental scanning electron microscopy images of (a,b) HA/CHI-Cl coacervates at 3rd day of incubation prepared with 300 mM NaCl

4.1.7 Dry Weight Analysis of Coacervates

Dry weight analysis was carried out to determine the water content inside the individual HA/CHI coacervates. Coacervates are viscous, dense liquid phases and they incorporate high water content [129]. The water content inside the biomaterials denotes the water retaining capacity which is highly related with the *in vivo* resorption of the scaffold by body fluid [195]. The water content inside the coacervates was determined by weighing after centrifugation and drying them in the oven.

Water content in the HA/CHI-Cl cocervates prepared in CaCl₂ and NaCl solutions was found 94 ± 0.1 % and 92 ± 0.4 %, respectively. HA/CHI-G cocervate was found 94 ± 0.2 %. The relatively higher water content for HA/CHI-Cl cocervates in CaCl₂ solution was expected because of the larger hydration number for Ca⁺² than Na⁺, as mentioned in ESEM results. When comparing the cocervates prepared in NaCl salt solution, the difference may come from the counterions found on the chitosan polymers. There was a weak dependence on salt concentration that was shown to increase the water content in poly (acrylic acid) (PAA)/poly (N,N-dimethylaminoethyl methacrylate) system [175]. This salt dependence could be due to the number of ions found in the system. Consequently, glutamate as counterion contains more ions than that of chloride, so it might be responsible for the more hydrated environment of the HA/CHI-G cocervates.

In the literature, water contents of the various types of cocervates have been reported generally between 65-85%, water content was found in the system of BSA/poly (diallyldimethylammonium chloride) as 73% [196], gelatin/PAA as up to 80% [197] and pectin/ β -lactoglobulin as up to 85% [198].

4.1.8 Degradation Behavior of the Cocervate Scaffolds

Biodegradable scaffolds have become favourable candidates for most of the tissue engineering applications. However, time and rate of biodegradation are very important factors for successful tissue regeneration. Degradation products should be biocompatible and provide suitable environment for the newly grown/formed tissue [199].

Figure 4.13 a,b shows the degradation ratio of HA/CHI-Cl and HA/CHI-G cocervates after different time points. Cocervates degraded fast during the first week. Total weights of 63.2 ± 0.9 % wt and 62.4 ± 1.5 % wt were lost for HA/CHI-Cl and HA/CHI-G cocervates, respectively. This quick degradation can be attributed to the leaching of constituents from the scaffold network. The degradation rate slowed down in the next 2 weeks and weight remained constant at 34.6 ± 2.4 % wt for HA/CHI-Cl, 29.9 ± 2.6 % wt for HA/CHI-G cocervates by conserving structural integrity until the end of 16 weeks.

It is a promising result that the durability of HA/CHI coacervates could allow new ECM development, mostly degrading by surface erosion to reach 16 weeks, although fast degrading profile was observed in the early time points.

It was shown that after 2 weeks of degradation, as a synthetic polymer blend of poly(propylene fumarate) with poly(DL-lactic-co-glycolic acid) scaffold decreased the buffer pH, meaning that released by-products of the scaffolds were acidic [200]. Unlike synthetic polymer originated scaffolds, natural polymer originated ones like in our study did not lead to acidic by-products after degradation [201].

Figure 4.13 c,d shows the change of pH value of HA/CHI-Cl and HA/CHI-G coacervates during 16 weeks *in situ* incubation. During the first day of degradation, the pH value of the buffer decreased from 7.44 to 7.12 ± 0.03 and 7.11 ± 0.04 for HA/CHI-Cl and HA/CHI-G coacervates, respectively. This might be explained by the ongoing exchange of the ions at the initial days between buffer (pH of 7.44) and coacervates (preparation pH of 6.25). After 30 days of incubation, the equilibrium pH ~ 7.0 was established. During the next 8 weeks, the pH value fluctuated in a mild and stable range for the HA/CHI-Cl, from 6.88 ± 0.06 to 7.04 ± 0.06 ; HA/CHI-G from 7.0 ± 0.08 to 7.16 ± 0.03 .

Both HA/CHI coacervates had steady degradation rate and their pH was in physiological range, which made them favourable to the further *in vitro* applications. Nevertheless, those pH measurements only represent *in situ* results and may change in *in vivo* conditions.

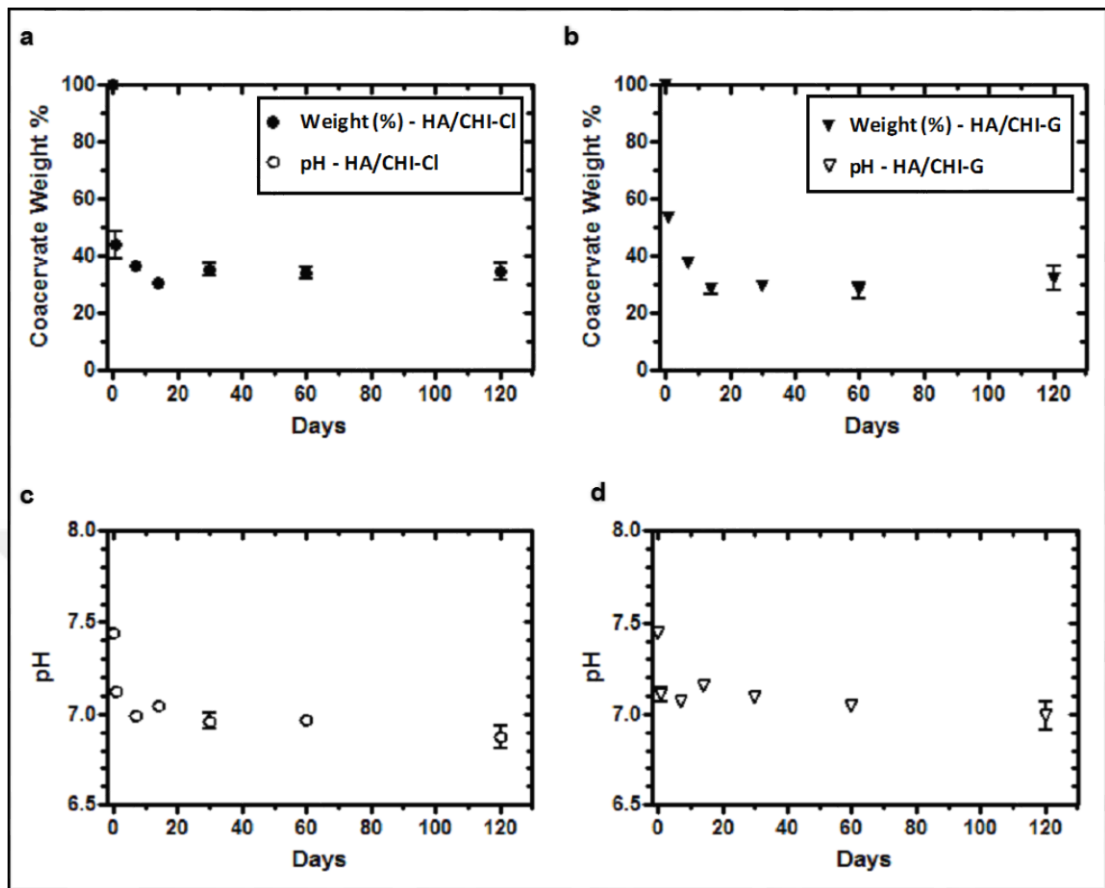


Figure 4.13. *In situ* degradation behavior of (a,c) HA/CHI-Cl and (b,d) HA/CHI-G coacervates in phosphate-buffered saline containing sodium azide (pH 7.5) at different incubation time intervals (up to 120 days). (a,b) shows the weight loss percentages of the coacervates and (c,d) shows the pH changes of the buffer. Values are reported as mean \pm SD (n = 3)

4.1.9 Antimicrobial Activity

Although our aim was to fabricate a scaffold for the purposes of cartilage tissue engineering, we were curious about the antimicrobial properties of the prepared coacervates. In the literature, plenty of reports have shown that chitosan has antimicrobial activity against a great number of bacteria, fungi and yeast [202-204]. The antimicrobial properties of chitosan can be variable due to its characteristics [205, 206], such as molecular weight, degree of acetylation or physical features [202, 207], such as hybridization with other polymers, pH and ionic strength. This activity is assigned to the

cationic nature of the chitosan thus it can interact and disturb the negatively charged cell membrane of the microorganisms [208].

Zone of inhibition around the contacted area of the coacervates and control disks were shown in the Figure 4.14. Ofloxacin antibiotic which is a well-known and frequently used antimicrobial agent was used as positive control. It is active against both gram positive and gram negative bacteria [209]. Very clear inhibition zones were observed around ofloxacin disks in both *Esheria coli* and *Staphylococcus aureus* bacteria (Figure 4.14). It means that used bacteria were not resistant to antimicrobial agents. The gram-positive bacteria, *S. aureus* was more susceptible when compared to the gram-negative bacteria *E. coli* for assessing the local inhibition area visually on coacervates prepared using NaCl salt. However, no considerable difference was noted due to the small area of inhibition among the HA/CHI-Cl and HA/CHI-G coacervates for *S. aureus* bacteria. Almost no inhibition zone was observed for the coacervates prepared using CaCl₂ salt, this might be the reason of using divalent calcium ion. Low antimicrobial activity of the coacervates could be due to the moderate polycationic nature, almost neutral and the low chitosan concentrations (0.09 %wt.) which were utilized at physiological pH and ionic strength while preparing the coacervates.

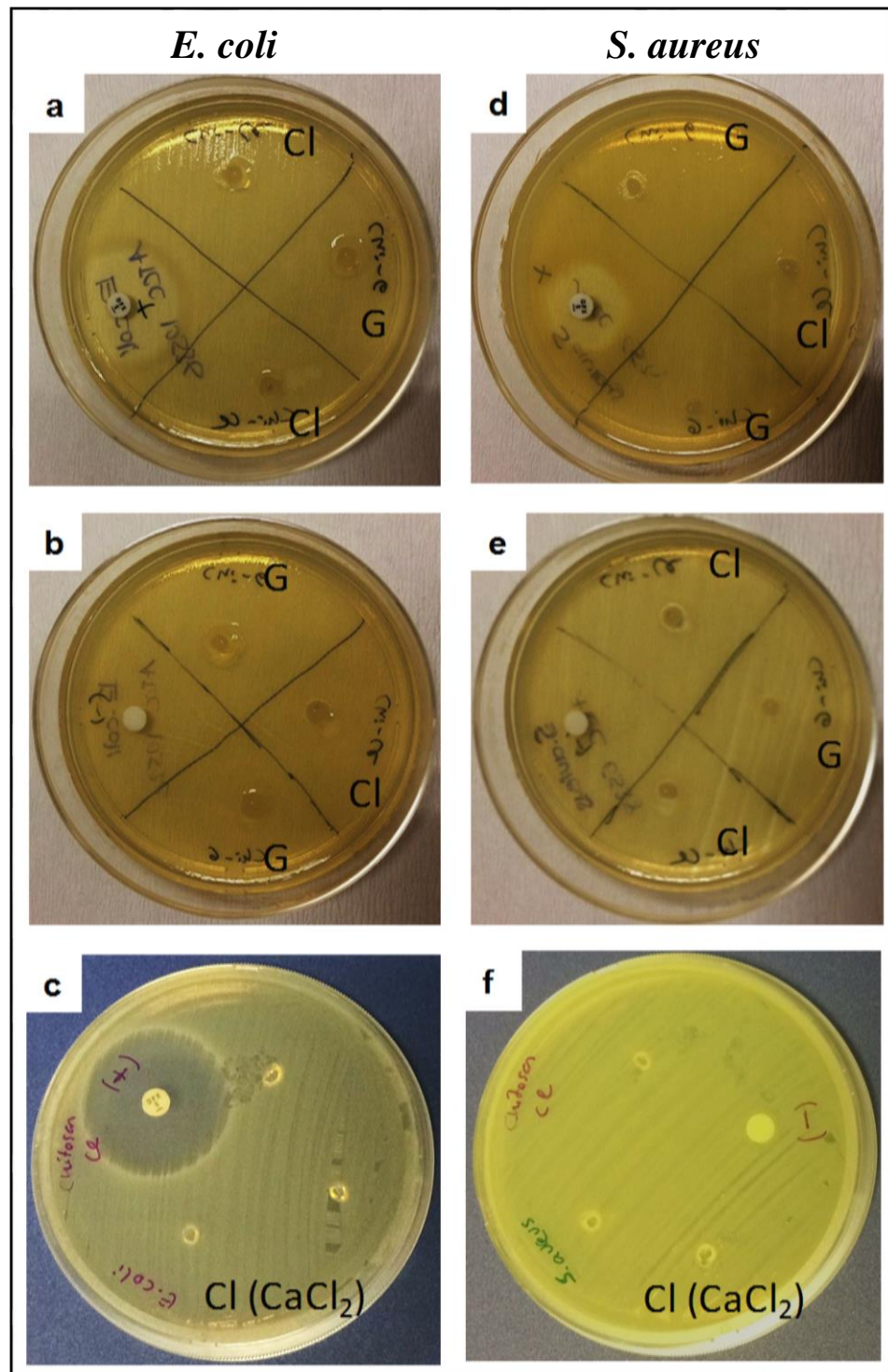


Figure 4.14. Bacterial growth inhibition of disc diffusion method. Coacervates were incubated at 37 °C for 24 h on agar plates cultured with *Esheria coli* (left panel a,b,c) and *Staphylococcus aureus* (right panel d,e,f); G indicates HA/CHI-G in NaCl, Cl indicates HA/CHI-Cl in NaCl, Cl (CaCl₂) indicates HA/CHI-Cl in CaCl₂ solution, (+) indicates the positive control (Ofloxacin disk) and (−) indicates the negative control (empty disk)

4.2 CHARACTERIZATION OF BONE MARROW STEM CELLS

MSC utilization becoming more and more popular due to the capacity of the differentiation towards a needed cell type. The advantage of using MSCs in cartilage tissue engineering was extensively shown for the cells isolated from multiple sources such as bone marrow [210], adipose tissue [211], teeth [212], umbilical cord [213] etc.

In accordance with the standards of the ISCT, identified CD markers should be positive (CD29, CD44, CD73, CD90, CD105, CD146, CD166 and STRO-1) and negative (CD11a, CD2, CD31, CD34, CD45, CD117 and HLA-DR) for the cells to be approved as mesenchymal stem cells [55].

Flow cytometry was performed on confluent P2 and P3 cells that were isolated from rat bone marrow. The quantitative expressions (percentage) of CD29, CD31, CD45, CD90 and CD11a were calculated. Data are presented as the mean \pm SDs obtained from the percentage of each CD marker and representative flow histogram are shown in Figure 4.15. It was found that CD29 (99.7 ± 0.16 %) and CD90 (99.82 ± 0.20 %), mesenchymal stem cell markers were positive in expression, while CD31 (2.18 ± 0.18 %), CD45 (1.27 ± 0.11 %) and CD11a (1.36 ± 0.15 %), hematopoietic stem cell markers were negative (Table 4.1). Expressions of cell surface markers showed that isolated cells from bone marrow had properties of mesenchymal stem cells and consistent with the literature [214, 215].

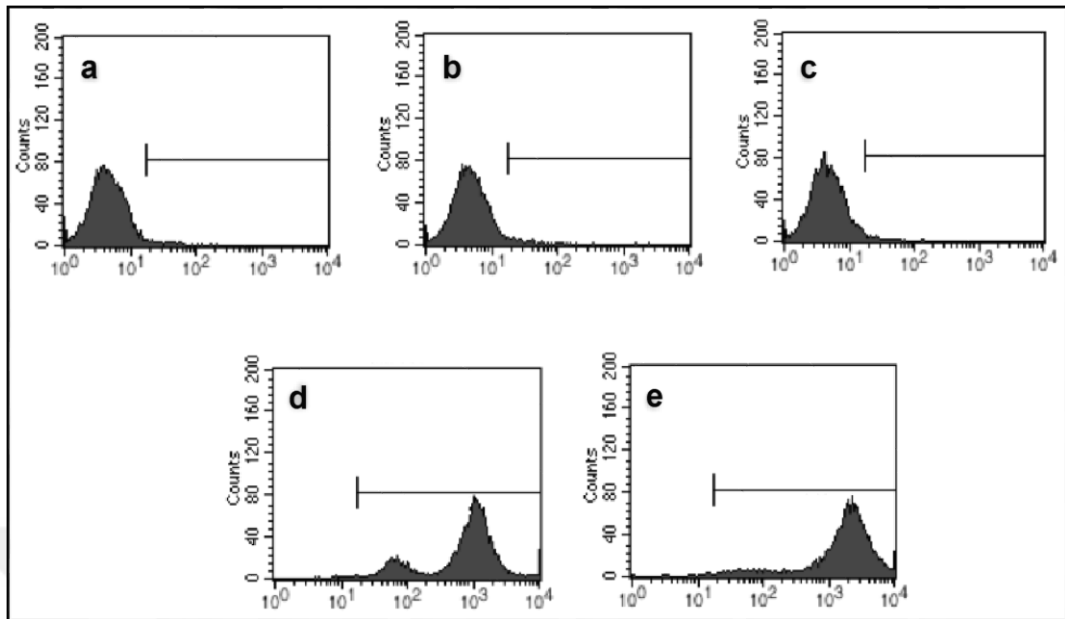


Figure 4.15. Flow cytometry histogram of rBMSC labeled with (a) CD11a, (b) CD 31, (c) CD45, (d) CD29 and (e) CD90. Positive gated cell fractions were indicated on histograms

Table 4.1 Positivity (%) of the CD markers

Antibody	Conjugate	Positivity %
CD11a (-)	FITC	1.36 ± 0.15
CD45 (-)	PE-Cy	1.27 ± 0.11
CD29 (+)	FITC	99.7 ± 0.16
CD90 (+)	FITC	99.82 ± 0.20
CD31 (-)	PE	2.18 ± 0.18

4.3 CELL CONTAINING COACERVATES

There are two strategies that cells can be involved in the tissue engineering system. In the first one, after formation of the scaffolds, cells can be seeded on them. This is very common and easy due to the post processing availability such as lyophilization, removal of the toxic molecules, sterilization etc. to the prepared scaffold before seeding. In the second one, cells can be encapsulated while preparing the scaffold. This is a very competitive way because of the selection of convenient materials and mild processing conditions. However, cell encapsulation has been a very promising way that it takes place in tissue engineering

applications for various type of tissues. Typically hydrogels are used for encapsulation of the cells from natural polymers such as chitosan [216], hyaluronic acid [217], fibrin [218], collagen and alginate [219]. In our system, we generated coacervates using both chitosan and hyaluronic acid biopolymers to apply cell seeding and cell encapsulation strategies.

4.3.1 Bright Field and Fluorescent Microscopy

Complex coacervation of HA and CHI biopolymers established semi-opaque scaffolds. Figure 4.16 shows bright field microscopy images of cell encapsulated coacervates.

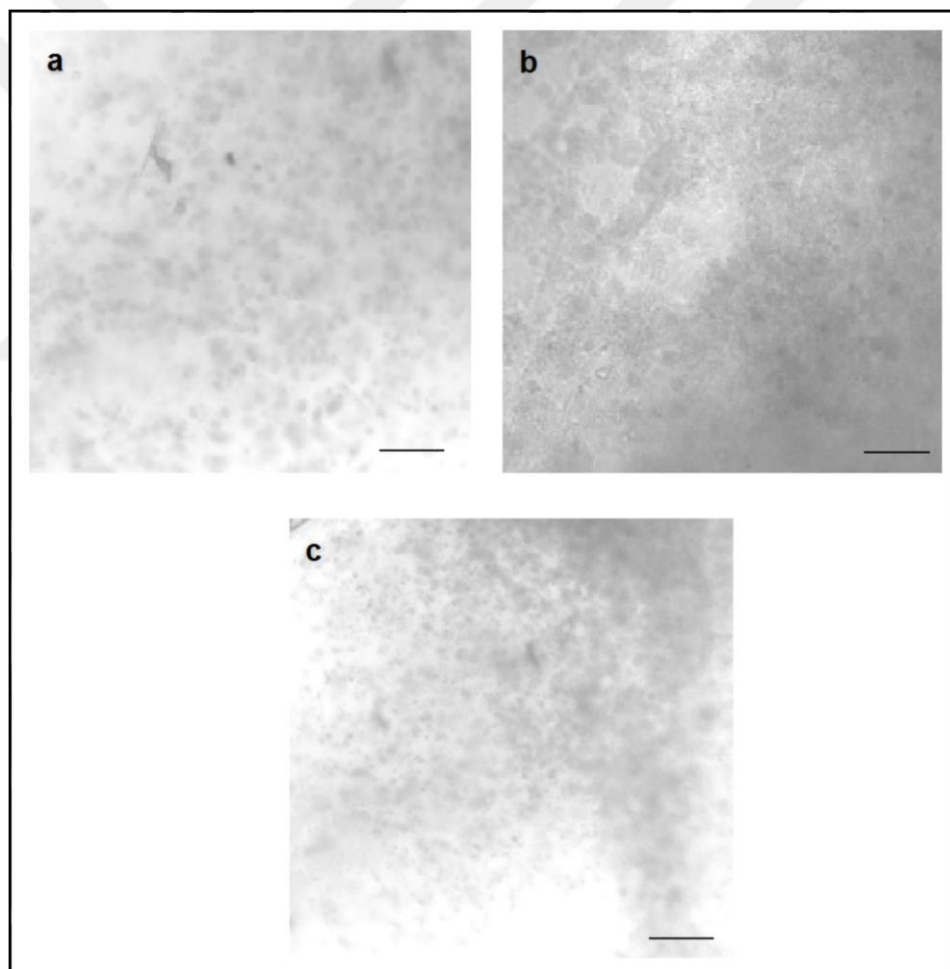


Figure 4.16. Bright field microscopy images of MSC encapsulated in (a) HA/CHI-Cl in CaCl_2 (b) HA/CHI-Cl in NaCl and (c) HA/CHI-G prepared in NaCl solutions after 1 day of incubation. The scale bars represent 500 μm

In order to control the successive cell seeding or cell encapsulation and evaluate the cell distribution by microscopy, fluorescently pre-labelled cells by CM-DiI dye were used. CM-DiI dye is retained in living cells through several generations and transferred to daughter cells; therefore, useful for long-term labelling [220]. CM-DiI labeled cells seeded on the coacervates or encapsulated inside the coacervates were detected using fluorescence microscope (Figure 4.17). Spread and well distributed cells were observed for encapsulated samples (500,000 cells/coacervate, Figure 4.17 a-c). Less number of cells (100,000 cells/coacervate) were seeded on the coacervates to prevent cell leakage and those cells remained mostly around the center of the coacervate surface (Figure 4.17 d-f).



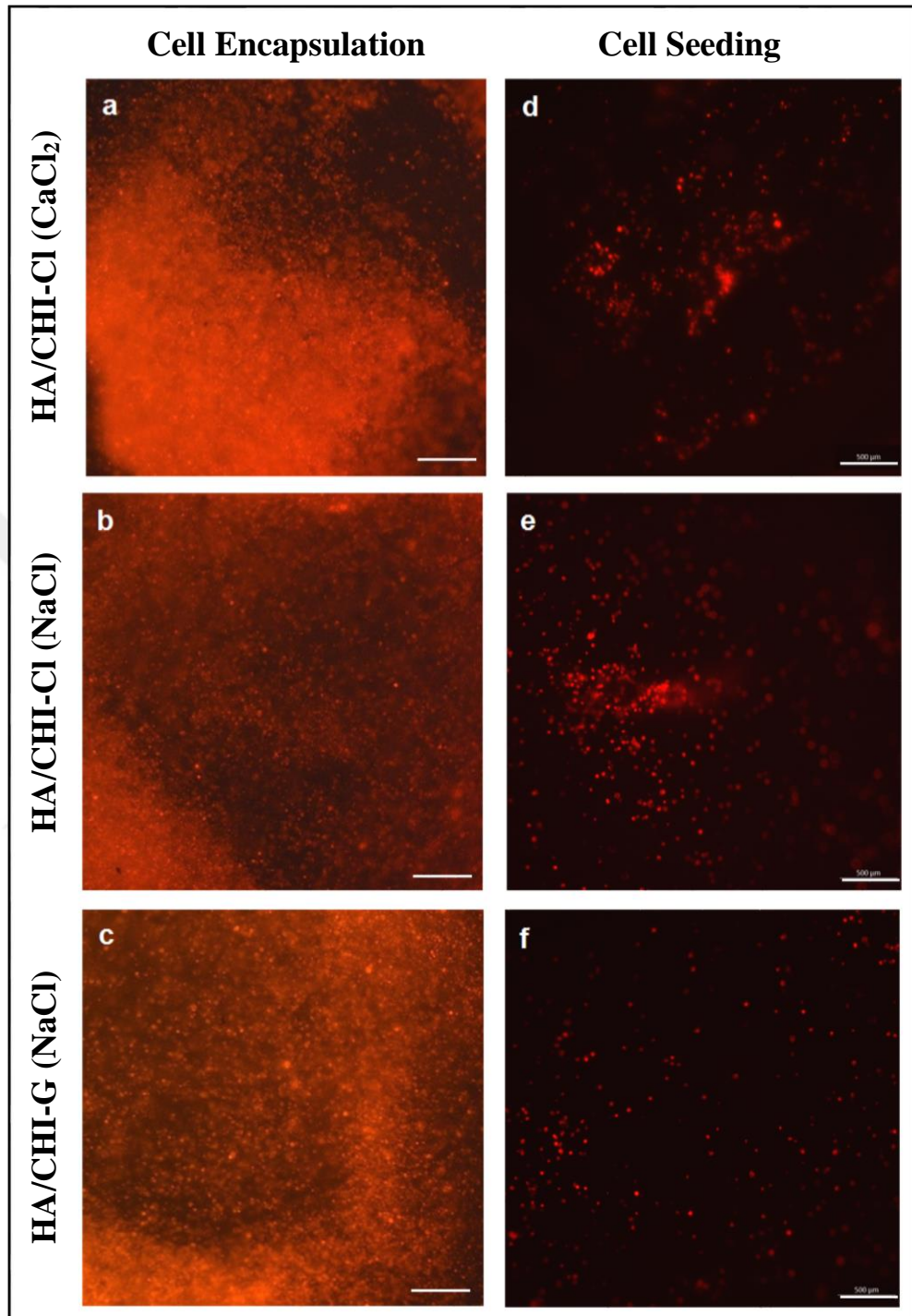


Figure 4.17. Fluorescent microscopy of CM-Dil-labeled MSCs at first day of incubation for coacervates HA/CHI-Cl and HA/CHI-G prepared using NaCl and CaCl₂ solutions. Left panel (a-c) shows encapsulated cells, right panel (d-f) shows seeded cells. The scale bars represent 500 μm

4.3.2 Scanning Electron Microscopy (SEM)

In addition to the ESEM observations, microstructure of the coacervates and their interactions with cells were also observed by SEM analysis after lyophilization. Both empty (blank) and cell-encapsulated coacervates were evaluated through SEM. Figure 4.18 represents the SEM images of empty coacervates while Figure 4.19 represents the SEM images of cell-encapsulated coacervates.

SEM micrographs showed that pores of the freeze-dried coacervates were much smaller than the native (wet) ones. Which is likely related to the collapse of the pores and structure shrinkage after water removal by lyophilization.

Coacervates prepared using CaCl_2 resulted in smaller pore sizes than that of the ones prepared using NaCl salt solution. The pores of the coacervates prepared using CaCl_2 salt solution were observed around 5-10 μm in diameter (Figure 4.18 a,b), while for the ones prepared using NaCl salt solution, the pore diameters were distributed between the range of 10-30 μm for both HA/CHI-Cl (Figure 4.18 c,d) and HA/CHI-G coacervates (Figure 4.18 e,f). This could be attributed to the more hydrated behaviour of the coacervates prepared using CaCl_2 salt solution.

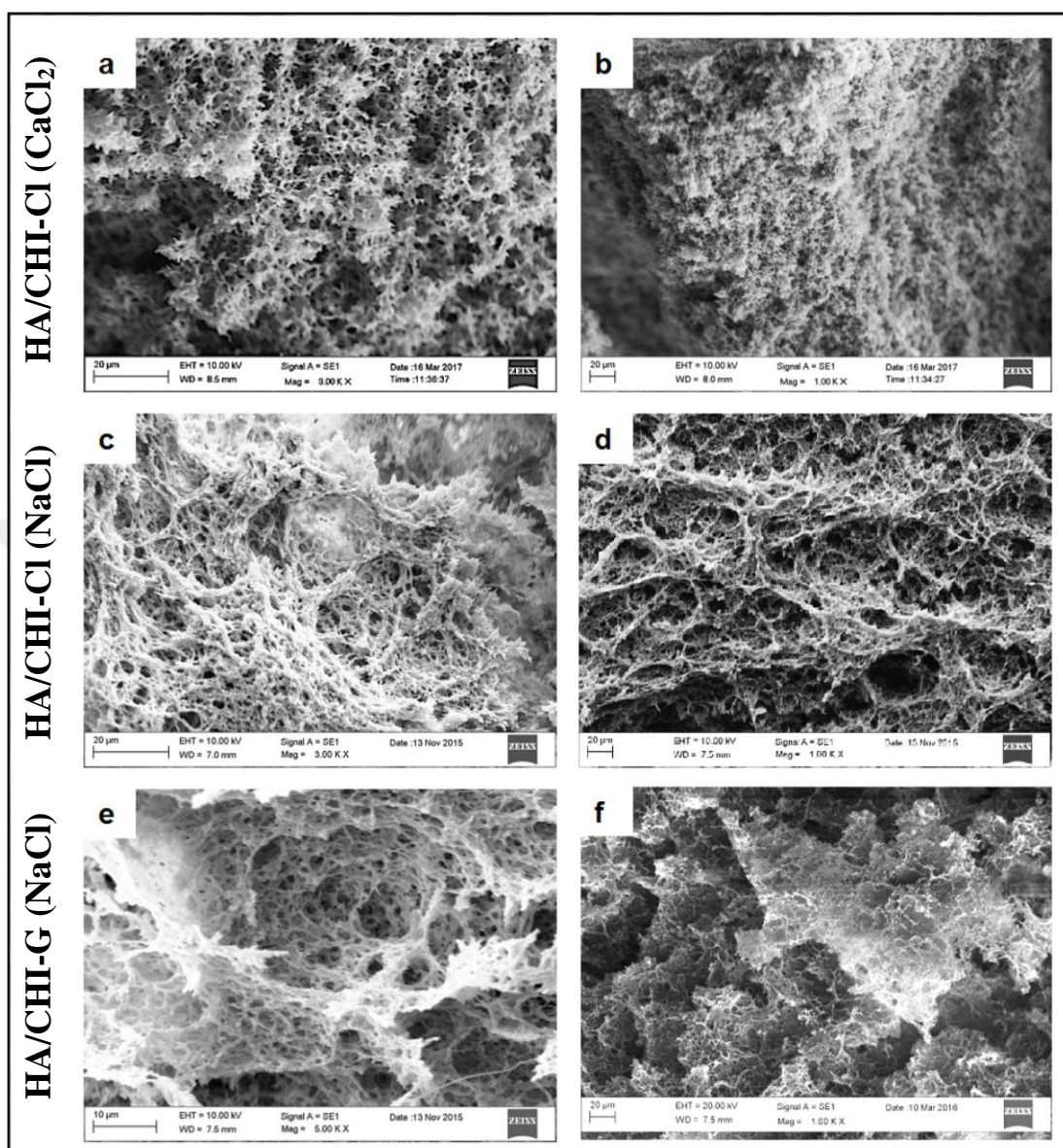


Figure 4.18. Scanning electron microscopy images of HA/CHI-Cl coacervates prepared in (a,b) CaCl₂, (c,d) NaCl and (e,f) HA/CHI-G coacervate prepared in NaCl solutions, original magnifications were: (a,c,e) 3.00 K \times ; (b,d,e) 1.00 K \times

In a recent review, the cell encapsulated scaffolds having pore sizes larger than 10 μm were shown to allow adequate gas exchange, nutrient transportation and removal of cellular wastes in addition to maintaining viability of those cells [221]. There were minor differences in pore sizes among the coacervates; therefore, all coacervates had highly porous and interconnected network structure that would support cell survival. It should be noted that it was hard to distinguish cells from polymer networks in SEM images so arrows were used to indicate cells in the Figure 4.19. We can conclude that, the cells were well

embedded within the coacervates, maintained their structural integrity and showed spread morphology after 3 days of incubation. Furthermore, the degradation profiles (see part 4.1.8) could enhance the migration and proliferation of the cells inside the coacervates for the increased cultivation time points.

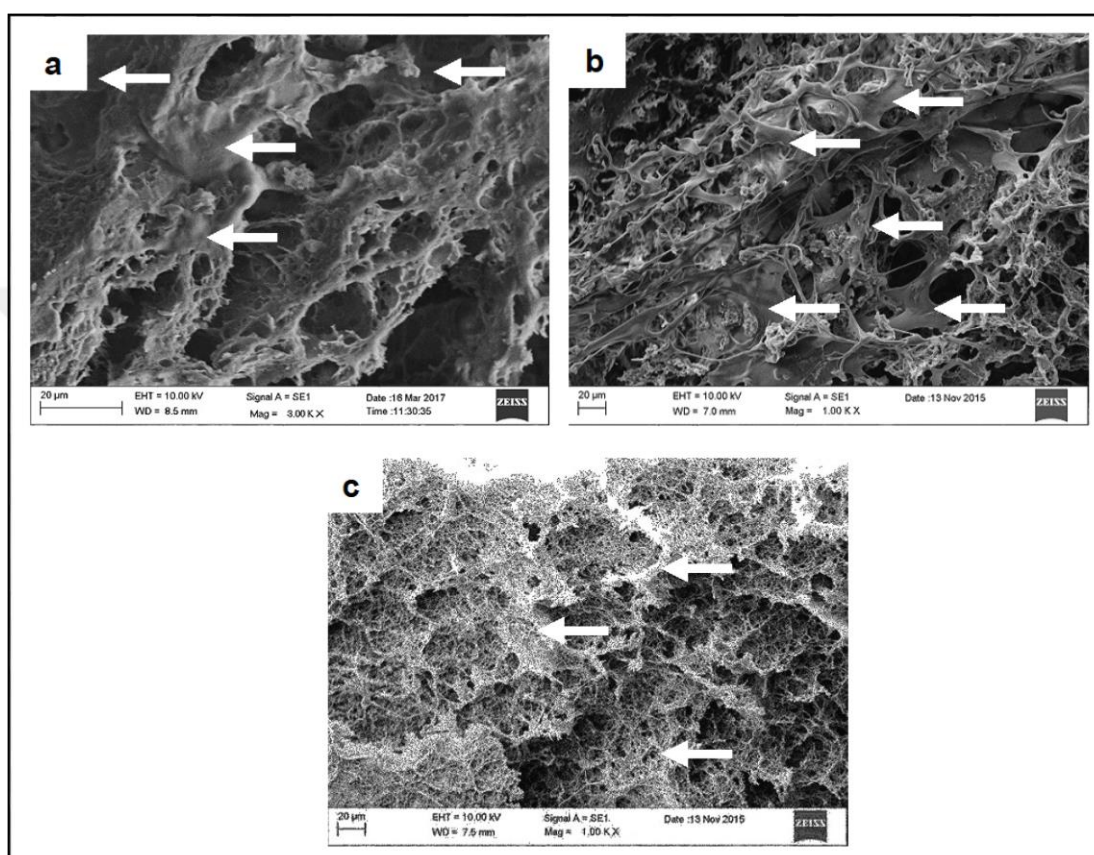


Figure 4.19. Scanning electron microscopy images of cell encapsulated HA/CHI-Cl coacervates prepared in (a) CaCl_2 , (b) NaCl and (c) HA/CHI-G coacervate prepared in NaCl solutions after 3 days of incubation, original magnifications were: (a) 3.00 K \times ; (b,c) 1.00 K \times . Arrows indicate cells

4.3.3 LIVE/DEAD Cell Viability Assay

To assess the HA/CHI coacervates as a cell feasible system, the rBMSCs were first labeled with CM-DiI dye and successive seeding or encapsulation was shown in part 4.3.1. This time isolated cells directly without pre-labeling seeded or encapsulated and examined

whether the polymers (or by-products) or encapsulation process affected the viability and morphology of the cells throughout the incubation time.

To qualitatively visualize the living and dead cells, live/dead assay staining was applied to rBMSCs seeded or encapsulated in the coacervates over three weeks of culture period. In addition to viability, this staining was also used for visualizing the cellular shape and membrane integrity [222]. This assay incorporates the fluorescent dyes calcein-AM and ethidium homodimer-1 (EthD-1). Live cells were distinguished from dead cells by measuring plasma membrane integrity and intracellular esterase activity. By using this assay, cells within the coacervates were imaged as in green color (alive) or red color (dead).

To quantitatively estimate the living and dead cells, 3 different zones were processed after calculating the number of green and red spots using the ImageJ software. The ratio (cell-viability percentage) of the number of live cells to the number of total cells was calculated.

4.3.3.1 Cell Seeded Coacervates

Live dead assay was first applied to rBMSCs that were seeded on the prepared coacervates to control their attachment and survival. Assay was applied on the incubation days of 1, 7, 14 and 21 to the HA/CHI-G (Figure 4.20 a-d), HA/CHI-Cl (Figure 4.20 e-h) coacervates prepared in NaCl and HA/CHI-Cl coacervate prepared in CaCl₂ (Figure 4.20 i-l) salt solutions.

Live dead staining studies showed that after 24 hour, seeded cells were highly alive with round morphology. Cell viabilities were around $86 \pm 3.4 \%$, $87 \pm 5.5 \%$ and $89 \pm 4.9 \%$ (Figure 4.22 a) for coacervates HA/CHI-Cl (NaCl), HA/CHI-G (NaCl) and HA/CHI-Cl (CaCl₂), respectively. Seeded cells exhibited a normal cellular morphology and maintained a survival level above 88 % after 3 weeks of incubation (Figure 4.20). We can conclude that both considering the live cell percentage and qualitative images, coacervates did not contain any toxic or harmful by-products and supported cell adhesion and spreading at the following time points that the cells could highly survive on those coacervates.

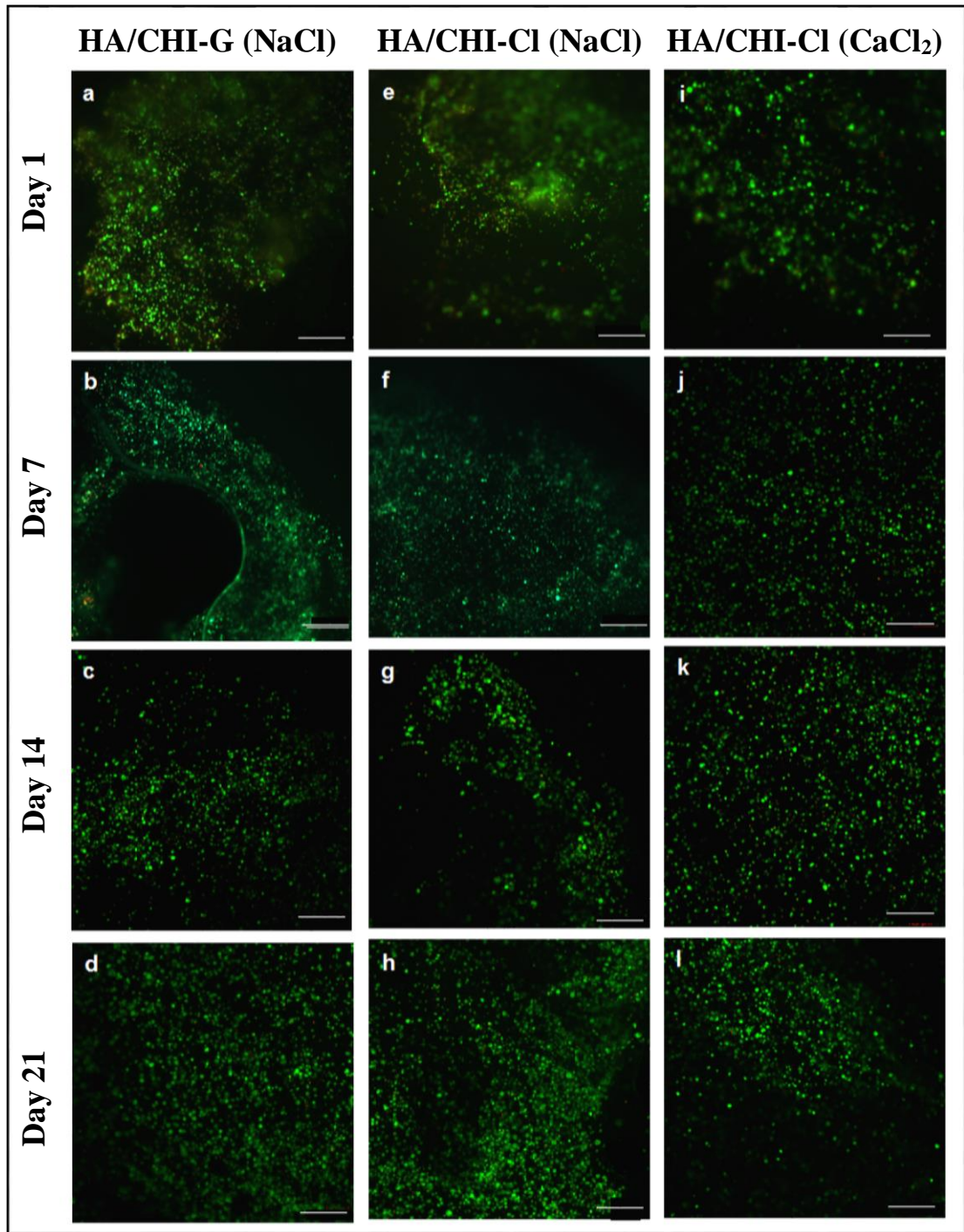


Figure 4.20. Images of rBMSCs seeded coacervates after LIVE/DEAD assay analysis. It represents the cell viability on coacervates prepared using (a-d) HA/CHI-G in NaCl, (e-h) HA/CHI-Cl in NaCl and (i-l) HA/CHI-Cl in CaCl₂ solutions, after (a,e,i) Day 1; (b,f,j) Day 7; (c,g,k) Day 14 and (d,h,l) Day 21. Living cells were stained by calcium-AM (green), and dead cells were stained by ethidium homodimer (red). The scale bars represent 200 μ m

4.3.3.2 Cell Encapsulated Coacervates

This time, live dead assay was applied to rBMSCs that were encapsulated inside the coacervates to control their survival after coacervation process and conditions. Stained rBMSCs inside coacervates were shown in Figure 4.21 as HA/CHI-Cl coacervates prepared in CaCl₂ salt solution (Figure 4.21 a-d) and NaCl salt solution (Figure 4.21 e-h), HA/CHI-G coacervates prepared in NaCl salt solution (Figure 4.21 i-l) for up to 21 days of incubation.

Figure 4.21 a,e,i show stained rBMSCs in coacervates after one day post-encapsulation. Overwhelming majority of the rBMSCs survived after the coacervation process. Cell viabilities were around $90 \pm 2.7 \%$, $93 \pm 0.8 \%$ and $86 \pm 0.9 \%$ (Figure 4.22 b) for coacervates HA/CHI-Cl (CaCl₂), HA/CHI-Cl (NaCl) and HA/CHI-G (NaCl), respectively. Significant difference ($p < 0.05$) was only observed between the coacervates prepared in NaCl for the first day. We can say that the encapsulation process did not affect the cells and cells could remain alive in those conditions such as pH and I of the preparation solution in addition to centrifugation time.

Based on stainings at different time points, rBMSCs, which initially had a rounded morphology, started to extend their ECM after 7 days of incubation as shown in Figure 4.21 b,f,j. Few dead cells appeared after 14 days of incubation; however, the number of cells observed alive were clearly much higher ($\geq 84 \%$). Moreover, cell viability observed in HA/CHI-Cl both in NaCl ($p < 0.05$) and CaCl₂ salts ($p < 0.01$) were found significantly higher than that of HA/CHI-G coacervate. After 21 days of incubation (Figure 4.21 d,h,l), cells perceptibly exhibited a more fibroblast-like morphology when compared to earlier time points, while still showing good cell viability levels ($\geq 88 \%$) with hardly any detectable cell death. It can be concluded from those results that coacervates enabled encapsulation of rBMSCs efficiently without decreasing the viability and encapsulated cells easily accessed to nutrient and oxygen through the porous HA/CHI coacervate microstructure.

These results show that coacervation system could provide a favourable microenvironment to support the cultivation and proliferation of rBMSCs using HA and CHI polymers for *in vitro* cultures.

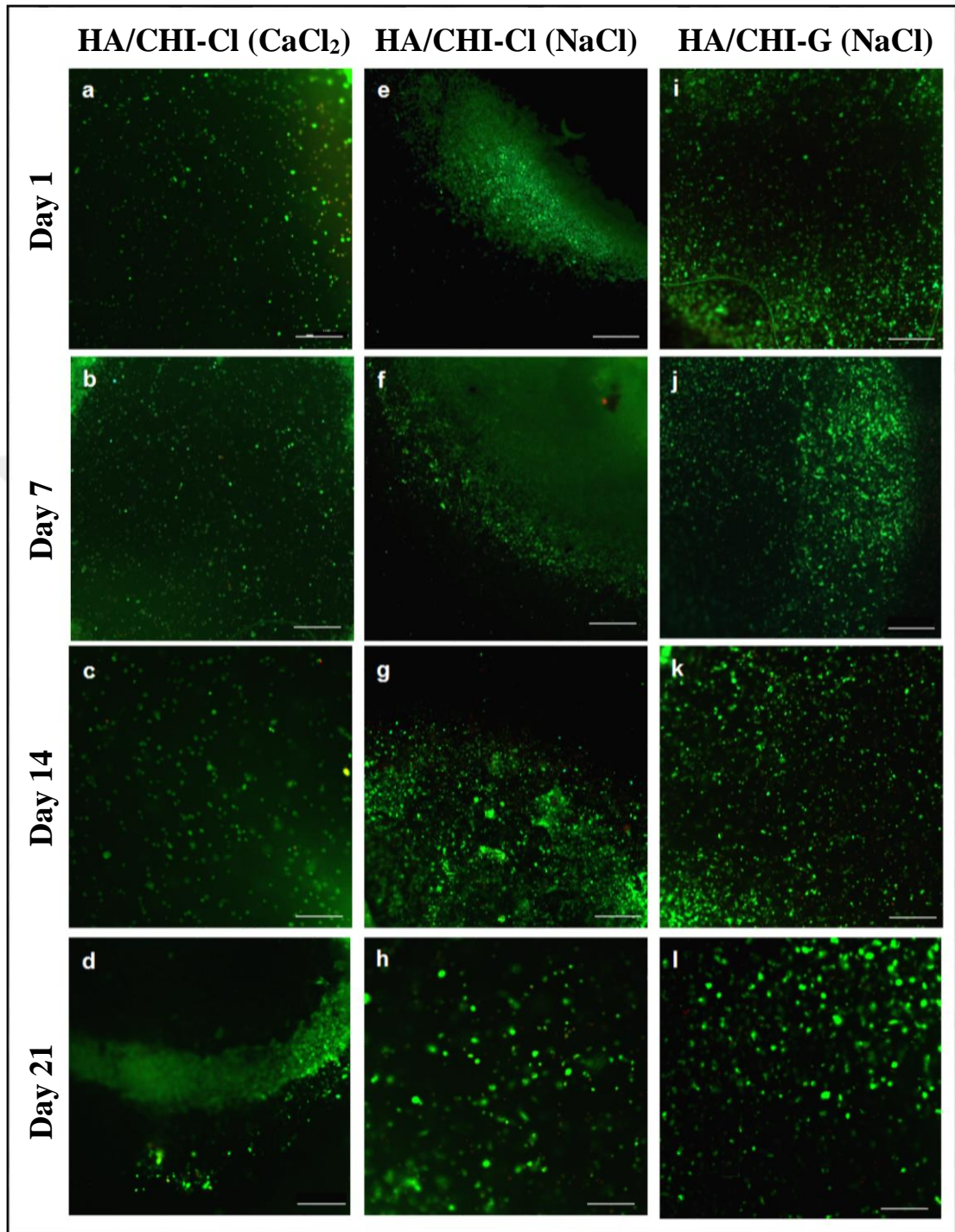


Figure 4.21. Images of rBMSCs encapsulated coacervates after LIVE/DEAD assay analysis. It represents the cell viability inside HA/CHI-Cl coacervates prepared using (a-d) CaCl₂ and (e-h) NaCl, HA/CHI-G coacervates prepared using (i-l) NaCl solutions, after (a,e,i) Day 1; (b,f,j) Day 7; (c,g,k) Day 14 and (d,h,l) Day 21. Living cells were stained by calcium-AM (green), and dead cells were stained by ethidium homodimer (red). The scale bars represent 200 μ m

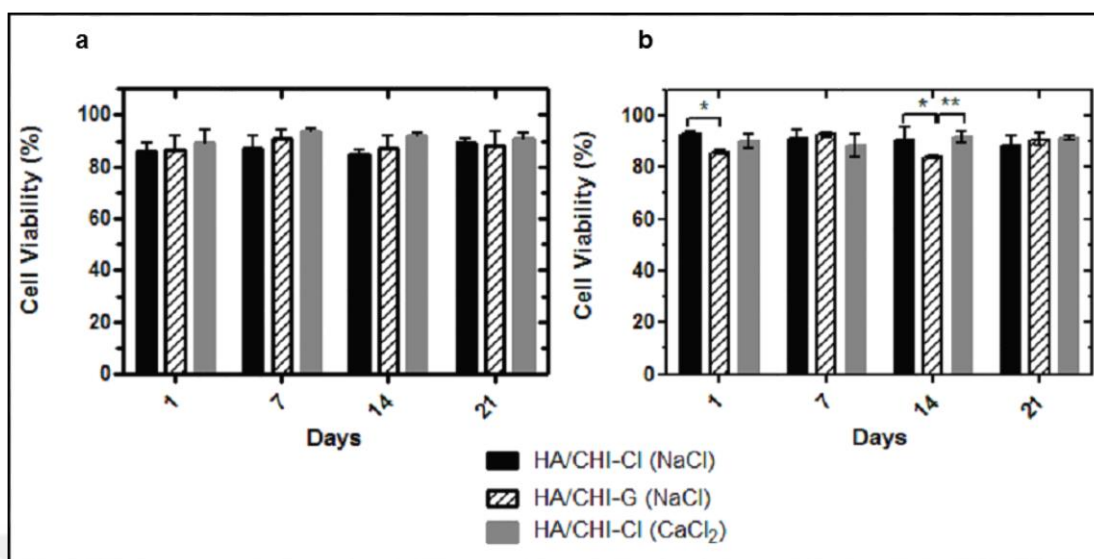


Figure 4.22. The graphs show the mean values \pm standard deviations for live cells from 3 different zones for each experimental group, (a) Cell seeded, (b) Cell encapsulated coacervates. ** $p < 0.01$ and * $p < 0.05$ showed statistically significant differences

4.3.4 Immunofluorescence Staining to Analyze Cell Morphology

In cell homeostasis, cytoskeleton organization has a fundamental role such as showing an apoptotic or proliferative signs [222]. It is a convenient way to control cellular morphologies in addition to live dead stainings.

Immunofluorescence stainings were used to study cytoskeleton organization of the cells, i.e. DAPI stained the nucleus in blue while the Alexa fluor 568 phalloidin stained the actin filaments in red color. Cellular structure and spreading were demonstrated by confocal microscopy after phalloidin and DAPI stainings.

Possessing cell adhesion moieties are important features of scaffolds. They provide attachment and spreading for the cells. RGD (arginine-glycine-aspartic acid) is the most commonly incorporated cell adhesion motif [223] but HA and CHI polymers are lack of RGD sequences. However, HA polymer is included in our coacervates and it interacts with CD44 and RHAMM cell surface receptors that is advantageous for cell attachment, proliferation and differentiation [224] by activation of the various signalling pathways [225-227].

4.3.4.1 Cell Seeded Coacervates

Figure 4.23 shows the confocal microscopy images of cell seeded coacervates after 3 days of incubation. After cell seeding process on the tissue culture plates, rBMSCs exhibited spread morphology; however, after 3 days later of seeding on the coacervates, rBMSCs showed predominantly rounded morphology (Figure 4.23 a-c) and only small amount of the cells started to extend their filopodia. Nevertheless, our observations were consistent with the reports about the seeded MSCs [228, 229] on the soft (gel-like) scaffolds thus producing smaller and less focal adhesions than that of those on harder scaffolds [230].

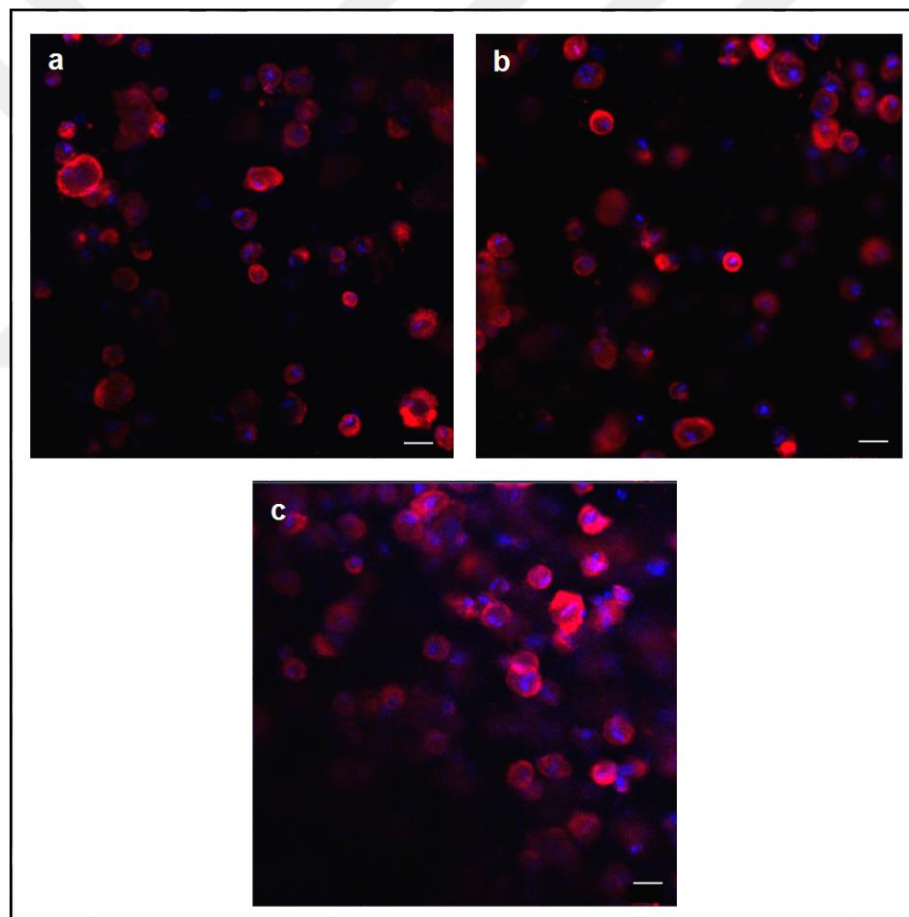


Figure 4.23. Phalloidin/DAPI stainings of rBMSCs seeded on HA/CHI-Cl coacervates prepared with (a) CaCl_2 , (b) NaCl salt solutions, (c) HA/CHI-G coacervate prepared with NaCl salt solution after 3 days of incubation. The scale bars represent 20 μm for images

4.3.4.2 Cell Encapsulated Coacervates

Confocal microscopy images of cells encapsulated inside the coacervates are shown in Figure 4.24 a-c (after 3 days of incubation) and Figure 4.24 d-f (after 21 days of incubation). Cellular morphologies were recorded at lower and higher magnifications.

Following the encapsulation process, cells preserved their spherical morphology up to 72 hours of incubation for all coacervate samples without visible cellular protrusions (Figure 4.24 a-c). Unless stimulated by special inducers like growth factors etc., cells gained a well-spread, natural MSC morphology with distinguishable F-actin filaments under normal circumstances after 21 days of incubation (Figure 4.24 d-f). Nevertheless, when culturing the cell encapsulated coacervates in chondrogenic differentiation media, normally observed well-spread morphology was affected and turned into be more rounded and larger appearance (see below part 4.3.5.1).

Moreover, after 21 days of biodegradation, the coacervate matrix established available spaces for supporting cell spreading by filopodia growth and extension inside the scaffolds. Multi-dimensional growth of the cellular network and cell to cell interaction as observed from Figure 4.25 would be a desirable property for the growing/healing tissue integration [231]. Distinctive differences among the coacervate samples could not be observed even from the images with higher magnification as shown in Figure 4.25.

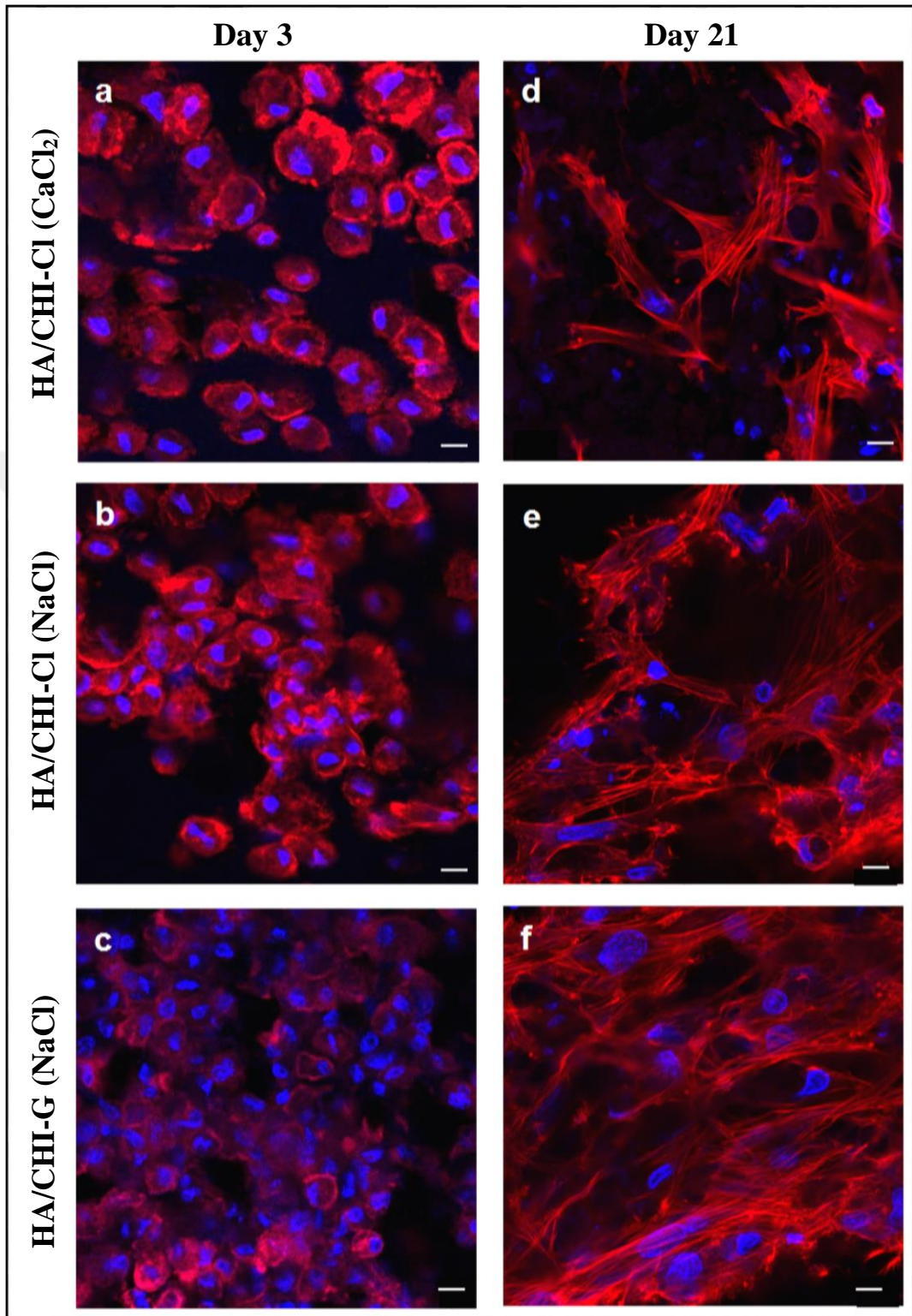


Figure 4.24. Images of encapsulated rBMSCs stained with phalloidin/DAPI representing the cell morphology inside HA/CHI-Cl cocervates prepared with (a,d) CaCl₂, (b,e) NaCl, (c,f) HA/CHI-G cocervates prepared with NaCl solutions after (a-c) 3 days, (d-f) 21 days of incubation (10× magnification). The scale bars represent 10 μm

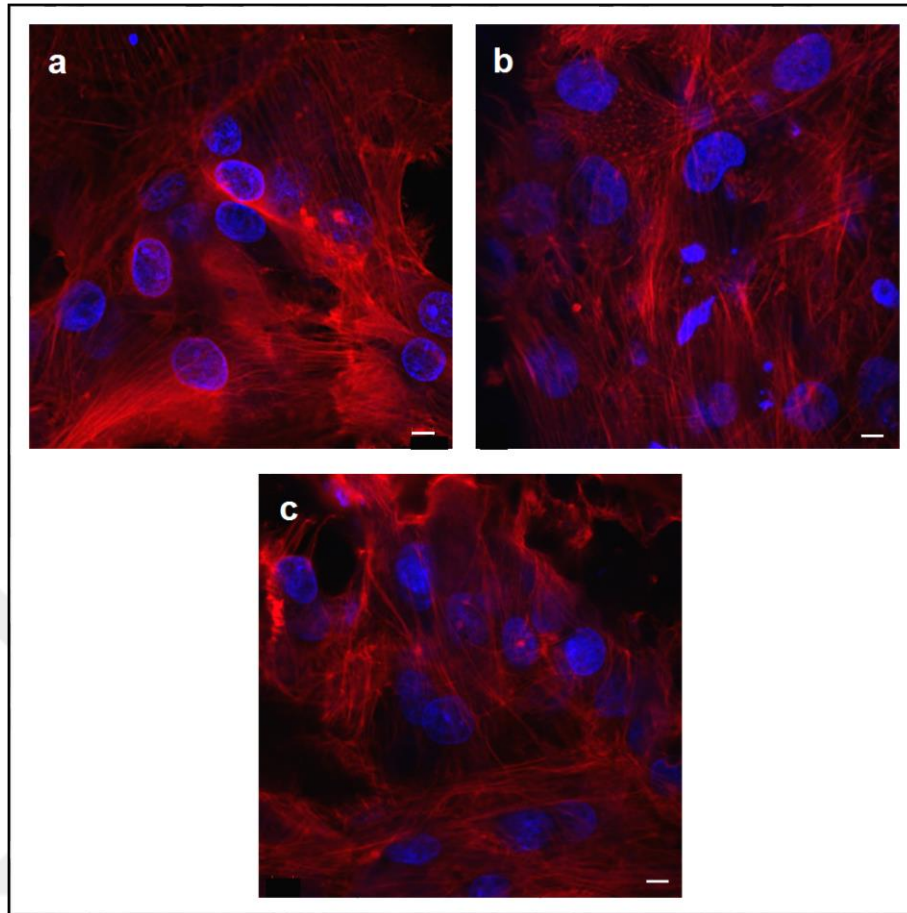


Figure 4.25. Images of encapsulated rBMSCs stained with phalloidin/DAPI representing the cell morphology inside HA/CHI-Cl coacervates prepared with (a) CaCl_2 , (b) NaCl , (c) HA/CHI-G coacervate prepared with NaCl solutions after 21 days of incubation (40 \times magnification). The scale bars represent 5 μm

Both cell seeding and encapsulation studies were promising due to the high cell survival and good cellular morphology results for the various tissue engineering applications but our aim was to investigate the chondrogenic differentiation capacity of the prepared coacervates, so differentiation experiments were continued with cell encapsulation strategy. Spherical morphology of the encapsulated cells has been shown to be more easily maintained and chondrogenic differentiation could be promoted by this attitude [232].

Also, we decided to reduce the experimental groups due to having similar results by omitting coacervates prepared in CaCl_2 salt solution. HA/CHI-Cl and HA/CHI-G coacervates prepared in NaCl salt solution were used for further chondrogenic differentiation experiments.

4.3.5 *In Vitro* Chondrogenic Differentiation

MSC chondrogenesis inside HA/CHI coacervates was promoted with a chondrogenic differentiation media formulation that includes TGF- β 1 [233] and dexamethasone [234]. Those components have already shown to induce chondrogenesis using different cell types or scaffolds for tissue engineering applications [235, 236].

In literature, chondrogenic differentiation is characterized in four stages, (i) cell commitment takes place in 0-48 hours, (ii) those committed cells start proliferation between 1-10 days, (iii) chondrogenic differentiation of the committed cells are observed by cartilage-specific gene expressions between 7-28 days and (iv) differentiated cells start cartilage-specific matrix production between 10-42 days [237].

Chondrogenic differentiation is qualified by the production of cartilage-specific markers, such as collagen type II (COL2A1), aggrecan (ACAN) and sulfated glycosaminoglycans (sGAG). Furthermore, SOX9 is considered to be the main chondrogenic transcription factor that promotes BMSCs to synthesize collagen type II and aggrecan [238, 239] during limb bud development.

In our study, prepared coacervate samples were examined for the expression of chondrogenic markers by real-time polymerase chain reaction (SOX9, COL2A1 and ACAN) and immunofluorescence staining (COL2A1 and ACAN).

4.3.5.1 *Immunofluorescence Staining*

Cartilage matrix is mainly constituted from collagen and proteoglycans. Collagen type II is the most abundant protein and aggrecan is the primary proteoglycan found in articular cartilage [18]. Those proteins are the major contributors and essential for the maintenance of a healthy ECM [240]. Immunofluorescence was used for the qualitative evaluation of chondrogenic differentiation and matrix synthesis was detected by the presence of collagen type II and aggrecan after 7, 14, 21 and 30 days of induction.

All coacervates were stained for antibodies against aggrecan (red), collagen type II (green) and cell nuclei (blue) (Figure 4.26 and Figure 4.27). Collagen type II immunofluorescence was observed strongly even after 7 days of induction in both HA/CHI-CI and HA/CHI-G

coacervates (Figure 4.26 a,b); however, only low level of aggrecan staining was observed after 7 days of induction. Increased quantity of ECM proteins was detected after especially 14 days of chondrogenic induction by the more intense immunofluorescence stainings (Figure 4.26 c,d). Both coacervates were positive for COL2A1 signal but ACAN production was still very slight. Furthermore, aggrecan staining in HA/CHI-G coacervates was also greater than that of in HA/CHI-Cl coacervates. After 21 days of induction, stained rBMSCs resembled the typical lacunae embedded chondrocytes that were large and round in phenotype (Figure 4.27 a-d). Collagen type II and aggrecan proteins were mainly distributed within ECM surrounding the cells and accumulated mostly in the pericellular region. In general immunofluorescence staining results indicated that, rBMSCs encapsulated in HA/CHI-G coacervates were observed to have more chondrogenic potential than that of HA/CHI-Cl coacervates.

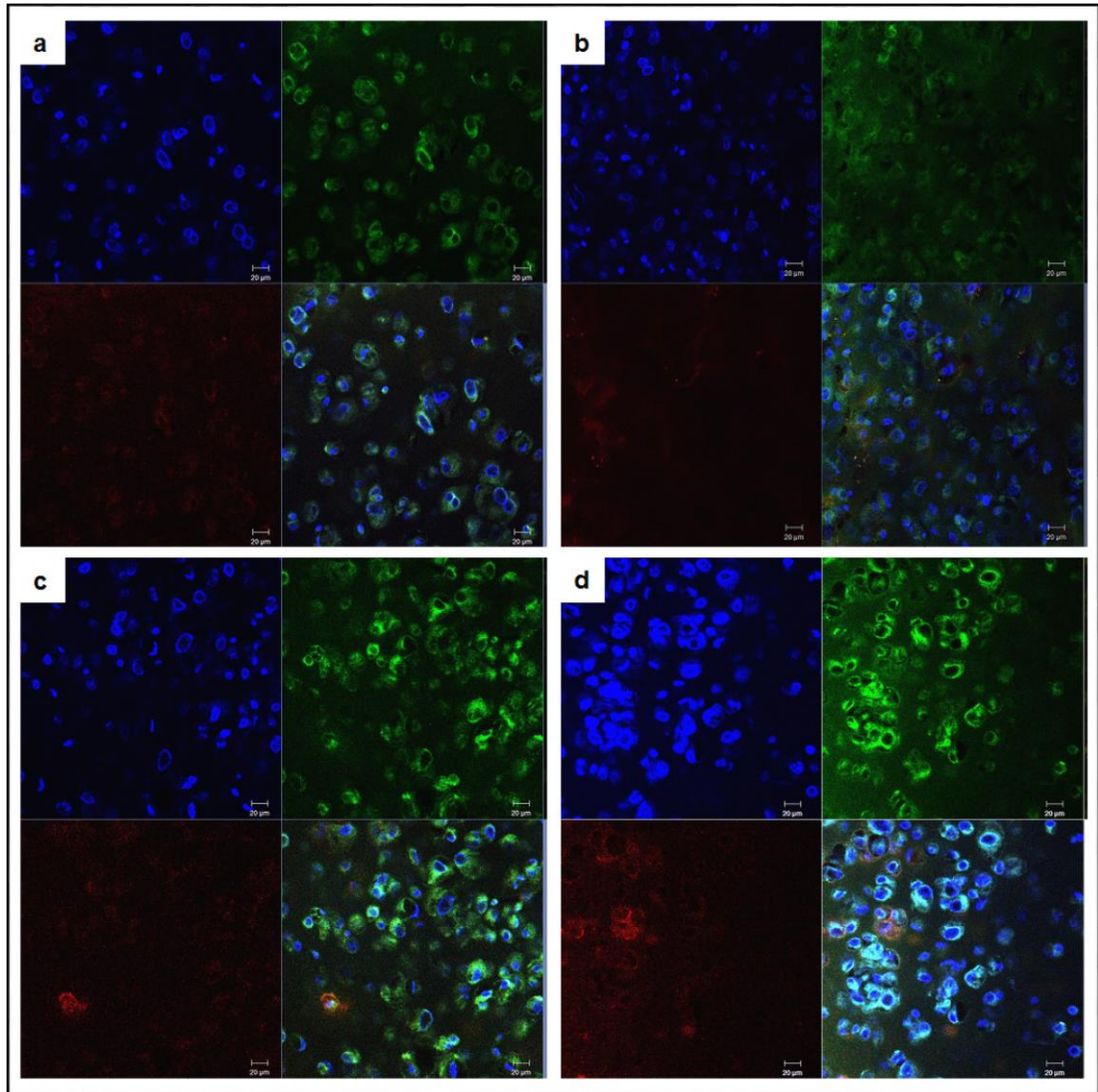


Figure 4.26. Collagen type II, aggrecan and cell nuclei immunostaining images of rBMSCs encapsulated in (a,c) HA/CHI-Cl and (b,d) HA/CHI-G coacervates after chondrogenic induction of (a,b) 7 days and (c,d) 14 days. All images were taken at magnification of 40 \times and scale bars represent 20 μ m. COL2A1 (green), ACAN (red) and cell nuclei (blue)

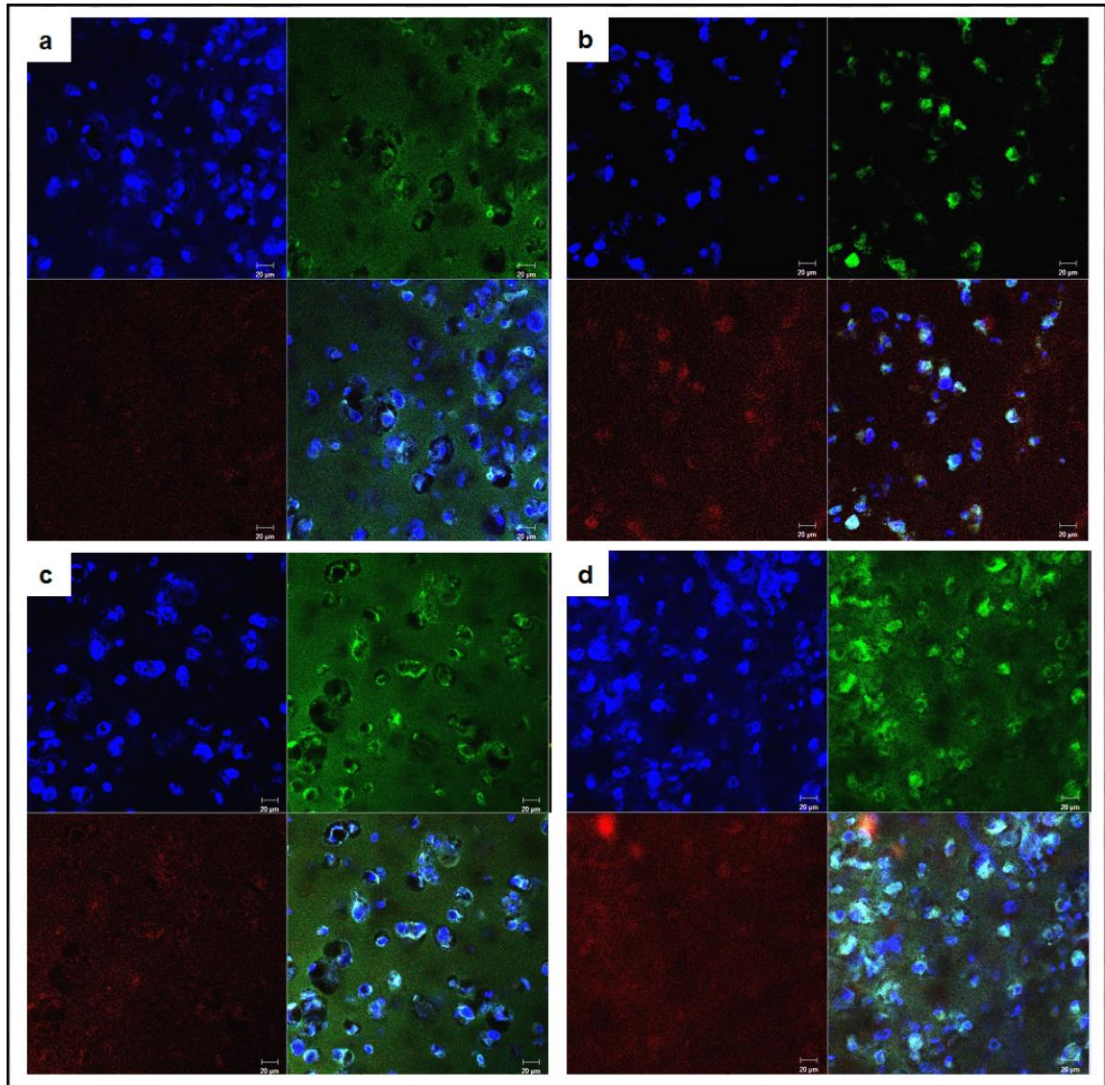


Figure 4.27. Collagen type II, aggrecan and cell nuclei immunostaining images of rBMSCs encapsulated in (a,c) HA/CHI-C1 and (b,d) HA/CHI-G coacervates after chondrogenic induction of (a,b) 21 days and (c,d) 30 days. All images were taken at magnification of 40 \times and scale bars represent 20 μ m. COL2A1 (green), ACAN (red) and cell nuclei (blue)

4.3.5.2 Gene Expression Profiles

In addition to immunofluorescence staining, chondrogenic gene expressions (SOX9, COL2A1 and ACAN) were quantitatively determined by q-PCR from the rBMSCs encapsulated coacervates (HA/CHI-C1 and HA/CHI-G) cultured under chondrogenic differentiation media (14 and 21 days of incubation) and growth media (21 days of incubation).

Gene expression profiles of rBMSCs encapsulated inside both HA/CHI-Cl and HA/CHI-G coacervates showed an increase in all chondrogenic genes over 2 weeks of cultivation with differentiation media (Figure 4.28 a-c). After 21 days of chondrogenic induction, expression levels from rBMSCs encapsulated inside HA/CHI-Cl coacervates were up-regulated for COL2A1 (1.7 fold, $p < 0.01$), ACAN (1.1 fold) and down-regulated for SOX9 (0.7 fold) when compared to the values for day 14. If the same data was compared for HA/CHI-G coacervates, all gene expressions were up-regulated for 21 days of induction, as COL2A1 (1.2 fold), ACAN (1.4 fold) and SOX9 (1.1 fold).

Expression levels from rBMSCs encapsulated inside HA/CHI-G coacervates were higher than HA/CHI-Cl coacervates at all time points. In more detail, after 14 days of chondrogenic induction of HA/CHI-G coacervates, expression of COL2A1 (1.9 fold; $p < 0.01$), ACAN (1.7 fold; $p < 0.05$), SOX9 (1.1 fold) and after 21 days of induction similarly, COL2A1 (1.3 fold; $p < 0.05$), ACAN (2.1 fold; $p < 0.01$), SOX9 (1.7 fold) were higher, respectively when compared to HA/CHI-Cl coacervates. Furthermore, the enhancement of mRNA expressions of the cartilage-specific markers during the chondrogenic induction in HA/CHI-G coacervate was consistent with the results of immunofluorescence staining. This can be interpreted as the potential chondrogenic effect of HA/CHI-G coacervate on rBMSC differentiation.

SOX9 is a regulatory transcription factor and its expression starts at early stages and continues in all stages of chondrogenesis. In literature, TGF- β has been shown to increase SOX9 expression and consequently chondrogenic differentiation potential [241]. It activates the cartilage specific gene expressions, especially COL2A1. After that activation, chondrogenic cells begin to express ACAN, collagen types IX and XI.

In our study we did not control the early SOX9 expression levels. After 14 days of induction, high level of SOX9 expression was observed but one week later, expression levels were down-regulated. In another study, our findings were in agreement with their results as highest SOX9 expression level was shown at 14 days of incubation [242].

Interestingly, all of the coacervates (HA/CHI-Cl and HA/CHI-G) with (+) and without (-) induction exhibited chondrogenic differentiation after 3 weeks of culture (Figure 4.28 d); however, the results of q-PCR showed that the expression levels of COL2A1, ACAN and SOX9 in both coacervates with induction (HA/CHI-Cl (+) and HA/CHI-G (+)) were

significantly higher than those of without induction (HA/CHI-Cl (-) and HA/CHI-G (-)) (Figure 4.28 d). In HA/CHI-Cl cocervates with (+) induction, levels of COL2A1, aggrecan and SOX9, were significantly higher as 2 ($p<0.001$), 1.5 ($p<0.01$) and 4.7 ($p<0.001$) fold, respectively than that of same cocervate without (-) induction. Likewise, from HA/CHI-G cocervates with (+) induction, levels of COL2A1, aggrecan and SOX9, were significantly higher as 1.7 ($p<0.001$), 2.4 ($p<0.001$) and 5.8 ($p<0.001$) fold, respectively than that of same cocervate without (-) induction. It can be speculated that rBMSC encapsulation in HA/CHI cocervates (without induction) had an influence on cell commitment but differentiation media including TGF- β 1 had an additional positive effect on differentiation of the stem cells. It was also reported that Methacrylated HA scaffolds slightly promoted differentiation of encapsulated MSCs to chondrocytes under incubation of growth media [243].

Our quantitative data of cartilaginous gene expressions agreed with the immunostaining results, indicating that both rBMSC encapsulated cocervates had chondrogenesis capability but a better potential was observed for the HA/CHI-G cocervates than that of HA/CHI-Cl ones.

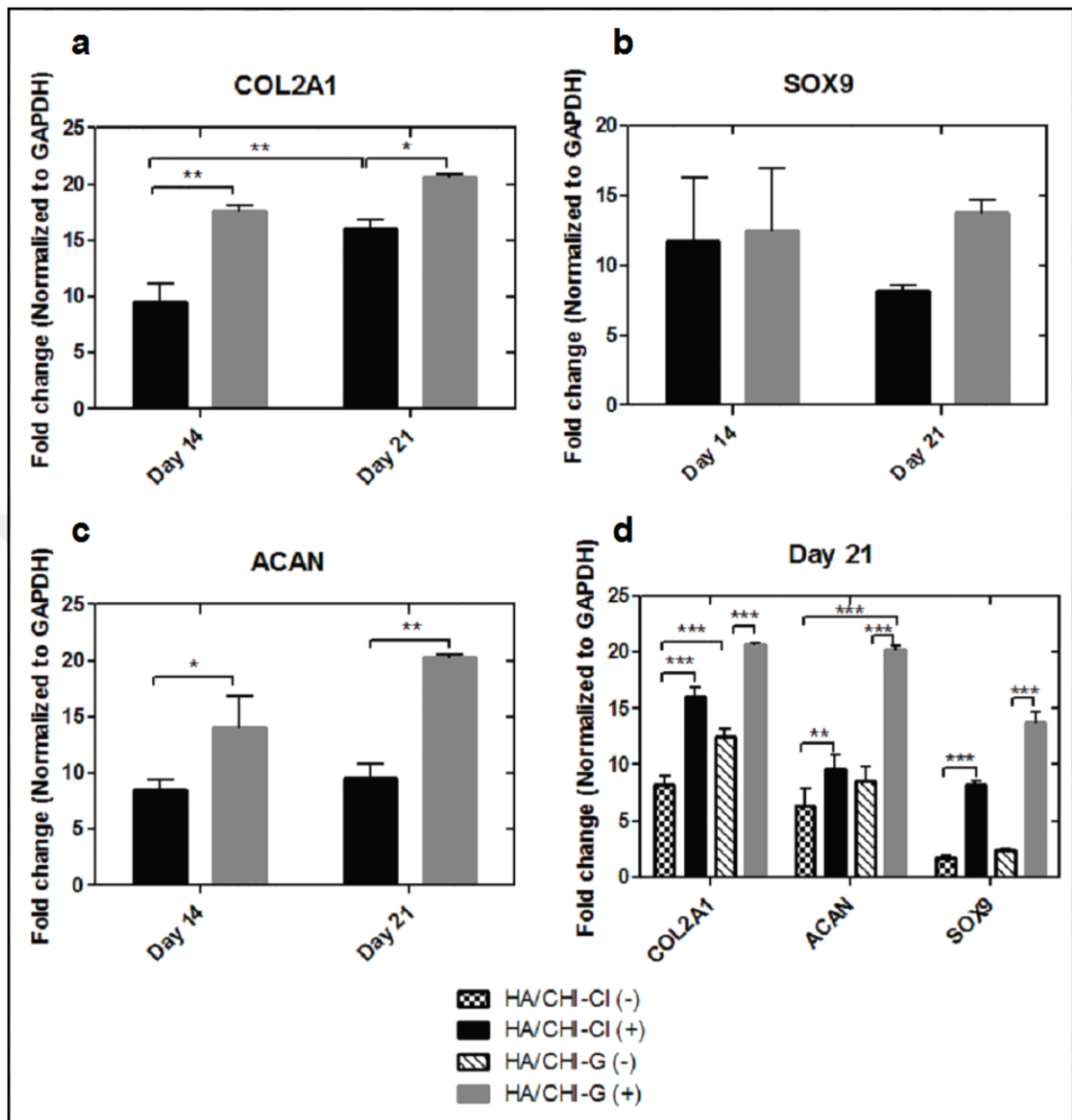


Figure 4.28. Analysis of gene expression levels for the coacervates after cultured in differentiation media (+) for 14 and 21 days (a) COL2A1, (b) SOX9, (c) ACAN, (d) comparison of all gene expressions within the coacervates that were cultured in differentiation (+) and growth media (-) for 21 days. Gene expression was normalized by only cell control and GAPDH was used for housekeeping gene. *** $p < 0.001$, ** $p < 0.01$ and * $p < 0.05$ showed statistically significant differences

5. CONCLUSION

Complex coacervation of oppositely charged biopolymers have become very promising for establishing biodegradable and moldable scaffolds in physiological conditions. Preparation and characterization of the coacervate based scaffolds containing HA and CHI polymers were investigated in this study. In the second part, those scaffolds were used as a cell compatible system and encapsulated rBMSCs in coacervates were further investigated for their chondrogenic differentiation potential.

For characterization purpose, prepared coacervate suspensions were first optimized to find the regions of phase separation and the transition points from coacervation to precipitation. DLS and light microscopy results showed that coacervate suspensions had spherical droplet morphology and good size distributions at the charge ratio of $[-]/[+] = 0.31$ for HA/CHI-C1 and 0.48 for HA/CHI-G system, respectively. Furthermore, to be used as a scaffold, centrifugation was applied to the HA/CHI suspensions and coacervate layers were achieved in both systems. Those scaffolds demonstrated highly porous and viscoelastic nature, consequently advantageous matrix for tissue engineering purposes.

The presented coacervation method also provided an effective protocol to produce scaffolds with cell encapsulation capacity. HA/CHI coacervates were formed under very narrow range of pH (6.25) and ionic strength (300 mM) to be used as a cell available and biocompatible system. rBMSCs were both seeded and encapsulated in HA/CHI-C1 or HA/CHI-G coacervates and those coacervates highly promoted cell viability and spread morphology.

This rBMSC encapsulated coacervate systems which contain HA and CHI polymers that show structural similarity to GAG showed remarkable potential for cartilage tissue engineering. This potential was also demonstrated by up-regulation of the cartilage-specific genes (COL2A1, SOX9 and ACAN) in both HA/CHI-C1 and HA/CHI-G coacervates. Moreover, cartilaginous matrix synthesis was concurrently shown by intense immunostaining results. Slightly better chondrogenic potential was found for HA/CHI-G than that of HA/CHI-C1 coacervate. Those positive results made coacervates encouraging candidates for further tissue engineering studies.

6. FUTURE PROSPECTS

The hypothesis of this thesis was to create a novel scaffold using HA and CHI biopolymers by complex coacervation technique and show the potential of this system *in vitro* through chondrogenic differentiation. The research outlined in this thesis represents promising results but further work should be required to understand cartilage regeneration in more detail.

The mechanical properties of the coacervates were not directly controlled but due to the viscosity of the materials used, strength and durability of the generated scaffolds should be improved. To better mimic the native cartilage tissue, instead of static culture, especially bioreactors with dynamic culture can be included. Consequently, this may also improve the physical and mechanical properties of the coacervates.

In cartilage tissue engineering, MSCs are promising cell sources but their differentiation potential affects the healing tissue. Due to the avascular nature of the native cartilage tissue, culturing MSC embedded coacervates under hypoxia conditions might enhance their chondrogenic potential. Furthermore, hypertrophy or dedifferentiation can be examined by the target gene markers (collagen type X or I, respectively). Moreover, changing cell source with co-cultures of MSCs with chondrocytes might improve the chondrogenesis.

To observe the actual potential of those cell embedded coacervates, long-term cartilage repair should be generated for the investigation of the newly formed tissue using *in vivo* animal models.

Generated coacervates are challenging scaffolds to investigate since the positive charge of the chitosan polymer and cell embedding make RNA, DNA and protein isolation very difficult or the isolated amount very low. Acidic pH of the used buffers may disrupt the coacervates before imaging and prevent the application of most of the differentiation studies. Therefore, more sophisticated techniques such as mass spectrometry, silver staining, ELISA assay or western blot can be involved to evaluate the chondrogenesis in more detail.

REFERENCES

1. Kuettner KE. Biochemistry of articular cartilage in health and disease. *Clin Biochem.* 1992;25(3):155-63.
2. Langer R, Vacanti JP. Tissue engineering. *Science.* 1993;260(5110):920-6.
3. Jung CK. Articular Cartilage: Histology and Physiology. In: Shetty AA, Kim S-J, Nakamura N, Brittberg M, editors. *Techniques in Cartilage Repair Surgery.* Berlin, Heidelberg: Springer Berlin Heidelberg; 2014. p. 17-21.
4. Standring S. *Gray's anatomy: the anatomical basis of clinical practice.* forty first edition ed: Elsevier Health Sciences; 2015.
5. Minuth WW, Strehl R, Schumacher K. *Tissue Engineering. Tissue Engineering: Essentials for Daily Laboratory Work: Wiley-VCH Verlag GmbH & Co. KGaA;* 2005. p. 113-29.
6. Schumacher BL, Block JA, Schmid TM, Aydelotte MB, Kuettner KE. A novel proteoglycan synthesized and secreted by chondrocytes of the superficial zone of articular cartilage. *Arch Biochem Biophys.* 1994;311(1):144-52.
7. Buckwalter J, Mankin H. Articular cartilage: tissue design and chondrocyte-matrix interactions. *Instr Course Lect.* 1997;47:477-86.
8. Aydelotte MB, Kuettner KE. Differences between sub-populations of cultured bovine articular chondrocytes. I. Morphology and cartilage matrix production. *Connect Tissue Res.* 1988;18(3):205-22.
9. van der Kraan PM, Buma P, van Kuppevelt T, van den Berg WB. Interaction of chondrocytes, extracellular matrix and growth factors: relevance for articular cartilage tissue engineering. *Osteoarthritis Cartilage.* 2002;10(8):631-7.

10. Mobasher A, Kalamegam G, Musumeci G, Batt ME. Chondrocyte and mesenchymal stem cell-based therapies for cartilage repair in osteoarthritis and related orthopaedic conditions. *Maturitas*. 2014;78(3):188-98.
11. Fratzl P. Collagen: Structure and Mechanics, an Introduction. In: Fratzl P, editor. *Collagen: Structure and Mechanics*. Boston, MA: Springer US; 2008. p. 1-13.
12. Buckwalter JA, Mankin HJ. Articular cartilage: tissue design and chondrocyte-matrix interactions. *Instr Course Lect*. 1998;47:477-86.
13. Alexopoulos LG, Youn I, Bonaldo P, Guilak F. Developmental and osteoarthritic changes in Col6a1-knockout mice: Biomechanics of type VI collagen in the cartilage pericellular matrix. *Arthritis & Rheumatism*. 2009;60(3):771-9.
14. Schmid TM, Linsenmayer TF. Immunohistochemical localization of short chain cartilage collagen (type X) in avian tissues. *J Cell Biol*. 1985;100(2):598-605.
15. Freeman MAR. *Adult articular cartilage*. 2nd revised edition ed: Pitman Medical; 1979.
16. Miosge N, Flachsbarth K, Goetz W, Schultz W, Kresse H, Herken R. Light and electron microscopical immunohistochemical localization of the small proteoglycan core proteins decorin and biglycan in human knee joint cartilage. *Histochem J*. 1994;26(12):939-45.
17. LeBaron RG, Athanasiou KA. Ex vivo synthesis of articular cartilage. *Biomaterials*. 2000;21(24):2575-87.
18. Mescher AL. *Junqueira's basic histology: text and atlas*. Thirteenth edition ed: McGraw-hill; 2013.
19. Chung C, Burdick JA. Engineering cartilage tissue. *Adv Drug Deliv Rev*. 2008;60(2):243-62.

20. Poole CA. Articular cartilage chondrons: form, function and failure. *J Anat.* 1997;191 (Pt 1):1-13.
21. Goldring MB, Tsuchimochi K, Ijiri K. The control of chondrogenesis. *J Cell Biochem.* 2006;97(1):33-44.
22. Minuth WW, Strehl R, Schumacher K. *Tissue engineering: From cell biology to artificial organs*: John Wiley & Sons; 2006.
23. Zhou S, Cui Z, Urban JP. Factors influencing the oxygen concentration gradient from the synovial surface of articular cartilage to the cartilage-bone interface: a modeling study. *Arthritis Rheum.* 2004;50(12):3915-24.
24. Widuchowski W, Widuchowski J, Trzaska T. Articular cartilage defects: study of 25,124 knee arthroscopies. *Knee.* 2007;14(3):177-82.
25. Radin EL, Burr DB, Caterson B, Fyhrie D, Brown TD, Boyd RD. Mechanical determinants of osteoarthritis. *Semin Arthritis Rheum.* 1991;21(3 Suppl 2):12-21.
26. Outerbridge RE. The etiology of chondromalacia patellae. *J Bone Joint Surg Br.* 1961;43-b:752-7.
27. Puett DW, Griffin MR. Published trials of nonmedicinal and noninvasive therapies for hip and knee osteoarthritis. *Ann Intern Med.* 1994;121(2):133-40.
28. Laupattarakasem W, Laopaiboon M, Laupattarakasem P, Sumananont C. Arthroscopic debridement for knee osteoarthritis. *Cochrane Db Syst Rev.* 2008(1).
29. Goymann V. [Abrasion arthroplasty]. *Orthopade.* 1999;28(1):11-8.
30. Magnussen RA, Dunn WR, Carey JL, Spindler KP. Treatment of focal articular cartilage defects in the knee: a systematic review. *Clin Orthop Relat Res.* 2008;466(4):952-62.

31. Steadman JR, Rodkey WG, Singleton SB, Briggs KK. Microfracture technique for full-thickness chondral defects: Technique and clinical results. *Oper Tech Orthop.* 7(4):300-4.
32. Shapiro F, Koide S, Glimcher MJ. Cell origin and differentiation in the repair of full-thickness defects of articular cartilage. *J Bone Joint Surg Am.* 1993;75(4):532-53.
33. Mankin HJ. The response of articular cartilage to mechanical injury. *J Bone Joint Surg Am.* 1982;64(3):460-6.
34. Robert H. Chondral repair of the knee joint using mosaicplasty. *Orthop Traumatol Surg Res.* 2011;97(4):418-29.
35. Gross AE, Kim W, Las Heras F, Backstein D, Safir O, Pritzker KPH. Fresh Osteochondral Allografts for Posttraumatic Knee Defects: Long-term Followup. *Clin Orthop Relat Res.* 2008;466(8):1863-70.
36. Brittberg M, Lindahl A, Nilsson A, Ohlsson C, Isaksson O, Peterson L. Treatment of deep cartilage defects in the knee with autologous chondrocyte transplantation. *N Engl J Med.* 1994;331(14):889-95.
37. Peterson L, Minas T, Brittberg M, Lindahl A. Treatment of osteochondritis dissecans of the knee with autologous chondrocyte transplantation: results at two to ten years. *J Bone Joint Surg Am.* 2003;85-A Suppl 2:17-24.
38. Gooding CR, Bartlett W, Bentley G, Skinner JA, Carrington R, Flanagan A. A prospective, randomised study comparing two techniques of autologous chondrocyte implantation for osteochondral defects in the knee: Periosteum covered versus type I/III collagen covered. *Knee.* 2006;13(3):203-10.
39. Cherubino P, Grassi F, Bulgheroni P, Ronga M. Autologous chondrocyte implantation using a bilayer collagen membrane: a preliminary report. *Journal of Orthopaedic Surgery.* 2003;11(1):10-5.

40. Makris EA, Gomoll AH, Malizos KN, Hu JC, Athanasiou KA. Repair and tissue engineering techniques for articular cartilage. *Nat Rev Rheumatol*. 2015;11(1):21-34.
41. Newman JH. Unicompartmental knee replacement. *The Knee*. 2000;7(2):63-70.
42. McGloughlin TM, Kavanagh AG. Wear of ultra-high molecular weight polyethylene (UHMWPE) in total knee prostheses: a review of key influences. *Proc Inst Mech Eng H*. 2000;214(4):349-59.
43. Julin J, Jamsen E, Puolakka T, Kontinen YT, Moilanen T. Younger age increases the risk of early prosthesis failure following primary total knee replacement for osteoarthritis. A follow-up study of 32,019 total knee replacements in the Finnish Arthroplasty Register. *Acta Orthop*. 2010;81(4):413-9.
44. Nestic D, Whiteside R, Brittberg M, Wendt D, Martin I, Mainil-Varlet P. Cartilage tissue engineering for degenerative joint disease. *Adv Drug Deliv Rev*. 2006;58(2):300-22.
45. Revell CM, Athanasiou KA. Success rates and immunologic responses of autogenic, allogenic, and xenogenic treatments to repair articular cartilage defects. *Tissue Eng Part B Rev*. 2009;15(1):1-15.
46. Moskalewski S, Hyc A, Osiecka-Iwan A. Immune response by host after allogeneic chondrocyte transplant to the cartilage. *Microsc Res Tech*. 2002;58(1):3-13.
47. Brodtkin K, Garcia A, Levenston M. Chondrocyte phenotypes on different extracellular matrix monolayers. *Biomaterials*. 2004;25(28):5929-38.
48. Bhardwaj N, Devi D, Mandal BB. Tissue-Engineered Cartilage: The Crossroads of Biomaterials, Cells and Stimulating Factors. *Macromol Biosci*. 2015;15(2):153-82.
49. Wakitani S, Takaoka K, Hattori T, Miyazawa N, Iwanaga T, Takeda S, *et al*. Embryonic stem cells injected into the mouse knee joint form teratomas and subsequently destroy the joint. *Rheumatology (Oxford)*. 2003;42(1):162-5.

50. Fortier LA. Stem cells: classifications, controversies, and clinical applications. *Vet Surg.* 2005;34(5):415-23.
51. Alexander PG, Hofer HR, Clark KL, Tuan RS. Chapter 54 - Mesenchymal Stem Cells in Musculoskeletal Tissue Engineering A2 - Lanza, Robert. In: Langer R, Vacanti J, editors. *Principles of Tissue Engineering (Fourth Edition)*. Boston: Academic Press; 2014. p. 1171-99.
52. De Bari C, Dell'Accio F, Tylzanowski P, Luyten FP. Multipotent mesenchymal stem cells from adult human synovial membrane. *Arthritis Rheum.* 2001;44(8):1928-42.
53. Pittenger MF, Mackay AM, Beck SC, Jaiswal RK, Douglas R, Mosca JD, *et al.* Multilineage potential of adult human mesenchymal stem cells. *Science.* 1999;284(5411):143-7.
54. Salgado AJ, Coutinho OP, Reis RL. Bone tissue engineering: state of the art and future trends. *Macromol Biosci.* 2004;4(8):743-65.
55. Dominici M, Le Blanc K, Mueller I, Slaper-Cortenbach I, Marini F, Krause D, *et al.* Minimal criteria for defining multipotent mesenchymal stromal cells. The International Society for Cellular Therapy position statement. *Cytotherapy.* 2006;8(4):315-7.
56. Winter A, Breit S, Parsch D, Benz K, Steck E, Hauner H, *et al.* Cartilage-like gene expression in differentiated human stem cell spheroids: a comparison of bone marrow-derived and adipose tissue-derived stromal cells. *Arthritis Rheum.* 2003;48(2):418-29.
57. Kopesky PW, Lee HY, Vanderploeg EJ, Kisiday JD, Frisbie DD, Plaas AH, *et al.* Adult equine bone marrow stromal cells produce a cartilage-like ECM mechanically superior to animal-matched adult chondrocytes. *Matrix Biol.* 2010;29(5):427-38.
58. Lutolf MP, Hubbell JA. Synthetic biomaterials as instructive extracellular microenvironments for morphogenesis in tissue engineering. *Nat Biotech.* 2005;23(1):47

59. Lee HJ, Yu C, Chansakul T, Hwang NS, Varghese S, Yu SM, *et al.* Enhanced chondrogenesis of mesenchymal stem cells in collagen mimetic peptide-mediated microenvironment. *Tissue Eng Part A*. 2008;14(11):1843-51.
60. Melton D. Chapter 2 - 'Stemness': Definitions, Criteria, and Standards. *Essentials of Stem Cell Biology (Third Edition)*. Boston: Academic Press; 2014. p. 7-17.
61. Mummery C, Wilmot SI, van de Stolpe A, Roelen BAJ. Chapter 5 - Origins and Types of Stem Cells. *Stem Cells*. San Diego: Academic Press; 2011. p. 87-107.
62. Takahashi K, Tanabe K, Ohnuki M, Narita M, Ichisaka T, Tomoda K, *et al.* Induction of pluripotent stem cells from adult human fibroblasts by defined factors. *Cell*. 2007;131(5):861-72.
63. Yoshida Y, Yamanaka S. Recent Stem Cell Advances: Induced Pluripotent Stem Cells for Disease Modeling and Stem Cell-Based Regeneration. *Circulation*. 2010;122(1):80-7.
64. Puetzer JL, Petite JN, Lobo EG. Comparative review of growth factors for induction of three-dimensional *in vitro* chondrogenesis in human mesenchymal stem cells isolated from bone marrow and adipose tissue. *Tissue Eng Part B Rev*. 2010;16(4):435-44.
65. Arita NA, Pelaez D, Cheung HS. Activation of the extracellular signal-regulated kinases 1 and 2 (ERK1/2) is needed for the TGFbeta-induced chondrogenic and osteogenic differentiation of mesenchymal stem cells. *Biochem Biophys Res Commun*. 2011;405(4):564-9.
66. Grimaud E, Heymann D, Redini F. Recent advances in TGF-beta effects on chondrocyte metabolism. Potential therapeutic roles of TGF-beta in cartilage disorders. *Cytokine Growth Factor Rev*. 2002;13(3):241-57.
67. Sekiya I, Colter DC, Prockop DJ. BMP-6 enhances chondrogenesis in a subpopulation of human marrow stromal cells. *Biochem Biophys Res Commun*. 2001;284(2):411-8.

68. Chen D, Zhao M, Mundy GR. Bone morphogenetic proteins. *Growth Factors*. 2004;22(4):233-41.
69. Kuroda R, Usas A, Kubo S, Corsi K, Peng H, Rose T, *et al*. Cartilage repair using bone morphogenetic protein 4 and muscle-derived stem cells. *Arthritis Rheum*. 2006;54(2):433-42.
70. Fortier LA, Mohammed HO, Lust G, Nixon AJ. Insulin-like growth factor-I enhances cell-based repair of articular cartilage. *J Bone Joint Surg Br*. 2002;84(2):276-88.
71. Solchaga LA, Penick K, Goldberg VM, Caplan AI, Welter JF. Fibroblast growth factor-2 enhances proliferation and delays loss of chondrogenic potential in human adult bone-marrow-derived mesenchymal stem cells. *Tissue Eng Part A*. 2010;16(3):1009-19.
72. Sekiya I, Larson BL, Vuoristo JT, Reger RL, Prockop DJ. Comparison of effect of BMP-2, -4, and -6 on *in vitro* cartilage formation of human adult stem cells from bone marrow stroma. *Cell Tissue Res*. 2005;320(2):269-76.
73. Park JS, Yang HN, Woo DG, Chung HM, Park KH. *In vitro* and *in vivo* chondrogenesis of rabbit bone marrow-derived stromal cells in fibrin matrix mixed with growth factor loaded in nanoparticles. *Tissue Eng Part A*. 2009;15(8):2163-75.
74. Portner R, Goepfert C, Wiegandt K, Janssen R, Ilinich E, Paetzold H, *et al*. Technical strategies to improve tissue engineering of cartilage-carrier-constructs. *Adv Biochem Eng Biotechnol*. 2009;112:145-81.
75. Temenoff JS, Mikos AG. Review: tissue engineering for regeneration of articular cartilage. *Biomaterials*. 2000;21(5):431-40.
76. Sucusky P, Osorio DF, Brown JB, Neitzel GP. Fluid mechanics of a spinner-flask bioreactor. *Biotechnol Bioeng*. 2004;85(1):34-46.

77. Concaro S, Gustavson F, Gatenholm P. Bioreactors for Tissue Engineering of Cartilage. In: Kasper C, van Griensven M, Pörtner R, editors. *Bioreactor Systems for Tissue Engineering*. Berlin, Heidelberg: Springer Berlin Heidelberg; 2009. p. 125-43.
78. Tran SC, Cooley AJ, Elder SH. Effect of a mechanical stimulation bioreactor on tissue engineered, scaffold-free cartilage. *Biotechnol Bioeng*. 2011;108(6):1421-9.
79. Freed LE, Vunjak-Novakovic G. Microgravity tissue engineering. *In Vitro Cell Dev Biol Anim*. 1997;33(5):381-5.
80. Sladkova M, de Peppo G. Bioreactor Systems for Human Bone Tissue Engineering. *Processes*. 2014;2(2):494.
81. Khan WS, Adesida AB, Hardingham TE. Hypoxic conditions increase hypoxia-inducible transcription factor 2alpha and enhance chondrogenesis in stem cells from the infrapatellar fat pad of osteoarthritis patients. *Arthritis Res Ther*. 2007;9(3):R55.
82. Wang DW, Fermor B, Gimble JM, Awad HA, Guilak F. Influence of oxygen on the proliferation and metabolism of adipose derived adult stem cells. *J Cell Physiol*. 2005;204(1):184-91.
83. Qu C, Lindeberg H, Ylärinne JH, Lammi MJ. Five percent oxygen tension is not beneficial for neocartilage formation in scaffold-free cell cultures. *Cell Tissue Res*. 2012;348(1):109-17.
84. Athanasiou KA, Darling EM, Hu JC. Articular cartilage tissue engineering. Kyriacos A. Athanasiou and J. Kent Leach UoC, Davis, editor. Davis: Morgan & Claypool; 2009. 1-182 p.
85. Peter SJ, Miller MJ, Yasko AW, Yaszemski MJ, Mikos AG. Polymer concepts in tissue engineering. *J Biomed Mater Res*. 1998;43(4):422-7.

86. Tsang VL, Bhatia SN. Fabrication of Three-Dimensional Tissues. In: Lee K, Kaplan D, editors. *Tissue Engineering II: Basics of Tissue Engineering and Tissue Applications*. Berlin, Heidelberg: Springer Berlin Heidelberg; 2007. p. 189-205.
87. Cima LG, Vacanti JP, Vacanti C, Ingber D, Mooney D, Langer R. Tissue Engineering by Cell Transplantation Using Degradable Polymer Substrates. *J Biomech Eng*. 1991;113(2):143-51.
88. BaoLin G, Ma PX. Synthetic biodegradable functional polymers for tissue engineering: a brief review. *Sci China Chem*. 2014;57(4):490-500.
89. Hsu SH, Chang SH, Yen HJ, Whu SW, Tsai CL, Chen DC. Evaluation of biodegradable polyesters modified by type II collagen and Arg-Gly-Asp as tissue engineering scaffolding materials for cartilage regeneration. *Artif Organs*. 2006;30(1):42-55.
90. Li WJ, Danielson KG, Alexander PG, Tuan RS. Biological response of chondrocytes cultured in three-dimensional nanofibrous poly(epsilon-caprolactone) scaffolds. *J Biomed Mater Res A*. 2003;67(4):1105-14.
91. Li WJ, Tuli R, Okafor C, Derfoul A, Danielson KG, Hall DJ, *et al*. A three-dimensional nanofibrous scaffold for cartilage tissue engineering using human mesenchymal stem cells. *Biomaterials*. 2005;26(6):599-609.
92. Haleem AM, Chu CR. Advances in Tissue Engineering Techniques for Articular Cartilage Repair. *Oper Tech Orthop*. 2010;20(2):76-89.
93. Nair LS, Laurencin CT. Biodegradable polymers as biomaterials. *Progress in Polymer Science*. 2007;32(8-9):762-98.
94. Dong C, Lv Y. Application of Collagen Scaffold in Tissue Engineering: Recent Advances and New Perspectives. *Polymers*. 2016;8(2):42.

95. Pieper JS, van der Kraan PM, Hafmans T, Kamp J, Buma P, van Susante JLC, *et al.* Crosslinked type II collagen matrices: preparation, characterization, and potential for cartilage engineering. *Biomaterials*. 2002;23(15):3183-92.
96. Yokoyama A, Sekiya I, Miyazaki K, Ichinose S, Hata Y, Muneta T. *In vitro* cartilage formation of composites of synovium-derived mesenchymal stem cells with collagen gel. *Cell Tissue Res*. 2005;322(2):289-98.
97. Jockenhoevel S, Zund G, Hoerstrup SP, Chalabi K, Sachweh JS, Demircan L, *et al.* Fibrin gel-advantages of a new scaffold in cardiovascular tissue engineering. *Eur J Cardiothorac Surg*. 2001;19(4):424-30.
98. Silverman RP, Passaretti D, Huang W, Randolph MA, Yaremchuk MJ. Injectable tissue-engineered cartilage using a fibrin glue polymer. *Plast Reconstr Surg*. 1999;103(7):1809-18.
99. Khabarov VN, Boykov PY, Selyanin MA. *Hyaluronic Acid: Production, Properties, Application in Biology and Medicine*: John Wiley & Sons; 2014.
100. Balazs EA, Laurent TC, Jeanloz RW. Nomenclature of hyaluronic acid. *Biochem J*. 1986;235(3):903-.
101. Ivanov D. Hyaluronic Acid-Based Biomaterials. *Encyclopedia of Biomedical Polymers and Polymeric Biomaterials*: CRC Press; 2015. p. 3743-59.
102. Grigolo B, Roseti L, Fiorini M, Fini M, Giavaresi G, Aldini NN, *et al.* Transplantation of chondrocytes seeded on a hyaluronan derivative (hyaff-11) into cartilage defects in rabbits. *Biomaterials*. 2001;22(17):2417-24.
103. Mauck RL, Yuan X, Tuan RS. Chondrogenic differentiation and functional maturation of bovine mesenchymal stem cells in long-term agarose culture. *Osteoarthritis Cartilage*. 2006;14(2):179-89.

104. Chi W-J, Chang Y-K, Hong S-K. Agar degradation by microorganisms and agar-degrading enzymes. *Appl Microbiol Biotechnol.* 2012;94(4):917-30.
105. Hauselmann HJ, Fernandes RJ, Mok SS, Schmid TM, Block JA, Aydelotte MB, *et al.* Phenotypic stability of bovine articular chondrocytes after long-term culture in alginate beads. *J Cell Sci.* 1994;107 (Pt 1):17-27.
106. Caterson EJ, Nesti LJ, Li WJ, Danielson KG, Albert TJ, Vaccaro AR, *et al.* Three-dimensional cartilage formation by bone marrow-derived cells seeded in polylactide/alginate amalgam. *J Biomed Mater Res.* 2001;57(3):394-403.
107. Yang T-L. Chitin-based Materials in Tissue Engineering: Applications in Soft Tissue and Epithelial Organ. *Int J Mol Sci.* 2011;12(3):1936-63.
108. Ravi Kumar MNV. A review of chitin and chitosan applications. *React Funct Polym.* 2000;46(1):1-27.
109. VandeVord PJ, Matthew HW, DeSilva SP, Mayton L, Wu B, Wooley PH. Evaluation of the biocompatibility of a chitosan scaffold in mice. *J Biomed Mater Res.* 2002;59(3):585-90.
110. Lahiji A, Sohrabi A, Hungerford DS, Frondoza CG. Chitosan supports the expression of extracellular matrix proteins in human osteoblasts and chondrocytes. *J Biomed Mater Res.* 2000;51(4):586-95.
111. Matsiko A, Levingstone T, Brien F. Advanced Strategies for Articular Cartilage Defect Repair. *Materials.* 2013;6(2):637.
112. Mikos AG, Temenoff JS. Formation of highly porous biodegradable scaffolds for tissue engineering 2000.
113. Ma PX, Langer R. Fabrication of Biodegradable Polymer Foams for Cell Transplantation and Tissue Engineering. In: Morgan JR, Yarmush ML, editors. *Tissue Engineering Methods and Protocols.* Totowa, NJ: Humana Press; 1999. p. 47-56.

114. Shi G, Cai Q, Wang C, Lu N, Wang S, Bei J. Fabrication and biocompatibility of cell scaffolds of poly(L-lactic acid) and poly(L-lactic-co-glycolic acid). *Polymers for Advanced Technologies*. 2002;13(3-4):227-32.
115. Schoof H, Apel J, Heschel I, Rau G. Control of pore structure and size in freeze-dried collagen sponges. *J Biomed Mater Res*. 2001;58(4):352-7.
116. Xia W, Liu W, Cui L, Liu Y, Zhong W, Liu D, *et al*. Tissue engineering of cartilage with the use of chitosan-gelatin complex scaffolds. *Journal of Biomedical Materials Research Part B: Applied Biomaterials*. 2004;71B(2):373-80.
117. Li W-J, Laurencin CT, Caterson EJ, Tuan RS, Ko FK. Electrospun nanofibrous structure: A novel scaffold for tissue engineering. *J Biomed Mater Res*. 2002;60(4):613-21.
118. Subramony SD, Dargis BR, Castillo M, Azeloglu EU, Tracey MS, Su A, *et al*. The Guidance of Stem Cell Differentiation by Substrate Alignment and Mechanical Stimulation. *Biomaterials*. 2013;34(8):1942-53.
119. Lu T, Li Y, Chen T. Techniques for fabrication and construction of three-dimensional scaffolds for tissue engineering. *International Journal of Nanomedicine*. 2013;8:337-50.
120. Pham QP, Sharma U, Mikos AG. Electrospinning of polymeric nanofibers for tissue engineering applications: a review. *Tissue Eng*. 2006;12(5):1197-211.
121. Woodfield TB, Guggenheim M, von Rechenberg B, Riesle J, van Blitterswijk CA, Wedler V. Rapid prototyping of anatomically shaped, tissue-engineered implants for restoring congruent articulating surfaces in small joints. *Cell Prolif*. 2009;42(4):485-97.
122. Skardal A. Chapter 1 - Bioprinting Essentials of Cell and Protein Viability A2 - Atala, Anthony. In: Yoo JJ, editor. *Essentials of 3D Biofabrication and Translation*. Boston: Academic Press; 2015. p. 1-17.

123. Cui X, Breitenkamp K, Lotz M, D'Lima D. Synergistic action of fibroblast growth factor-2 and transforming growth factor-beta1 enhances bioprinted human neocartilage formation. *Biotechnol Bioeng*. 2012;109(9):2357-68.
124. Patwekar SL, Ashwini P. Potulwar, Snehal R. Pedewad, Manoj S. Gaikwad, Shaz. A Khan, Arvind B Suryawanshi. Review on Polyelectrolyte Complex as Novel Approach for Drug Delivery System. *Ijppr.Human*; 2016. p. 97-104.
125. Bohidar H. Coacervates: a novel state of soft matter: an overview. *J Surf Sci Technol*. 2008;24(4):105-24.
126. Bungenberg de Jong H. Complex colloid systems. *Colloid science*. 1949;2:335-432.
127. Overbeek JT, Voorn MJ. Phase separation in polyelectrolyte solutions; theory of complex coacervation. *J Cell Physiol Suppl*. 1957;49(S1):7-26.
128. de Kruif CG, Weinbreck F, de Vries R. Complex coacervation of proteins and anionic polysaccharides. *Current Opinion in Colloid & Interface Science*. 2004;9(5):340-9.
129. Priftis D, Tirrell M. Phase behaviour and complex coacervation of aqueous polypeptide solutions. *Soft Matter*. 2012;8(36):9396-405.
130. Sarmiento B, Ribeiro A, Veiga F, Sampaio P, Neufeld R, Ferreira D. Alginate/chitosan nanoparticles are effective for oral insulin delivery. *Pharm Res*. 2007;24(12):2198-206.
131. Shahidi F, Han XQ. Encapsulation of food ingredients. *Crit Rev Food Sci Nutr*. 1993;33(6):501-47.
132. Chu H, Gao J, Chen C-W, Huard J, Wang Y. Injectable fibroblast growth factor-2 coacervate for persistent angiogenesis. *P Natl Acad Sci USA*. 2011;108(33):13444-9.

133. Sakai S, Ono T, Ijima H, Kawakami K. *In vitro* and *in vivo* evaluation of alginate/sol-gel synthesized aminopropyl-silicate/alginate membrane for bioartificial pancreas. *Biomaterials*. 2002;23(21):4177-83.
134. Poshadri A, Aparna K. Microencapsulation technology: a review. *Journal of Research ANGRAU*. 2010;38(1):86-102.
135. Lim F, Sun AM. Microencapsulated islets as bioartificial endocrine pancreas. *Science*. 1980;210(4472):908-10.
136. Orive G, Hernandez RM, Gascon AR, Calafiore R, Chang TM, De Vos P, *et al*. Cell encapsulation: promise and progress. *Nat Med*. 2003;9(1):104-7.
137. Haque T, Chen H, Ouyang W, Martoni C, Lawuyi B, Urbanska AM, *et al*. *In vitro* study of alginate-chitosan microcapsules: an alternative to liver cell transplants for the treatment of liver failure. *Biotechnol Lett*. 2005;27(5):317-22.
138. Johnson NR, Wang Y. Controlled delivery of heparin-binding EGF-like growth factor yields fast and comprehensive wound healing. *J Control Release*. 2013;166(2):124-9
139. Wu J, Ye J, Zhu J, Xiao Z, He C, Shi H, *et al*. Heparin-based coacervate of FGF2 improves dermal regeneration by asserting a synergistic role with cell proliferation and endogenous facilitated VEGF for cutaneous wound healing. *Biomacromolecules*. 2016;17(6):2168-77.
140. Lee K-W, Johnson NR, Gao J, Wang Y. Human progenitor cell recruitment via SDF-1 α coacervate-laden PGS vascular grafts. *Biomaterials*. 2013;34(38):9877-85.
141. Toh Y-C, Ho ST, Zhou Y, Hutmacher DW, Yu H. Application of a polyelectrolyte complex coacervation method to improve seeding efficiency of bone marrow stromal cells in a 3D culture system. *Biomaterials*. 2005;26(19):4149-60.

142. Hwang DS, Waite JH, Tirrell M. Promotion of osteoblast proliferation on complex coacervation-based hyaluronic acid–recombinant mussel adhesive protein coatings on titanium. *Biomaterials*. 2010;31(6):1080-4.
143. Chen M, Le DQ, Baatrup A, Nygaard JV, Hein S, Bjerre L, *et al.* Self-assembled composite matrix in a hierarchical 3-D scaffold for bone tissue engineering. *Acta Biomater*. 2011;7(5):2244-55.
144. Shao H, Stewart RJ. Biomimetic Underwater Adhesives with Environmentally Triggered Setting Mechanisms. *Adv Mater*. 2010;22(6):729-33.
145. Kim HJ, Choi BH, Jun SH, Cha HJ. Sandcastle Worm-Inspired Blood-Resistant Bone Graft Binder Using a Sticky Mussel Protein for Augmented *In Vivo* Bone Regeneration. *Adv Healthc Mat*. 2016;5(24):3191-202.
146. Wang W, Xu Y, Li A, Li T, Liu M, von Klitzing R, *et al.* Zinc induced polyelectrolyte coacervate bioadhesive and its transition to a self-healing hydrogel. *Rsc Advances*. 2015;5(82):66871-8.
147. Winslow BD, Shao H, Stewart RJ, Tresco PA. Biocompatibility of adhesive complex coacervates modeled after the sandcastle glue of *Phragmatopoma californica* for craniofacial reconstruction. *Biomaterials*. 2010;31(36):9373-81.
148. Lawrence PG, Lapitsky Y. Ionically cross-linked poly (allylamine) as a stimulus-responsive underwater adhesive: ionic strength and pH effects. *Langmuir*. 2015;31(4):1564-74.
149. Zhou D, Pierucci L, Gao Y, O’Keeffe Ahern J, Huang X, Sigen A, *et al.* Thermo- and pH-Responsive, Coacervate-Forming Hyperbranched Poly (β -amino ester) s for Selective Cell Binding. *ACS Appl Mater Inter*. 2017;9(7):5793-802.
150. Shimada N, Saito M, Shukuri S, Kuroyanagi S, Kuboki T, Kidoaki S, *et al.* Reversible monolayer/spheroid cell culture switching by UCST-type thermoresponsive ureido polymers. *ACS Appl Mater Inter*. 2016;8(46):31524-9.

151. Kayitmazer AB, Seeman D, Minsky BB, Dubin PL, Xu Y. Protein-polyelectrolyte interactions. *Soft Matter*. 2013;9(9):2553-83.
152. Comert F, Malanowski AJ, Azarikia F, Dubin PL. Coacervation and precipitation in polysaccharide-protein systems. *Soft Matter*. 2016;12(18):4154-61.
153. van Oss CJ. *Interfacial Forces in Aqueous Media*, Second Edition: CRC Press; 2006.
154. Ahmed EM. Hydrogel: Preparation, characterization, and applications: A review. *Journal of Advanced Research*. 2015;6(2):105-21.
155. Yan Q, Hoffman AS. Synthesis of macroporous hydrogels with rapid swelling and deswelling properties for delivery of macromolecules. *Polymer*. 1995;36(4):887-9.
156. Decher G, Hong JD, Schmitt J. Buildup of ultrathin multilayer films by a self-assembly process: III. Consecutively alternating adsorption of anionic and cationic polyelectrolytes on charged surfaces. *Thin Solid Films*. 1992;210:831-5.
157. Lee JS, Lee EK. Original Paper: Newborn Calf Serum Retards Loss of the Chondrocytic Phenotype during *In Vitro* Cell Expansion. 2009;6(1):229-35.
158. Gulrez SK, Phillips GO, Al-Assaf S. *Hydrogels: methods of preparation, characterisation and applications*. Progress in Molecular and Environmental Bioengineering: INTECH Open Access Publisher; 2011.
159. Sabaratnam S, Coleman P, Badrick E, Mason R, Levick J. Interactive effect of chondroitin sulphate C and hyaluronan on fluid movement across rabbit synovium. *The Journal of physiology*. 2002;540(1):271-84.
160. Desbrieres J. Viscosity of semiflexible chitosan solutions: influence of concentration, temperature, and role of intermolecular interactions. *Biomacromolecules*. 2002;3(2):342-9.

161. Yan H, Nykanen A, Ruokolainen J, Farrar D, Miller AF. Protein fibrillar hydrogels for three-dimensional tissue engineering. *Journal of Nanotechnology*; 2009.
162. McNaught AD, McNaught AD. *Compendium of chemical terminology*: Blackwell Science Oxford; 1997.
163. Wayne P. National Committee for Clinical Laboratory Standards, 1997. Approved Standard M7–A4 Search PubMed.
164. Black KA, Priftis D, Perry SL, Yip J, Byun WY, Tirrell M. Protein encapsulation via polypeptide complex coacervation. *ACS Macro Lett.* 2014;3(10):1088-91.
165. Priftis D, Xia X, Margossian KO, Perry SL, Leon L, Qin J, *et al.* Ternary, tunable polyelectrolyte complex fluids driven by complex coacervation. *Macromolecules.* 2014;47(9):3076-85.
166. Aumiller Jr WM, Keating CD. Phosphorylation-mediated RNA/peptide complex coacervation as a model for intracellular liquid organelles. *Nat Chem.* 2015;8(2):129-35.
167. Perry S, Li Y, Priftis D, Leon L, Tirrell M. The Effect of Salt on the Complex Coacervation of Vinyl Polyelectrolytes. *Polymers.* 2014;6(6):1756.
168. Kizilay E, Kayitmazer AB, Dubin PL. Complexation and coacervation of polyelectrolytes with oppositely charged colloids. *Adv Colloid Interface Sci.* 2011;167(1):24-37.
169. Comert F, Nguyen D, Rushanan M, Milas P, Xu AY, Dubin PL. Precipitate–Coacervate Transformation in Polyelectrolyte–Mixed Micelle Systems. *J Phys Chem B.* 2017;121(17):4466-73.
170. Turgeon SL, Laneuville SI. Protein+ polysaccharide coacervates and complexes: from scientific background to their application as functional ingredients in food products. *Modern biopolymer science.* 2009:327-63.

171. Schmitt C, Aberkane L, Sanchez C. Protein-polysaccharide complexes and coacervates. *Handbook of hydrocolloids*. 2009:420-76.
172. Wang Q, Schlenoff JB. The Polyelectrolyte Complex/Coacervate Continuum. *Macromolecules*. 2014;47(9):3108-16.
173. Weinbreck F, de Vries R, Schrooyen P, de Kruif CG. Complex coacervation of whey proteins and gum arabic. *Biomacromolecules*. 2003;4(2):293-303.
174. Kayitmazer AB, Koksal AF, Kilic Iyilik E. Complex coacervation of hyaluronic acid and chitosan: effects of pH, ionic strength, charge density, chain length and the charge ratio. *Soft Matter*. 2015;11(44):8605-12.
175. Spruijt E, Westphal AH, Borst JW, Cohen Stuart MA, van der Gucht J. Binodal compositions of polyelectrolyte complexes. *Macromolecules*. 2010;43(15):6476-84.
176. Anema SG, de Kruif CK. Phase separation and composition of coacervates of lactoferrin and caseins. *Food Hydrocolloids*. 2016;52:670-7.
177. Yan Y, Kizilay E, Seeman D, Flanagan S, Dubin PL, Bovetto L, *et al.* Heteroprotein complex coacervation: bovine β -lactoglobulin and lactoferrin. *Langmuir*. 2013;29(50):15614-23.
178. Anema SG, de Kruif CK. Complex coacervates of lactotransferrin and β -lactoglobulin. *J Colloid Interface Sci*. 2014;430:214-20.
179. Instruments M. Achieving high sensitivity at different scattering angles with different optical configurations. Technical Note Malvern, MRK656-01. 2014:1-6.
180. Kwon TK, Kim J-C. Complex coacervation-controlled release from monoolein cubic phase containing silk fibroin and alginate. *Biomacromolecules*. 2010;12(2):466-71.

181. Zhou H, Sun X, Zhang L, Zhang P, Li J, Liu Y-N. Fabrication of biopolymeric complex coacervation core micelles for efficient tea polyphenol delivery via a green process. *Langmuir*. 2012;28(41):14553-61.
182. Qin J, Priftis D, Farina R, Perry SL, Leon L, Whitmer J, *et al.* Interfacial tension of polyelectrolyte complex coacervate phases. *ACS Macro Letters*. 2014;3(6):565-8.
183. Zhang R, Shklovskii B. Phase diagram of solution of oppositely charged polyelectrolytes. *Physica A*. 2005;352(1):216-38.
184. Srivastava A, Waite JH, Stucky GD, Mikhailovsky A. Fluorescence investigations into complex coacervation between polyvinylimidazole and sodium alginate. *Macromolecules*. 2009;42(6):2168-76.
185. Iwasaki N, Kasahara Y, Yamane S, Igarashi T, Minami A, Nisimura S-i. Chitosan-based hyaluronic acid hybrid polymer fibers as a scaffold biomaterial for cartilage tissue engineering. *Polymers*. 2010;3(1):100-13.
186. Correia CR, Moreira-Teixeira LS, Moroni L, Reis RL, van Blitterswijk CA, Karperien M, *et al.* Chitosan scaffolds containing hyaluronic acid for cartilage tissue engineering. *Tissue Engineering Part C: Methods*. 2011;17(7):717-30.
187. Miranda DG, Malmonge SM, Campos DM, Attik NG, Grosogeat B, Gritsch K. A chitosan-hyaluronic acid hydrogel scaffold for periodontal tissue engineering. *Journal of Biomedical Materials Research Part B: Applied Biomaterials*. 2016;104(8):1691-702.
188. Nair S, Remya N, Remya S, Nair PD. A biodegradable in situ injectable hydrogel based on chitosan and oxidized hyaluronic acid for tissue engineering applications. *Carbohydrate polymers*. 2011;85(4):838-44.
189. Kaushik P, Dowling K, McKnight S, Barrow CJ, Adhikari B. Microencapsulation of flaxseed oil in flaxseed protein and flaxseed gum complex coacervates. *Food research international*. 2016;86:1-8.

190. Yin X, Stöver HD. Hydrogel Microspheres Formed by Complex Coacervation of Partially MPEG-Grafted Poly (styrene-*a* It-maleic anhydride) with PDADMAC and Cross-Linking with Polyamines. *Macromolecules*. 2003;36(23):8773-9.
191. Kizilay E, Seeman D, Yan Y, Du X, Dubin PL, Donato-Capel L, *et al.* Structure of bovine β -lactoglobulin–lactoferrin coacervates. *Soft matter*. 2014;10(37):7262-8.
192. O'brien FJ. Biomaterials & scaffolds for tissue engineering. *Materials today*. 2011;14(3):88-95.
193. Schlenoff JB, Rmaile AH, Bucur CB. Hydration contributions to association in polyelectrolyte multilayers and complexes: visualizing hydrophobicity. *J Am Chem Soc*. 2008;130(41):13589-97.
194. Nava MM, Draghi L, Giordano C, Pietrabissa R. The effect of scaffold pore size in cartilage tissue engineering. *Journal of Applied Biomaterials & Functional Materials*. 2016;14(3):0-.
195. Zhao F, Yao D, Guo R, Deng L, Dong A, Zhang J. Composites of Polymer Hydrogels and Nanoparticulate Systems for Biomedical and Pharmaceutical Applications. *Nanomaterials*. 2015;5(4):2054.
196. Bohidar H, Dubin P, Majhi P, Tribet C, Jaeger W. Effects of protein– polyelectrolyte affinity and polyelectrolyte molecular weight on dynamic properties of bovine serum albumin– poly (diallyldimethylammonium chloride) coacervates. *Biomacromolecules*. 2005;6(3):1573-85.
197. Mathieu F, Ugazio S, Carnelle G, Ducini Y, Legrand J. Complex coacervation of the gelatin–poly (acrylic acid) system. *Journal of applied polymer science*. 2006;101(1):708-14.
198. Wang X, Lee J, Wang Y-W, Huang Q. Composition and rheological properties of β -lactoglobulin/pectin coacervates: effects of salt concentration and initial protein/polysaccharide ratio. *Biomacromolecules*. 2007;8(3):992-7.

199. Zhang H, Zhou L, Zhang W. Control of scaffold degradation in tissue engineering: a review. *Tissue Eng Part B Rev.* 2014;20(5):492-502.
200. Hedberg EL, Shih CK, Lemoine JJ, Timmer MD, Liebschner MA, Jansen JA, *et al.* *In vitro* degradation of porous poly(propylene fumarate)/poly(DL-lactic-co-glycolic acid) composite scaffolds. *Biomaterials.* 2005;26(16):3215-25.
201. Srichana T, Domb AJ. Polymeric Biomaterials. In: Narayan R, editor. *Biomedical Materials.* Boston, MA: Springer US; 2009. p. 83-119.
202. Raafat D, Sahl HG. Chitosan and its antimicrobial potential—a critical literature survey. *Microbial biotechnology.* 2009;2(2):186-201.
203. Seyfarth F, Schliemann S, Elsner P, Hipler U-C. Antifungal effect of high-and low-molecular-weight chitosan hydrochloride, carboxymethyl chitosan, chitosan oligosaccharide and N-acetyl-D-glucosamine against *Candida albicans*, *Candida krusei* and *Candida glabrata*. *Int J Pharm.* 2008;353(1):139-48.
204. Kong M, Chen XG, Xing K, Park HJ. Antimicrobial properties of chitosan and mode of action: a state of the art review. *Int J Food Microbiol.* 2010;144(1):51-63.
205. No HK, Park NY, Lee SH, Meyers SP. Antibacterial activity of chitosans and chitosan oligomers with different molecular weights. *Int J Food Microbiol.* 2002;74(1):65-72.
206. Tsai GJ, Su WH, Chen HC, Pan CL. Antimicrobial activity of shrimp chitin and chitosan from different treatments and applications of fish preservation. *Fisheries science.* 2002;68(1):170-7.
207. Chung YC, Wang HL, Chen YM, Li SL. Effect of abiotic factors on the antibacterial activity of chitosan against waterborne pathogens. *Bioresource technology.* 2003;88(3):179-84.

208. Rhoades J, Roller S. Antimicrobial actions of degraded and native chitosan against spoilage organisms in laboratory media and foods. *Appl Environ Microbiol.* 2000;66(1):80-6.
209. Sato K, Inoue Y, Fujii T, Aoyama H, Mitsuhashi S. Antibacterial activity of ofloxacin and its mode of action. *Infection.* 1986;14:S226-S30.
210. Solchaga LA, Penick KJ, Welter JF. Chondrogenic Differentiation of Bone Marrow-Derived Mesenchymal Stem Cells: Tips and Tricks. In: Vemuri MCC, L.G.; Rao, M.S., editor. *Mesenchymal Stem Cell Assays and Applications.* 698: Humana Press; 2011. p. 253-78.
211. Sun H, Liu Y, Jiang T, Liu X, He A, Li J, *et al.* Chondrogenic differentiation and three dimensional chondrogenesis of human adipose-derived stem cells induced by engineered cartilage-derived conditional media. *Tissue Engineering and Regenerative Medicine.* 2014;11(1):59-66.
212. Svobodová J, Proks V, Karabiyik Ö, Çalıkoğlu Koyuncu AC, Torun Köse G, Rypáček F, *et al.* Poly (amino acid)-based fibrous scaffolds modified with surface-pendant peptides for cartilage tissue engineering. *J Tissue Eng Regen Med.* 2017;11(3):831-42.
213. Marquez-Curtis LA, Janowska-Wieczorek A, McGann LE, Elliott JAW. Mesenchymal stromal cells derived from various tissues: Biological, clinical and cryopreservation aspects. *Cryobiology.* 2015;71(2):181-97.
214. Harting M, Jimenez F, Pati S, Baumgartner J, Cox CJ. Immunophenotype characterization of rat mesenchymal stromal cells. *Cytotherapy.* 2008;10(3):243-53.
215. Boxall SA, Jones E. Markers for Characterization of Bone Marrow Multipotential Stromal Cells. *Stem Cells Int.* 2012;2012:12.
216. Hong Y, Song H, Gong Y, Mao Z, Gao C, Shen J. Covalently crosslinked chitosan hydrogel: properties of *in vitro* degradation and chondrocyte encapsulation. *Acta biomaterialia.* 2007;3(1):23-31.

217. Chung C, Erickson IE, Mauck RL, Burdick JA. Differential behavior of auricular and articular chondrocytes in hyaluronic acid hydrogels. *Tissue Engineering Part A*. 2008;14(7):1121-31.
218. Hou T, Xu J, Li Q, Feng J, Zen L. *In vitro* evaluation of a fibrin gel antibiotic delivery system containing mesenchymal stem cells and vancomycin alginate beads for treating bone infections and facilitating bone formation. *Tissue Engineering Part A*. 2008;14(7):1173-82.
219. Nguyen BNB, Moriarty RA, Kamalitinov T, Etheridge JM, Fisher JP. Collagen hydrogel scaffold promotes MSC and endothelial cell coculture for bone tissue engineering. *Journal of Biomedical Materials Research Part A*. 2017;105(4):1123-31.
220. Ferrari A, Hannouche D, Oudina K, Bourguignon M, Meunier A, Sedel L, *et al.* *In vivo* tracking of bone marrow fibroblasts with fluorescent carbocyanine dye. *J Biomed Mater Res*. 2001;56(3):361-7.
221. Fan C, Wang DA. Macroporous Hydrogel Scaffolds for Three-Dimensional Cell Culture and Tissue Engineering. *Tissue Eng Part B Rev*. 2017.
222. Joshi C, Karumuri B, Newman JJ, DeCoster MA. Cell morphological changes combined with biochemical assays for assessment of apoptosis and apoptosis reversal. *Curr Microsc Contrib to Adv Sci Technol (A Méndez-Vilas, Ed)*. 2012:756-62.
223. Mager MD, LaPointe V, Stevens MM. Exploring and exploiting chemistry at the cell surface. *Nat Chem*. 2011;3(8):582-9.
224. Knudson CB. Hyaluronan and CD44: strategic players for cell–matrix interactions during chondrogenesis and matrix assembly. *Birth Defects Research Part C: Embryo Today: Reviews*. 2003;69(2):174-96.
225. Dicker KT, Gurski LA, Pradhan-Bhatt S, Witt RL, Farach-Carson MC, Jia X. Hyaluronan: A Simple Polysaccharide with Diverse Biological Functions. *Acta Biomater*. 2014;10(4):1558-70.

226. Isacke CM, Yarwood H. The hyaluronan receptor, CD44. *Int J Biochem Cell Biol.* 2002;34(7):718-21.
227. Misra S, Hascall VC, Markwald RR, Ghatak S. Interactions between Hyaluronan and Its Receptors (CD44, RHAMM) Regulate the Activities of Inflammation and Cancer. *Front Immunol.* 2015;6:201.
228. Jha AK, Xu X, Duncan RL, Jia X. Controlling the adhesion and differentiation of mesenchymal stem cells using hyaluronic acid-based, doubly crosslinked networks. *Biomaterials.* 2011;32(10):2466-78.
229. Fraley SI, Feng Y, Krishnamurthy R, Kim D-H, Celedon A, Longmore GD, *et al.* A distinctive role for focal adhesion proteins in three-dimensional cell motility. *Nat Cell Biol.* 2010;12(6):598.
230. Bershadsky AD, Balaban NQ, Geiger B. Adhesion-dependent cell mechanosensitivity. *Annu Rev Cell Dev Biol.* 2003;19(1):677-95.
231. Burdick JA, Vunjak-Novakovic G. Engineered Microenvironments for Controlled Stem Cell Differentiation. *Tissue Engineering Part A.* 2009;15(2):205-19.
232. Varghese S, Theprungsirikul P, Ferran A, Hwang N, Canver A, Elisseeff J. Chondrogenic differentiation of human embryonic germ cell derived cells in hydrogels. *Conf Proc IEEE Eng Med Biol Soc.* 2006;1:2643-6.
233. Yu D-A, Han J, Kim B-S. Stimulation of Chondrogenic Differentiation of Mesenchymal Stem Cells. *International Journal of Stem Cells.* 2012;5(1):16-22.
234. Shintani N, Hunziker EB. Differential effects of dexamethasone on the chondrogenesis of mesenchymal stromal cells: influence of microenvironment, tissue origin and growth factor. *Eur Cell Mater.* 2011;22:302-19.

235. Hu J, Feng K, Liu X, Ma PX. Chondrogenic and osteogenic differentiations of human bone marrow-derived mesenchymal stem cells on a nanofibrous scaffold with designed pore network. *Biomaterials*. 2009;30(28):5061-7.
236. Awad HA, Halvorsen YD, Gimble JM, Guilak F. Effects of transforming growth factor beta1 and dexamethasone on the growth and chondrogenic differentiation of adipose-derived stromal cells. *Tissue Eng*. 2003;9(6):1301-12.
237. O'Driscoll SW, Fitzsimmons JS. The Role of Periosteum in Cartilage Repair. *Clin Orthop Relat Res*. 2001;391:S190-S207.
238. Vinatier C, Mrugala D, Jorgensen C, Guicheux J, Noël D. Cartilage engineering: a crucial combination of cells, biomaterials and biofactors. *Trends Biotechnol*. 2009;27(5):307-14.
239. De Crombrughe B, Lefebvre V, Behringer RR, Bi W, Murakami S, Huang W. Transcriptional mechanisms of chondrocyte differentiation. *Matrix Biol*. 2000;19(5):389-94.
240. Poole AR, Kojima T, Yasuda T, Mwale F, Kobayashi M, Lavery S. Composition and Structure of Articular Cartilage: A Template for Tissue Repair. *Clin Orthop Relat Res*. 2001;391:S26-S33.
241. Dy P, Wang W, Bhattaram P, Wang Q, Wang L, Ballock RT, *et al*. Sox9 Directs Hypertrophic Maturation and Blocks Osteoblast Differentiation of Growth Plate Chondrocytes. *Dev Cell*. 2012;22(3):597-609.
242. Hamid AA, Idrus RBH, Saim AB, Sathappan S, Chua K-H. Characterization of human adipose-derived stem cells and expression of chondrogenic genes during induction of cartilage differentiation. *Clinics*. 2012;67:099-106.
243. Chung C, Burdick JA. Influence of 3D Hyaluronic Acid Microenvironments on Mesenchymal Stem Cell Chondrogenesis. *Tissue engineering Part A*. 2009;15(2):243-54.